Identification of hypoxia-specific anti-cancer drugs using an *in vitro* spheroid model

vorgelegt von
M.Sc.
Saskia Klutzny
geb. in Brandenburg an der Havel

von der Fakultät III – Prozesswissenschaften
der Technischen Universität Berlin
zur Erlangung des akademischen Grades

Doktor der Naturwissenschaften
- Dr. rer. nat. –

genehmigte Dissertation

Promotionsausschuss:
Vorsitzender: Prof. Dr. Peter Neubauer
Gutachter: Prof. Dr. Juri Rappsilber
Gutachter: Prof. Dr. Roland Lauster
Gutachter: Dr. Patrick Steigemann

Tag der wissenschaftlichen Aussprache: 06. November 2017

Berlin 2018

This work was done at:

Bayer AG
Lead Discovery Berlin
Screening Cell Biology
High Content Analysis group of Dr. Patrick Steigemann

Declaration according to §5, Sec. 1 of the Doctoral Regulations

I hereby declare in lieu of an oath that I have independently completed the dissertation. All aids and sources have been listed and passages included from other works have been marked as such (additional remarks see pre-publication of the dissertation).

_____ _____

Location, Date Signature

Declaration pre-publication of the dissertation

Parts of this dissertation have previously been published:

> Klutzny, S., et al. (2017) „Functional inhibition of acid sphingomyelinase by Fluphenazine triggers hypoxia-specific tumor cell death." *Cell Death and Disease*, 8, e2709

Details of my own contributions according to §2, subpara 4 doctoral regulations are listed in the attachment of the "Application to commence the doctoral procedure at Faculty III - Process Sciences, Technische Universität Berlin".

The following chapters of this dissertation are essentially based on this pre-publication. The usage of verbatim passages from this pre-publication will not be marked separately as self-citation in this dissertation.

_____ _____

Location, Date Signature

.

Abstract

Cancer is among the leading causes of morbidity and mortality worldwide and the effectiveness of novel treatment approaches is often limited by the development of drug resistance. Owing to the rapid growth, high metabolic rates and lagging or insufficient neo-angiogenesis, many solid tumors are characterized by large regions of hypoxia. Tumor hypoxia is a main determinant for resistance development and treatment failure and is therefore an important target for cancer therapy. Most approaches for targeting hypoxic cells focus on the inhibition of hypoxia adaption pathways but only a limited number of compounds with the potential to specifically target hypoxic tumor regions have been identified.

Therefore, a tumor spheroid model that mimics regions of severe hypoxia in tumors was used to perform a high-content screen for the identification of hypoxia-sensitizing compounds that specifically induce cell death in hypoxic tumor spheroids. Using this unbiased phenotypic screening system, a set of compounds including the antipsychotic phenothiazine drug fluphenazine were identified as highly hypoxia-selective hits that act via a novel, yet unreported mode of action. It was discovered that fluphenazine functionally inhibits the lysosomal enzyme acid sphingomyelinase and induces cancer cell death in hypoxic tumor spheroids by sphingomyelin accumulation. Moreover, fluphenazine potentiates the transcriptional activity of hypoxia stress response pathways and causes hypoxia specific cell death via the ER-stress response transcription factor ATF4.

Taken together, the here presented data suggest a novel, yet unexplored mechanism in which induction of sphingolipid stress leads to the overactivation of hypoxia stress response pathways and thereby promotes their pro-apoptotic tumor suppressor functions to specifically kill cells in hypoxic tumor areas. This study provides further insight into the survival of cancer cells in hypoxic tumor regions and proposes the inhibition of sphingomyelin metabolism as potential novel target approach in hypoxic tumor regions that could lead to the identification of novel drugs to potentiate anti-cancer therapy.

Zusammenfassung

Krebserkrankungen gehören weltweit zu den häufigsten Ursachen für Morbidität und Mortalität. Trotz neuartiger Behandlungsansätze wird die Wirkung von Krebstherapeutika häufig durch die Entwicklung von Therapieresistenzen stark vermindert. Auf Grund des schnellen Wachstums, des hohen metabolischen Verbrauchs und der mangelnden oder unzureichenden Neubildung von sauerstoffversorgenden Blutgefäßen zeigen viele Tumore starke hypoxische Regionen auf. Tumorhypoxie ist eine der Hauptursachen für Resistenzentwicklung und Therapieversagen und zählt damit zu einem wichtigen Angriffspunkt für die Krebstherapie. Die häufigsten Therapieansätze für die zielgerichtete Behandlung von hypoxischen Tumorzellen sind auf die Inhibition von Anpassungssignalwegen fokussiert, welche unter starkem Sauerstoffmangel von den Krebszellen aktiviert werden um ihr Überleben zu sichern. Die Anzahl der bisher identifizierten hypoxiespezifischen Therapeutika ist jedoch sehr gering.

Daher wurde in dieser Arbeit ein Tumorsphäroid-Model, welches Tumorregionen mit schwerer Hypoxie nachahmt, verwendet, um einen phänotypischen Screen (sog. High-Content-Screen) durchzuführen und chemische Substanzen zu identifizieren, welche spezifisch den Zelltod von hypoxischen Krebszellen induzieren. Mithilfe dieses Screeningsystems war es möglich eine Gruppe von Wirkstoffen zu identifizieren, welche ihre hypoxiespezifische Wirkung über einen neuen, bisher nicht beschriebenen Mechanismus ausüben. Zu dieser Gruppe gehört unter anderem das antipsychotische Phenothiazin-Arzneimittel Fluphenazin. Es wurde herausgefunden, dass Fluphenazin das lysosomale Enzym saure Sphingomyelinase funktionell inhibiert und durch eine starke Akkumulation von Sphingomyelin den Zelltod in hypoxischen Tumorsphäroiden hervorruft. Darüber hinaus verstärkt Fluphenazin die transkriptionelle Aktivität von hypoxischen Stressadaptionssignalwegen und bewirkt so über den ER-Stress Transkriptionsfaktor ATF4 ein hypoxiespezifisches Absterben von Krebszellen.

Zusammenfassend lässt sich aus den hier vorgestellten Daten ein neuer, bisher unerforschter Mechanismus ableiten, welcher durch die Induktion von Sphingolipidstress zur Überaktivierung von hypoxischen Stressadaptionssignalwegen führt und so ihre pro-apoptotischen Tumorsupressorfunktionen aktiviert, um spezifisch Krebszellen in hypoxischen Tumorregionen zu töten. Diese Ergebnisse liefern neue wertvolle Einblicke in das Überleben von hypoxischen Tumorzellen und identifizieren den Sphingomyelinmetabolismus als potentiellen neuen Angriffspunkt für die Krebstherapie hypoxischer Tumore, was zur Entdeckung neuer Wirkstoffe beitragen könnte.

Table of contents

1. Introduction

1.1. Trends and obstacles in cancer research and therapy

Cancer is a live threatening condition that continuous to be one of the major causes of death in the developed countries (Sudhakar, 2009, who.int, 2017). In spite of all the efforts and ground-breaking discoveries over the last century, most cancer types remain incurable. Moreover, despite the development of novel treatment strategies, cancer cells seem to find a way to adapt and evolve in response to therapy, causing resistance development and treatment failure (Yates and Campbell, 2012). The following chapters will give an overview of the milestones achieved in cancer research in the past as well as highlight future trends and challenges faced in cancer research and treatment.

1.1.1. Milestones and current trends in cancer research

The beginning to understand cancer biology

Cancer is an ancient disease and evidence shows that already the ancient Egyptians were affected by it (Sudhakar, 2009, Prates et al., 2011). Nevertheless, it was not until the end of the 19th century that researches started to understand the fundamental principles of cancer. Thus, in 1863 Rudolf Virchow was the first to identify enhanced cell proliferation in severely irritated tissue as the origin of cancer (Virchow, 1863) and in 1889 Stephen Paget proposed his “Seed and Soil”-hypothesis to explain tumor cell spreading to promote metastasis (Paget, 1889). Moreover, in 1890 David von Hansemann, and a few years later, Theodor Boveri identified the incorrect combination of chromosomes caused by aberrant cell divisions as genetic basis for cancer (von Hansemann, 1890, Boveri, 1914). Additionally, Peyton Rous discovered in 1910 that certain types of cancer can be transmitted by viral particles (Rous, 1910).

Carcinogens and gene mutations

However, it needed further ground-breaking findings, such as the discovery of the DNA structure by Watson and Crick (1953) and the deciphering of the genetic code by Nirenberg and Matthaei (1961), for these early findings to be fully appreciated in cancer biology in the second half of the 20th century. Researchers discovered that cancer can be caused not only by retroviral genes but also by inherited gene mutations as well as radiation and chemicals (Sudhakar, 2009). One of the first most prominent carcinogens identified in the 1950s was tobacco smoke (Wynder and Graham, 1950, Doll and Hill, 1956), which resulted in multiple countries in anti-smoking campaigns and eventually led

to a significant reduction of lung cancer cases (Rodu and Cole, 2002). Nowadays more than 100 carcinogens are known that induce DNA damage and thus induce gene mutations that cause cancer (monographs.iarc.fr, 2017).

Oncogenes and tumor suppressor genes

In the 1970s it was widely discussed that cancer is a disease of altered genes, which also led to the discovery of oncogenes and tumor suppressor genes (DeVita and Rosenberg, 2012). While it was shown that oncogenes such as the tyrosine-protein kinase *Src* are mutated genes that cause normal cells to grow uncontrollably (Huebner and Todaro, 1969, Oppermann et al., 1979), tumor suppressor genes like *p53* or *retinoblastoma gene* (*RB*) were discovered as genes that suppress tumorigenesis and only if rendered non-functional, for example by mutations, normal cells transform to tumor cells (Sudhakar, 2009). The discovery of oncogenes and tumor suppressor genes presented a more detailed genetic insight into the development of cancer and offered the possibility for new treatment strategies. In the early 1980s Harold Varmus and J. Michael Bishop introduced the idea of proto-oncogenes and that drugs could be designed that inactivate those cancer-causing genes (Oppermann et al., 1979, Parker et al., 1984), a treatment strategy that is nowadays known as targeted tumor therapy.

Advances in cancer diagnostics and adjuvant cancer therapy

Next to these fundamental molecular discoveries that helped to understand the origin of cancer, cancer therapy experienced major changes during this time. While radical surgery (e.g. mastectomy for breast cancer) was viewed for a long time as the best and only method to treat cancer, understanding the molecular basis of cancer development and spreading introduced new ideas and revolutionized cancer therapy. Additionally, the introduction of new diagnostic tools such as sonography, computed tomography (CT), magnetic resonance imaging (MRI) and positron emission tomography (PET) scanning in the early 1970s allowed clinicians to locate and treat the location of tumor tissue in a more precise way (Sudhakar, 2009, DeVita and Rosenberg, 2012).

Following the discovery of Sidney Farber in 1948 that the folic acid derivative aminopterin achieved a temporarily remission of childhood leukemia (Farber and Diamond, 1948), researchers investigated the use of chemicals, so called chemotherapeutics, to cure cancer. Soon adjuvant chemotherapy, e.g. with vinblastine (Cutts et al., 1960) or cisplatin (Rosenberg et al., 1969), became a common strategy to reduce the chance of metastasis after surgery (Bonadonna et al., 1976). Additionally, despite its first discovery as carcinogen, radiation therapy was increasingly used to inhibit cancer cell spreading, especially after the development of more local treatment methods in the early 1970s that

allowed a direct delivery of radiation to the tumor and spare healthy tissue (Fisher et al., 1985), such as Brachytherapy (Ward et al., 2015) or Gamma-knife radiosurgery (Leksell, 1983). These days, even more precise ways of delivering radiation therapy with less side effects on normal tissue are being developed such as nanoparticles carrying radioactive material (Mi et al., 2016) or radioprotective substances like palifermin or amifostine (Johnke et al., 2014).

Targeted - and immuno-therapy

Although the discovery of oncogenes and the idea of targeted cancer therapy were already introduced in the 1970s, it was not until 1998 that one of the first molecular-targeted drugs, called trastuzumab (Herceptin) was approved by the U. S. Food and Drug Administration (FDA). Trastuzumab is a humanized monoclonal antibody that blocks the HER2 receptor that is significantly upregulated especially in some breast cancer types (Molina et al., 2001). With the beginning of targeted therapy emerged also the field of cancer immunotherapy. The first production of monoclonal antibodies in 1975 by Köhler and Milstein (1975) paved the way to produce therapeutic antibodies for multiple different oncological targets. Besides trastuzumab several other therapeutic antibodies have been approved for cancer therapy since the turn of the millennium, for example bevacizumab (Avastin), cetuximab (Erbitux) and ipilimumab (Yervoy) (Scott et al., 2012). Immunotherapeutic antibodies can kill cancer cells via different mechanisms, such as by directly blocking a receptor or by specifically delivering a toxin or an immune cell like macrophages to the site of a tumor. Next to antibodies, further immune modulatory drugs have been developed to help the immune system to arm itself against cancer, including immune signaling molecules like interleukin-2 (Rosenberg et al., 1985) as well as vaccines like the HPV vaccine Gardasil (Harper et al., 2010) which enhance the ability of T cells to detect and destroy tumor cells.

Cancer expression profiling

With the beginning of the 21th century major scientific discoveries like the complete sequencing of the human genome (The-International-Human-Genome-Mapping-Consortium, 2001) lifted cancer research to a completely new level. The introduction of microarray technology made it possible to classify tumor types not only by their morphology but also by their genetic signature. Thus, morphologically undistinguishable tumors could be separated into different genetic subclasses (Alizadeh et al., 2000) and predictions about clinical outcome and therapy responsiveness could be made (van 't Veer et al., 2001). In addition to gene expression profiling, proteomics-based techniques

gained in importance as tool to discover novel biomarkers and therapeutic targets as well as to personalize cancer therapy (Swami, 2010).

Current trends and challenges in personalized cancer medicine

Owing to the increasing knowledge about the complexity of human tumor types, personalized cancer medicine has become an important treatment strategy these days (Dragani et al., 2016). Research fields like immunotherapy and RNA interference (RNAi), as well as new diagnostics strategies such as the analysis of circulating tumor DNA (ctDNA) or multi-omics data are gaining ground worldwide to identify the best and most effective personalized cancer therapy.

Already suggested by Paul Ehrlich at the beginning of the 1900th century (Ehrlich, 1909), immunotherapy has become one of the most advancing and promising treatment strategies these days. While the first vaccines for virus-caused tumor types such as the HPV vaccine Gardasil (Harper et al., 2010) have already been approved in the early 21th century, researches also aim to find vaccines to prevent non-viral cancers which are caused by mutations that develop and accumulate over time. However, in order to prevent tumor development at an early stage, it remains challenging to identify already small changes at the beginning of cancer to distinguish abnormal cells from healthy cells (Lohmueller et al., 2016, Gotwals et al., 2017).

Another promising strategy to study cancer and improve personalized medicine is to silence the expression of genes involved in the tumorigenic transformation of cells by RNAi (Hannon, 2002). In contrast to small molecule and antibody drugs, RNAi molecules show an extended number of possible cancer targets that have been considered undruggable (Wu et al., 2014). First clinical trials, for example using VEGF and KSP specific siRNA, have already demonstrated a high anti-cancer efficacy and a good tolerability in most patients (Davis et al., 2010). However, there are still a few challenges that need to be overcome such as the delivery of sufficient material to the site of the tumor (Wu et al., 2014), as well as potential side effects when escaping the tumor cell or when unspecifically taken up by normal cells, for example immune cells (Kanasty et al., 2012, Wu et al., 2014).

Nevertheless, in order to use these new treatment strategies as efficiently as possible, cancer diagnostics also need to improve and provide a complex and personalized profile for each patient. In recent years, research has drifted away from analyzing single datasets in an isolated way to combining all the existing data such as genomic, proteomic, transcriptional, metabolic and environmental information. This approach has been termed

multi-omics and helps to analyze complex datasets efficiently and to gain new insights in cancer research, such as novel biomarkers, and to personalize treatment (Cancer Genome Atlas, 2012)). Moreover, new diagnostics tools such as the detection of ctDNA facilitate the advances towards a more personalized cancer therapy. ctDNA molecules are fragments of cell-free nucleic acids (cfDNA) found in human blood that show mutations which are prognostic markers for cancer, such as KRAS mutations in plasma as marker for colorectal cancer (Wan et al., 2017). The comparably easy access to patient samples enables a dynamic tracking of mutations in response to treatment and thus could improve patient survival and prevent relapse (Dragani et al., 2016, Wan et al., 2017). One of the biggest challenges of ctDNA at the moment is its handling, which is only done by specialized laboratories and is owned by its short half-life of only 16 to 150 minutes (Wan et al., 2017).

Although, the high cost that come with more complex personalized cancer therapy are still a major challenge, more efficient diagnostic tools that provide more data within one assay and cheaper devices that measure health data are becoming available (Schork, 2015) and will facilitate the shift towards personalized cancer therapy. Moreover, personalized medicine has the potential to provide more efficient treatment strategies for each individual patient and, thus, could save money that is spent on inappropriate interventions (Schork, 2015).

1.1.2. Resistance development

Despite significant advances in understanding the complexity of cancer biology and in identifying novel treatment approaches, therapy resistance is still a major obstacle which significantly limits the effectiveness of various anti-cancer drugs (Housman et al., 2014). By using a diverse range of resistance mechanisms cancer cells are able to adapt and acquire new characteristics to evade the effects of an anti-cancer drug which often leads to tumor relapse weeks or months after an initial successful shrinkage. Moreover, owing to the cellular heterogeneity of most tumors, therapy-induced positive selection of a resistant minor subpopulation has become a common problem in cancer therapy (Holohan et al., 2013). Therefore, it seems to be a constant race between finding the next resistance mechanism and identifying novel and superior therapeutic approaches. Although the factors and mechanisms responsible for resistance development for molecular targeted therapy approaches are nowadays much better predictable than for systemic and broad-spectrum anti-cancer drugs, the general principles are similar (Holohan et al., 2013) and will be discussed in the following chapters. An overview of the most common resistance mechanisms is illustrated in Figure 1.

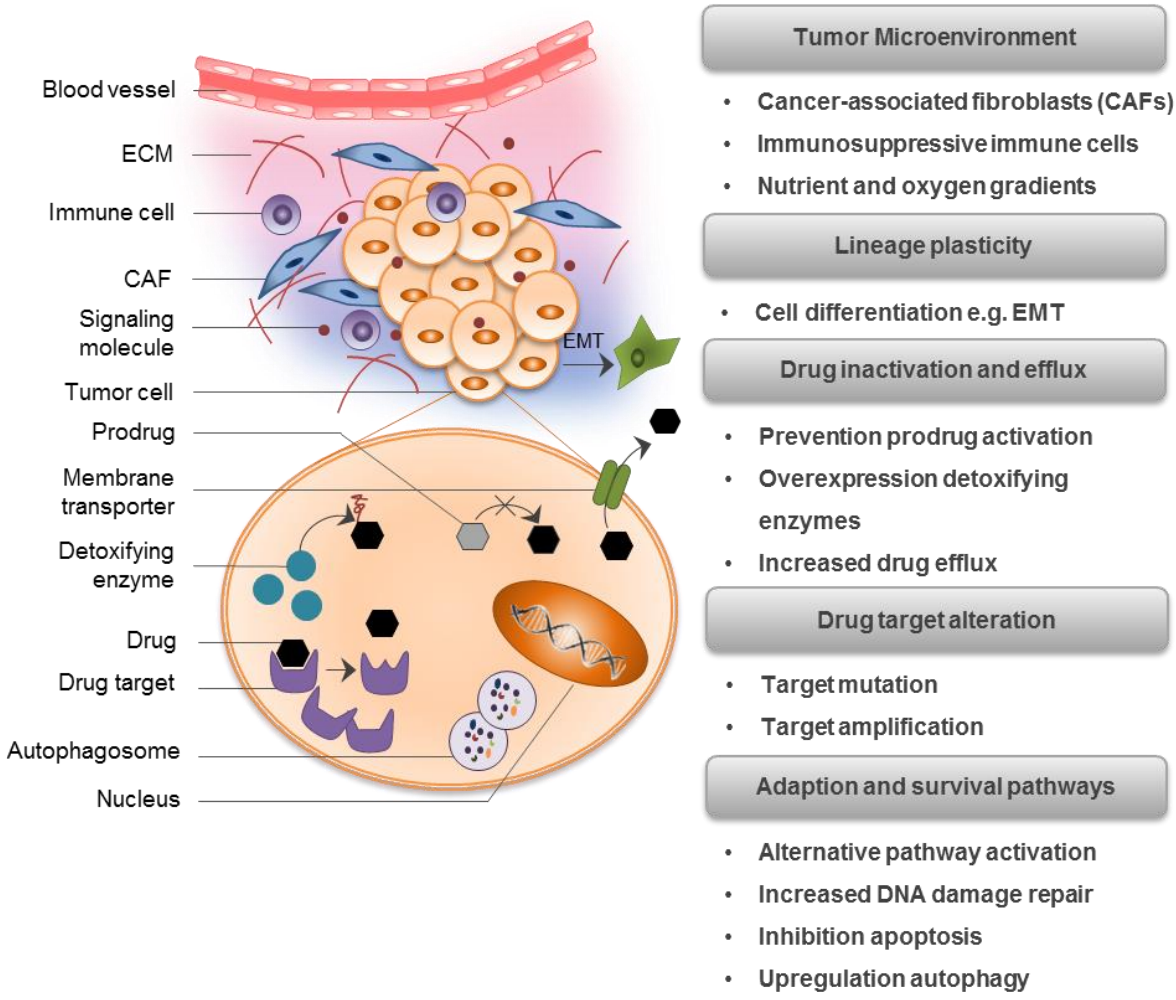

Figure 1: Overview mechanisms of cancer drug resistance. Resistance development is mediated by multiple, often overlapping, mechanisms and is significantly influenced by changes in the tumor microenvironment, such as the development of oxygen and nutrient gradients caused by an insufficient or damaged vascularization or the invasion of immunosuppressive immune cells. The activity of a drug can be limited by an increased drug efflux by membrane transporter proteins, an inactivation of the drug, an alteration or amplification of the drug target or the activation of adaption and survival pathways. Resistance may also be mediated by cell differentiation creating a cell of a different identity whose survival no longer depends on the drug target.

Drug inactivation and efflux

In order to minimize unwanted side effects on healthy tissue and to optimize tumor site specific delivery, anti-cancer prodrugs are a common strategy as they need to undergo enzymatic or chemical transformation *in vivo* before they gain their desired activity and clinical efficacy (Rautio et al., 2008, Giang et al., 2014). An example is the fluorouracil prodrug capecitabine which is converted by the enzyme thymidine phosphorylase (TP) to its active and much more toxic form 5-FU (Johnston and Kaye, 2001). Capecitabine has successfully been used as chemotherapeutic agent in various cancer types (Walko and Lindley, 2005). However, over time multiple patients developed a resistance caused by

DNA-methylation that significantly reduced the expression level of *TP* and hence prevented the transformation of capecitabine to 5-FU (Holohan et al., 2013).

In addition to preventing prodrug activation, another resistance mechanism applied by tumor cells to prevent cell death is the inactivation of reactive cancer drugs by overexpressing detoxifying enzymes like glutathione S-transferase (GST). GST reduces the reactivity of toxic compounds by linking them to the antioxidant glutathione and has been implicated in the development of resistance in multiple cancers (Townsend and Tew, 2003, Housman et al., 2014).

Moreover, not only the inactivation of anti-cancer drugs but also their enhanced efflux, which prevents drug accumulation within the cancer cell, is a well-known mechanism of drug resistance. In healthy cells efflux mechanisms are important to prevent the over-accumulation of toxins, but in cancer cells many of the membrane transporter proteins are overexpressed and promote the elimination of multiple anti-cancer compounds. Well-studied examples are ATP-binding cassette (ABC) transporter proteins like the multi-drug resistance protein 1 (MDR1) which is overexpressed in various tumors, but can also be induced by different stress conditions like chemotherapy or radiation therapy (Holohan et al., 2013, Santos and Paulo, 2013).

Drug target alteration

Especially for targeted-cancer-therapy, it is common for cancer cells to acquire resistance through gene mutations or expression changes of the drug target. Thus, for example, increased androgen receptor expression could be identified as mediator for drug resistance in prostate cancer patients receiving androgen deprivation therapy (Harris et al., 2009, Karantanos et al., 2013).

Many targeted-therapy approaches are based on the tumor-specific overexpression or mutation of a particular target such as the *epidermal growth factor receptor* (*EGFR*) which is mutated in the tyrosine kinase domain in approximately 10 % of non-small lung tumors (Pao et al., 2005). The antibody gefitinib takes advantage of this and inhibits EGFR activity in tumor cells with this mutation. However, after an early successful response most patients relapse as the tumor displays a second mutation, a so called gatekeeper mutation, which is not targeted by the drug but renders the receptor active again despite treatment (Kobayashi et al., 2005, Pao et al., 2005). Learning from examples like this, newer targeted drugs are often designed to recognize multiple mutations of a drug target (Holohan et al., 2013).

Activation of adaption and survival pathways

In other cases of resistance development, the drug-target remains unaltered but an alternative pathway is activated. For example, tumor cells resistance to EGFR targeted therapy bypass EGFR inhibition by activating downstream ERBB3/PI3K/Akt signaling through an amplification of the tyrosine-protein kinase MET (Engelman et al., 2007). In another example resistant prostate cancer cells evaded the effects of androgen receptor blockage by upregulating the glucocorticoid receptor which substitutes androgen signaling (Arora et al., 2013).

Ideally, anti-cancer drugs should result eventually in the induction of tumor cell death. However, by down-regulating apoptotic pathways and by activating distinct survival pathways cancer cells can survive. Radiation therapy and many chemotherapeutic agents are aimed to induce DNA damage that causes an accumulation of mutations which are at some point lethal to the cell. Whether the induced DNA damage is severe enough to induce apoptosis highly depends on the efficacy of DNA repair mechanisms present in a cell. Therefore, a common mechanism for resistant cancer cells to evade DNA-damage-induced cell death is to enhance their DNA repair capacity, for example by upregulating repair mechanisms like homologous recombination or nucleotide excision repair (NER) (Holohan et al., 2013, Housman et al., 2014). Thus, an overactivity of the excision repair cross-complementation group 1 (ERCC-1) protein, which plays an important role in NER-based DNA repair, has been closely linked to platinum-drug-based chemotherapy resistance (Kwon et al., 2007). For this reason, many chemotherapeutic and radiation-based treatments are nowadays combined with targeted drugs that inhibit DNA repair mechanisms (Gavande et al., 2016).

In addition to increased DNA repair, resistant cancer cells apply further methods to inactivate apoptosis, for example by overexpressing anti-apoptotic factors like B-cell lymphoma 2 (BCL-2) family proteins such as *BCL-W* or *BCL-2* (Yip and Reed, 2008, Ni Chonghaile et al., 2011). Additionally, cancer cells show an increased probability to survive anti-cancer treatment when displaying enhanced level of autophagy, an intracellular recycling process to manage stress-induced damage and to prevent apoptosis. Upregulation of autophagy is closely linked with resistance development in different malignancies and co-treatment of chemotherapeutic or targeted drugs with autophagy inhibitors like chloroquine or hydroxychloroquine has shown promising results in clinical trials (Sui et al., 2013). However, anti-autophagy treatment remains critical due to its dual function in tumor suppression and resistance development (White, 2012).

Lineage plasticity

Genetic mutations that alter the drug-target or activate adaption pathways are among the most common mechanisms of resistance development. In some cases these mutations can drive changes of an entire cellular phenotype, creating tumor cells of a different identity whose survival no longer depends on the drug target. This process of resistance development is called lineage plasticity (Mu et al., 2017). For example, prostate cancer cells that acquired a resistance to anti-androgen hormone therapy exhibited a loss-of-function mutation of the tumor suppressor genes *TP53* and *RB1* which promoted a differentiation of luminal epithelial cells to basal-like cells that did not rely on androgen signaling (Ku et al., 2017, Mu et al., 2017). Furthermore, it was shown that EGFR inhibitor resistance in hepatoma cells is mediated by epithelial-to-mesenchymal transition (EMT), a process characterized by the development of multipotent cells with increased motility and invasive capacity (Fuchs et al., 2008). EMT has also been identified as driving force for therapy resistance and increased tumor progression in multiple other tumor types, including prostate, pancreas and breast carcinomas and represents a major obstacle for anti-cancer treatment (Smith and Bhowmick, 2016).

Changes in tumor microenvironment

The tumor microenvironment (TME) has long been underestimated as extrinsic driver for resistance development but is gaining more and more attention these days. Various characteristics of the TME, such as nutrient availability, integrin and cytokine signaling of stroma cells or extracellular matrix (ECM) structures, modulate cancer cell signaling involved in drug-resistance or provide protective niches for tumor cells (Holohan et al., 2013, Barker et al., 2015, Sun, 2016).

During tumorigenesis cancer cells secrete signaling molecules that alter the host tissue stroma and provide a microenvironment that promotes growth, invasion, and metastasis. These changes include the transformation of normal fibroblast to cancer-associated fibroblasts (CAFs), which display aggressive proliferation and increased ECM and cytokine secretion characteristics and form a synergistic relationship with cancer cells that favors resistance development (Barker et al., 2015, Sun, 2016). For example, preclinical models in head and neck squamous cell carcinomas and lung cancer cells identified the close crosstalk between CAFs and cancer cells as crucial factor for resistance towards EGFR inhibition, such as by secreting matrix metalloproteinase proteins or hepatocyte growth factor molecules (Wang et al., 2009, Johansson et al., 2012).

However, not only CAFs but also immunosuppressive and tumor-permissive immune cells favor tumor progression and resistance development. Tumor associated macrophages (TAMs) cause chemoresistance in breast cancer cells by an enhanced IL-10 secretion that elevates *BCL-2* expression (Yang et al., 2015). Additionally, regulatory T cells and myeloid-derived suppressor cells (MDSCs) suppress tumor-specific immune responses by expressing high levels of suppressive cytokines like TGF-β or immune checkpoint receptors like cytotoxic T lymphocyte antigen 4 (CTLA4) (Barker et al., 2015).

Another important part of the TME is the tumor vasculature. Rapid tumor cell proliferation often results in an insufficient or disorganized vascularization, creating large gradients in oxygen and nutrient supply and promoting tumor hypoxia (Nagy et al., 2009, Rohwer and Cramer, 2011, Kyle et al., 2012, Semenza, 2014). Additionally, some anti-cancer treatments, such as irradiation, promote similar effects by causing endothelial cell death and vessel destruction (Barker et al., 2015). The lack of vasculature does not only limit the distribution of anti-cancer drugs, but also promotes metabolic adaptions and the activation of stress-response pathways in starved tumor regions, which both favor resistance development and cancer cell survival. Indeed, intratumoral hypoxia inversely correlates with clinical efficacy of cancer therapies and clinical outcome (Vaupel and Mayer, 2007, Sullivan et al., 2008, Wilson and Hay, 2011, Rebucci and Michiels, 2013, Multhoff et al., 2014). Hypoxia mediates resistance development through multiple mechanisms, including the stimulation of CAFs (Barker et al., 2015), the activation of autophagy and drug efflux (Rohwer and Cramer, 2011), the modification of DNA damage response (Bristow and Hill, 2008), as well as the reduction of cell proliferation and senescence (Sullivan et al., 2008, Rohwer and Cramer, 2011). Therefore, tumor hypoxia has emerged as promising target to treat resistance development.

1.2. Tumor hypoxia

Intratumoral hypoxia is a common feature of most solid tumors and substantially potentiates resistance development and treatment failure (Vaupel and Mayer, 2007, Sullivan et al., 2008, Rohwer and Cramer, 2011, Wilson and Hay, 2011, Rebucci and Michiels, 2013, Multhoff et al., 2014, Semenza, 2014). Moreover, hypoxic signaling is closely interlinked with several hallmarks of cancer, including neo-angiogenesis, metabolic reprogramming, invasion, metastasis and immune evasion (Kroemer and Pouyssegur, 2008, Cairns et al., 2011, Semenza, 2014, McIntyre and Harris, 2015, Chouaib et al., 2016, LaGory and Giaccia, 2016). Therefore, targeting cancer cells in hypoxic tumor areas is an important strategy for cancer treatment.

1.2.1. Hypoxic signaling mechanisms

To ensure survival under conditions of reduced oxygen accessibility, hypoxic cancer cells activate different but partially overlapping stress response pathways to adapt cellular metabolism and promote pro-survival signaling (Wilson and Hay, 2011). These include the stabilization of hypoxia-inducible transcription factors (HIF), the activation of endoplasmic reticulum (ER) stress induced unfolded protein response (UPR), as well as the inhibition of mechanistic target of rapamycin (mTOR) signaling (Figure 2) (Wouters and Koritzinsky, 2008).

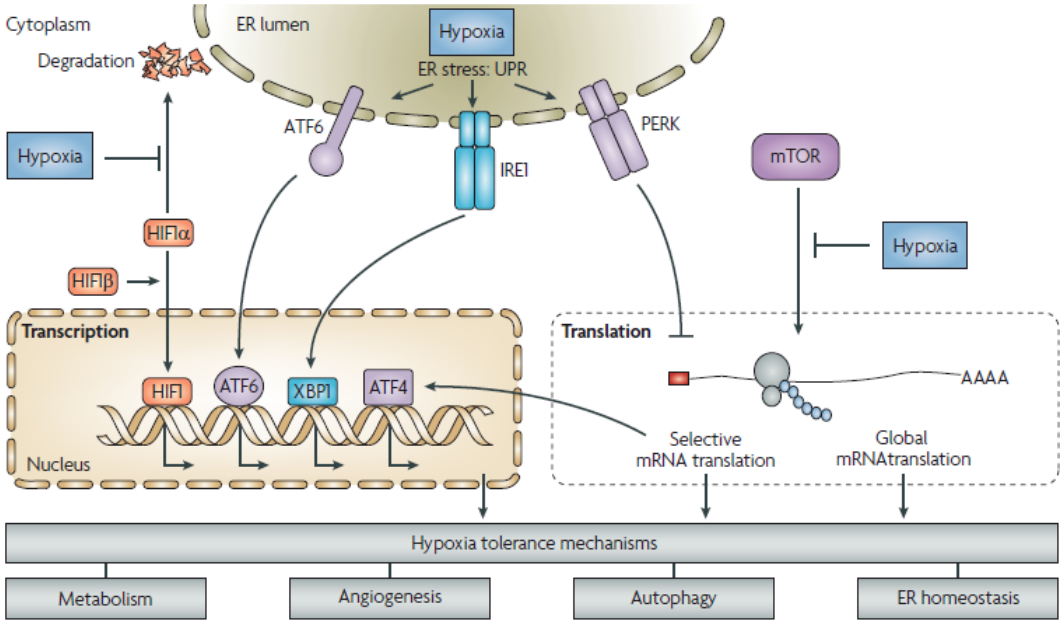

Figure 2: Cellular response pathways to low oxygen levels under hypoxic conditions. Stabilization of hypoxia-inducible transcription factors (HIF), activation of endoplasmic reticulum (ER) stress induced unfolded protein response (UPR) and inhibition of mTOR signaling are the three main response mechanisms to mediated cellular adaption to hypoxic conditions (figure taken from Wouters and Koritzinsky (2008)).

Stabilization of HIF as key regulator during hypoxia

Among these three response pathways, activation of the HIF protein family is the most extensively studied and has been identified as the master regulator of adaption to hypoxic conditions (Semenza, 2010). The HIF family consists of three members, HIF-1, HIF-2 and HIF-3, which are all heterodimeric transcription factors composed of a constitutively expressed beta subunit and an oxygen sensitive alpha subunit. Under normal oxygen conditions (normoxia) the α-subunit is constantly hydroxylated by members of the oxygen dependent Fe^{2+} containing prolyl hydroxylase domain (PHD) family which enables the recognition and ubiquitination by the von Hippel-Lindau tumor suppressor protein (VHL)-E3 ligase complex and the subsequent proteasomal degradation (Henze and Acker, 2014). Under hypoxic conditions the HIF-α unit remains unhydroxylated and translocates to the nucleus where it heterodimerizes with its β-subunit. Together with the co-activator proteins CBP and p300, this complex binds to the hypoxia responsive element (HRE) which induces the expression of many different genes to ensure cellular survival under reduced oxygen levels (Henze and Acker, 2014).

Of the three known HIF transcription factors, HIF-1 is the best characterized one, which is highly-conserved in almost all oxygen-consuming organisms and regulates the expression of multiple genes involved cell survival such as cellular metabolism (e.g. *solute carrier family 2 member 3* (*SLC2A3*)), neo-angiogenesis (e.g. *vascular endothelial growth factor A* (*VEGFA*)), as well as cell motility and invasion (e.g. *twist-related protein* (*TWIST*)) (Harris, 2002, Koh and Powis, 2012, Liu et al., 2012). In addition to pro-survival genes HIF-1 also stimulates the transcription of pro-apoptotic genes like *BCL2/ adenovirus E1B 19 kDa interacting protein 3* (*BNIP3*) or *Nix* which induce hypoxia-induced cell death (Sowter et al., 2001). Moreover, different co-regulatory pathways have been identified which fine-tune the dual role of HIF-1 to balance pro-survival and pro-apoptotic functions, including feedback mechanisms by the Cbp/p300-interacting transactivator 2 (CITED2) or the DNA-damage-inducible transcript 4 protein (DDIT4, also known as REDD1) or upregulation of translation by phosphoinositide 3-kinase (PI3K) (Henze and Acker, 2014, Masoud and Li, 2015). Owing to its pivotal role in multiple pathways that are interlinked with tumor growth and mortality, increased *HIF-1-α* expression levels have been correlated with a more aggressive cancer phenotype and poor patient prognosis after radiation and chemotherapy (Aebersold et al., 2001, Semenza, 2010, Burroughs et al., 2013).

mTOR inhibition and activation of ER stress in response to hypoxia

Severe stress conditions found in hypoxic tumor regions strongly affect protein expression and folding. This often leads to an accumulation of misfolded and non-functional proteins. In order to promote survival, hypoxic tumor cells reduce on the one hand the energy-intensive production of new proteins by inhibiting the master regulator of protein translation, mTOR. On the other hand, cancer cells activate the unfolded protein response (UPR) by three distinct ER pathways, including protein kinase R-like ER kinase (PERK), inositol-requiring protein 1 (IRE1) and activating transcription factor 6 (ATF6) (Wouters and Koritzinsky, 2008).

Similar to HIF-1 signaling these adaption pathways regulate both pro-survival and pro-apoptotic signals such as the activation of autophagy or the expression of *activating transcription factor 4* (*ATF4*), *X-box-binding protein 1* (*XBP1*), or *C/EBP homologous protein* (*CHOP*) (Rzymski and Harris, 2007, Wouters and Koritzinsky, 2008, Han et al., 2013). Therefore, mTOR and ER signaling in response to hypoxic stress are also closely correlated with tumor survival and resistance development (Giampietri et al., 2015, Corazzari et al., 2017). mTOR pathway inhibition reduces cell proliferation and is essential for tumor survival in oxygen and nutrient depleted regions to preserve energy homeostasis which drives the selection of treatment resistant cancer cells (Wouters and Koritzinsky, 2008). Furthermore, it has been shown that cancer cells strongly depend on functional UPR signaling during hypoxia. For example, the loss of *PERK* expression via gene knockdown reduces tumor growth and increases apoptosis specifically in hypoxic tumor regions (Bi et al., 2005). Additional, deletion of the IRE1 downstream effector *XBP1* impairs tumor growth and decreases survival in response to hypoxia (Romero-Ramirez et al., 2004).

1.2.2. Treatment strategies to target hypoxic tumor cells

While hypoxic signaling via the known pathways is relatively well characterized, less is known about how hypoxia response pathways interact to orchestrate different hypoxic responses and integrate other stress signals to balance pro-survival and pro-apoptotic signals (Harris, 2002, Wang and Kaufman, 2014). Furthermore, apart from the canonical hypoxia pathways, little is known about the adaptive mechanisms needed for cancer cells to survive severe hypoxia (oxygen level below 1 %) or even anoxia (complete depletion of oxygen), a condition that can be found in up to a third of tumor cells *in vivo* (Olive et al., 2002). Additionally, the development of hypoxia specific inhibitors poses the challenge of potential side effects due to the presence of low oxygen levels (between 1 and 5 %) in healthy tissue, such as in regions of the brain or in joints (Koumenis and Wouters, 2006).

Accordingly, so far there are only few drugs that act to specifically target hypoxic tumor cells (Semenza, 2012, Burroughs et al., 2013).

To date, two main treatment strategies have been applied for targeting hypoxic tumors. These include on the one hand the targeted delivery of cytotoxins by using bioreductive prodrugs and on the other hand the modulation of hypoxia-survival pathways. Although the activation of bioreductive prodrugs by enzymatic reduction is restricted to hypoxic tissue regions allowing a high selectivity, limited extravascular penetration and high cytotoxicity are the main challenges of this approach (Wilson and Hay, 2011).

Molecular targets of the second treatment strategy include proteins involved in UPR signaling, such as HSP90 or IRE1 (targeted by e.g. 17-AAG or salicaldehydes) or mTOR pathway signaling molecules like mTORC1 (targeted by e.g. temsirolimus). However, due to its strong predictive characteristics in tumor progression and patient survival, the most prominent molecular target has been HIF-1. Owing to the low druggability of HIF-1 a wide range of pharmacological strategies have been proposed, such as increasing HIF-1α degradation, reducing *HIF-1α* mRNA levels and protein synthesis, as well as decreasing HIF-1 subunit heterodimerization, DNA binding or accumulation of HIF-1 negative regulators (Wilson and Hay, 2011, Semenza, 2012, Masoud and Li, 2015). Nevertheless, to date there is no clear clinical evidence of antitumor activity due to HIF-1 inhibition and no specific HIF-1 inhibitor has been clinically approved and launched (Wilson and Hay, 2011, Burroughs et al., 2013).

1.2.3. 3D cell culture models as *in vitro* model for tumor hypoxia

One reason for the limited success rate of hypoxia and HIF-1 specific inhibitors might be the use of suboptimal *in vitro* models to mimic hypoxic conditions for compound screening and inhibitor identification. So far, most studies on HIF-1 inhibitors have applied biochemical or two-dimensional (2D) cell-based assays (Tan et al., 2005, Semenza, 2010, Masoud and Li, 2015, Hsu et al., 2016). However, due to the lack of complexity results from these assays can often only partially be translated to experimental outcomes *in vivo*. Tumor hypoxia commonly arises together with other microenvironmental adaptions such as nutrient and energy gradients that affect cellular signaling, metabolism and proliferation (Hirschhaeuser et al., 2010). Additionally, HIF-1 signaling is a complex pathway that is regulated at multiple levels, including mRNA expression by growth factors, protein stability by proteasomal degradation or transcriptional activity by co-factors or feedback pathways (Semenza, 2003, Henze and Acker, 2014, Masoud and Li, 2015).

Three-dimensional (3D) cell culture methods allow for the establishment of tissue-like structures that mimic many of these morphological and signaling complexities in an *in vitro*

setting, including physiological conditions like nutrient and oxygen depletion or the development of quiescent tumor regions. Moreover, multicellular tumor spheroids model cell-cell and cell-matrix interactions, which are important for cellular signaling, gene expression and growth, as well as their response to anti-cancer therapies (Hirschhaeuser et al., 2010, Thoma et al., 2014).

There are many different 3D cell culture techniques which can be roughly classified into scaffold-based and liquid-based systems (Thoma et al., 2014). Examples for the first group include natural ECM isolates from e.g. decellularized cancer tissue (Pinto et al., 2017), hydrogels like collagen (Jeong et al., 2016) or synthetic scaffolds such as polyethylene glycol (Girard et al., 2013). However, while most scaffold-based systems are highly specialized and customized to study the influence of extracellular and biophysical properties on tumor behavior, they are limited in their compatibility with high-throughput screening (HTS) and automated microscopy for the identification of novel cancer therapeutics (Thoma et al., 2014).

In contrast, many liquid-based systems offer various properties that are advantageous for spheroid-based cancer drug screening. These characteristics include the ability to form uniform spheroids in a HTS compatible multi-well-format with high reproducibility or the easy accessibility of spheroids, e.g. for modifications or imaging (Thoma et al., 2014, Ham et al., 2016). Scaffold-free liquid-based systems exploit the ability of cancer cells to self-organize to multicellular spheroids under conditions of limited adhesion through the formation of cell-cell contacts and ECM secretion. Examples include liquid overlay microplates with non-adherent surfaces such as an agarose coating (Wenzel et al., 2014), hanging drop cultured spheroids (Neto et al., 2015) or rotating vessel devices (Chang and Hughes-Fulford, 2009).

The variety of 3D cell culture models is vast and is constantly advancing, gaining more and more importance for the discovery of novel cancer therapies (Thoma et al., 2014). Hence, the complex nature of multicellular spheroid models may also help to identify new drug candidates that target hypoxic cancer cells in solid tumors.

1.3. Aim of this work

Resistant tumor cells are a major obstacle for cancer treatment and significantly limit the effectiveness of various anti-cancer drugs. Owing to the rapid and uncontrollable growth, many solid tumors lack a sufficient vasculature which promotes the development of oxygen depleted hypoxic tumor regions. Hypoxic adaption pathways significantly contribute to resistance development against anti-proliferative chemotherapeutics, radiotherapy and immunotherapy. Therefore, targeting cells in hypoxic tumor areas is an important strategy for cancer treatment, which, however, is limited by the availability of specific and effective drugs and physiologically-relevant *in vitro* screening models with high-throughput capability.

The aim of this work was firstly to characterize and validate *in vitro* generated multicellular spheroids as model system for tumor hypoxia and secondly to perform a small-molecule-screen to identify compounds which induce hypoxia specific cell death but do not affect the viability of cells in normoxia. For this purpose, a high-throughput and automated imaging -compatible HCT116 tumor spheroid model was established for the identification of hypoxia-sensitizing compounds. Moreover, it was aimed to create a geno- and phenotypic profile of those spheroids and compare them with *in vivo* and literature data from hypoxic tumors. Following these initial experiments, it was planned to perform a phenotypic screen on a library of known bioactive small molecules to identify hypoxia-sensitizing compounds that specifically induce cell death in hypoxic spheroid regions. Additionally, this work was aimed to classify the identified hits and elucidate their mode of action in order to better understand the adaptive mechanisms applied by tumor cells to survive severe hypoxia. This included the implementation of secondary assays using various molecular techniques, as well as the detailed characterization of the identified hits in regard to tumor metabolism, gene expression and hypoxia stress signaling.

In summary, the results of this work could provide further insight into the survival of cancer cells in hypoxic tumor regions and contribute to the development of new anti-cancer treatment strategies.

2. Materials and methods[1]

A detailed table with all materials and equipment can be found in the appendix under chapter A1 Materials.

2.1. Cell culture

All cell lines were obtained from American Type Culture Collection. HCT116, T47D, LnCap were cultured in RPMI 1640 (Gibco) supplemented with 10 % FCS (PAA Laboratories) and 1 % Penicillin/Streptomycin (P/S) (Sigma) (and 0.01 µg/ml Insulin for T47D cells (Gibco)). HCT116 cells carrying the Hypoxia-Response Element (HRE)-luciferase reporter construct (598-pGL3-Hif-RE-Luc- vector) (Ellinghaus et al., 2013) were cultured in DMEM (Gibco) supplemented with 10 % FCS, 1 % PS and 100 µg/ml Hygromycin B (Invitrogen). SUM149 and H460 were cultured in DMEM / Ham's F12 (Gibco) supplemented with 10 % FCS (PAA Laboratories) and 1 % Penicillin/Streptomycin (P/S) (Sigma). Cells were maintained at 37 °C in a 5 % CO_2 and humidified incubator. Cells were subjected to hypoxia by exposure to < 1 % O_2, 5 % CO_2 and balanced N_2 at 37 °C in an incubator chamber (C16, Labotect).

2.2. Immunohistochemistry: HCT116 tumor section

1.5 x 10^6 human colon cancer HCT116 cells were injected subcutaneously in cell medium into the left flank of female NMRI nude mice (Charles River) to establish a subcutaneous tumor. At a tumor size of an average of 100 mm^2 the animals were intravenously injected with Pimonidazole (Hypoxyprobe) according to manufactures instructions and sacrificed one hour later, the tumors were resected and fixed in 10 % formalin. The tumors were fixed in formalin for 48 h and further processed in an Autotechnicon (Leica ASP 200S), embedded in paraffin (Microm EC350-1), sliced and generated sections were transferred to object slides. Animal experiments were conducted in accordance with the German animal welfare law, approved by local authorities and in accordance with the ethical guidelines of Bayer AG.

Prior to immunostaining, slides were deparrafined using a decreasing alcohol dilution series. Afterwards heat mediated antigen retrieval was performed and unspecific binding sides reduced using Protein block (Dako). Vasculature was stained using a 1:100 dilution of anti-CD31 (ab28364)) and 1:100 fluorescent Alexa Fluor® 594 anti-

[1] The materials and methods part is adapted from Klutzny et al. (2017). The usage of verbatim passages will not be marked separately as self-citation (see declaration pre-publication of the dissertation).

rabbit secondary antibody (Jackson Immuno Research). Hypoxia was detected via bound pimonidazole adducts using a 1:100 mouse–anti-pimonidazole–FITC antibody (Hypoxyprobe, HP6-100Kit). Additionally, tissue sections were stained with Hoechst 33342 (Life Technologies) to label cell nuclei. Slides were imaged for fluorescence on the ImageXpress Micro widefield imaging system (Molecular Devices) with 10x air objective and attached CCD camera.

2.3. Spheroid generation

Spheroid generation was carried out using a modified version of the liquid overlay cultivation technique described by Wenzel et al. (2014). Briefly, 10 µl of a heated 1.5 % (w/v) agarose (in RPMI 1640, no FCS) solution was dispended by a liquid dispenser (Multidrop Combi, Thermo Fisher) into sterile 384-well clear bottom imaging plates (Greiner). For spheroid growth, a single-cell suspension was seeded into agarose-coated 384-well clear bottom plates in 40 µl culture medium using a liquid dispenser. Plates were incubated under standard cell culture conditions at 37 °C and 5 % CO_2 in humidified incubators for 4 days. To obtain spheroids with an approximate diameter of 400 µm on day 4, 300 cells were seeded per well for HCT116, 2000 cells per well for T47D, 300 cells per well for SUM149, 200 cells per well for H460 and 750 cells per well for LnCap.

2.4. Immunohistochemistry: Spheroids

3 hours prior to harvest, spheroids were incubated with 100 µM pimonidazole (Hypoxyprobe) under previous culture conditions. After 2 h pimonidazole incubation, spheroids were fixed for 1 h in 4 % PFA. Afterwards spheroids were transferred to 50 ml tubes, washed in DPBS (Dulbecco's Phosphate Buffered Saline) and equilibrated in 30 % sucrose/ 5 % glucose (w/v) DPBS solution for 1 h. Then, spheroids were transferred to cryomolds, excess DPBS solution removed and spheroids covered in Tissue-Tek OCT compound (Sakura). After equilibration, cryomolds were frozen by incubation in a mixture of dried ice and 2-Methylbutane (Sigma Aldrich). Prepared samples were cut into 5 µm sections by cryostat, mounted on SuperFrost Plus slides (Menzel-Glaser). Visualization of hypoxic areas was carried out using a mouse FITC-MAb against pimonidazole (Hypoxyprobe). Furthermore, sections were counterstained with Hoechst 33342 (Life Technologies) to stain nuclei. Slides were imaged on the ImageXpress Micro widefield imaging system (Molecular Devices) with 10x air objective and attached CCD camera.

2.5. Compound treatment

After 4 days of spheroid growth. 20 µl culture medium containing 80 nl compounds (ENZO Screen-Well ICCB Known Bioactives library (468 compounds), final compound dilution of 0.1 – 20 µM, depending on original stock concentration) were added and incubated for additional 3 days either at normal culture conditions (21 % O_2, 37 °C, 5 % CO_2) or in a hypoxic chamber (< 1 % O_2, 37 °C, 5 % CO_2). A 0.2 % DMSO solution was used as solvent control and staurosporine (Sigma-Aldrich) as general toxic control (10 µM).

Screening hits and further tool compounds (see A1 Materials) were purchased from Sigma-Aldrich, Tocris, Selleckchem or Santa Cruz Biotechnology. 1-stearoyl-2-arachidonoyl-sn-glycero-3-phosphocolin (18:0-20:4 PC) and 1-stearoyl-2-docosahexaenoyl-sn-glycerol-3-phosphocolin (18:0-22:6 PC) were purchased from Avanti lipids. All compounds, except for sphingomyelin and phosphocholines, were dissolved in DMSO (10 mM) and stored at -20 °C. Sphingomyelin and phosphocholines were dissolved in ethanol. Hypoxia mimicking agent deferoxamine mesylate (DFO, Sigma-Aldrich) was used at a final concentration of 1 mM (2D growth assays for 16-24 h).

2.6. Image acquisition and analysis of spheroids

Prior to imaging, spheroids were stained for a minimum of 2 hours by adding Hoechst 33342 (Life Technologies) as counterstain for all nuclei and SytoxGreen, as stain for dead cells (Life Technologies) at a final dilution of 1:10000 each. One image per spheroid and wavelength, focused on the spheroid center was captured by an Opera confocal spinning disc microscope system with a 4x air objective. Quantification of spheroid cell death was done with MetaXpress software (Molecular Devices) using custom written image analysis routines as described previously (Wenzel et al., 2014).

Normalization, quality control and fitting curves for EC50 determination of tested compounds were done with Genedata Screener® for high-content screening and Genedata Condoseo modules (Genedata AG). In detail, wells with no recognizable spheroid were masked and the average intensity of the dead cell signal (SytoxGreen) was normalized to the DMSO control (0 %) and the 10 µM staurosporine (100 %) control.

2.7. Real-time quantitative PCR (RT-qPCR)

Total RNA was isolated from HCT116 cells or spheroids using RNeasy Plus Mini Kit (Qiagen) and reverse-transcribed with the RevertAid H Minus First Strand cDNA Synthesis Kit (Thermo Fisher) according to manufacturer's instructions. To measure expression levels of target genes, sample concentrations were adjusted to 10 ng/µl cDNA and mixed with specific TaqMan Gene Expression Primer (Thermo Fisher) and TaqMan Fast Advanced Master Mix (Thermo Fisher). Real-time quantification was performed in quadruplicates on a MicroAmp optical 384-well reaction plate (Thermo Fisher) using a 7900 PCR machine (Applied Biosystems). Relative mRNA levels were calculated to the geometric mean of reference gene *RPL32* (encoding ribosomal protein L32).

TaqMan Primer used: RPL32 (ribosomal protein L32. Hs00851655_g1), SLC2a3 (solute carrier family 2 (facilitated glucose transporter), member 3, encoding Glut3 protein, Hs00359840_m1), VEGFA (vascular endothelial growth factor A, Hs00900055_m1), BNIP3 (BCL2/ adenovirus E1B 19 kDa interacting protein 3, Hs00969291_m1), DDIT4 (DNA-damage-inducible transcript 4, Hs01111686_g1), CITED2 (Cbp/p300-interacting transactivator 2, Hs01897804_s1), EIF2AK3 (eukaryotic translation initiation factor 2-alpha kinase 3, Hs00984006_m1), XBP1 (X-box binding protein 1, Hs00231936_m1), DDIT3 (DNA-damage-inducible transcript 3, Hs99999172_m1), (PPP1R15A (Protein phosphatase 1 regulatory subunit 15A, Hs00169585_m1), ATF4 (Activating transcription factor 4, Hs00909569_g1), HIF-1-α (Hypoxia inducible factor 1 alpha, Hs00153153_m1), EPAS1 (Endothelial PAS domain-containing protein 1, Hs01026149_m1).

2.8. DigiWest

HCT116 spheroids were incubated for 24 h under Normoxia or Hypoxia. Afterwards n > 100 spheroids were collected, lysed for 10 min with cold lysis buffer (0.5 M Tris-HCl, pH 7.4. 1.5 M NaCl, 2.5 % deoxycholic acid, 10 % NP-40, 10 mM EDTA; Merck Millipore) and proteins collected for DigiWest analysis. The NuPAGE SDS-PAGE gel system (Invitrogen) was used for protein separation and blotting. Proteins (20 µg per sample) were separated using 4-12 % Bis-Tris gels according to the manufacturer's instructions. Blotting onto PVDF membranes (Merck Millipore) was performed under standard conditions. For high content Western analysis, the DigiWest procedure was performed as previously described (Treindl et al., 2016). Briefly, proteins immobilized on the blotting membrane were biotinylated (NHS-PEG12-Biotin, Thermo Fisher) and individual sample lanes were cut into a comb-like structure (strip height 0.5 mm each,

strip width 6 mm) using an electronic cutting tool (Silhouette SD). The resulting 96 strips correspond to 96 molecular weight fractions immobilized on individual membrane strips and cover a range from 15 kDa to more than 250 kDa. To solubilize and elute proteins, the individual strips were placed in separate wells of a 96-well plate and incubated for 2 h in 10 µl elution buffer (8 M urea, 1 % Triton-X100 in 100 mM Tris-HCl, pH 9.5). After addition of 90 µl dilution buffer (5 % BSA in PBS, 0.02 % sodium azide, 0.05 % Tween-20), 96 different Neutravidin-coated Luminex bead sets (60,000 beads/well) were added to the individual wells and eluted biotinylated proteins were captured on the bead surface. After ON incubation the Luminex beads were pooled, washed and stored in storage buffer (1 % BSA, 0.05 % Tween-20, 0.05 % sodium azide in PBS) at 4°C.

For antibody incubation, an aliquot of each bead pool (approximately 0.3 % of the available bead pool) was transferred into an assay plate and 30 µl diluted western blot antibody (650 different antibodies) in assay buffer (Blocking Reagent (Sigma-Aldrich), 0.05 % Tween 20, 0.02 % sodium azide, 0.2 % milk powder) was added per well and incubated ON at 4 °C. For read-out, beads were washed twice with 100 µl PBST before species-specific fluorescently-labeled secondary antibodies (Jackson ImmunoResearch) were added in 30 µl assay buffer for 1 h. After 2 washes with 100 µl PBST a fluorescent signal was generated and measured in a FlexMAP 3D instrument (Luminex). Data generated by the Luminex instrument were analyzed using a dedicated analysis tool that visualizes the fluorescent signals as bar graphs and identifies antibody specific peaks. Each graph is composed of the 96 values derived from the 96 molecular weight fractions obtained after antibody incubation. The software tool identifies specific peaks and a molecular weight is assigned to each of the 96 fractions. After background correction, specific signal intensities are calculated as the integral of the identified peak.

2.9. Lipidomics analysis

After compound treatment for 24 h at 37 °C and 21 % O_2 (n = 3). HCT116 cells were washed twice with cold sodium chloride (0.9 %) and incubated for 15 min with 1 ml 80 % methanol at -80 °C. Subsequently, cells were harvest using a cell scraper and transferred together with the methanol into a new tube. Wells were washed once with 500 µl 80 % methanol and added into the same tube. The resulting extracts were freeze-dried and resolved in 100 µl 100 % methanol followed by a centrifugation step. Afterwards, 10 µl of these extracts were used for target metabolite profiling by using the LC-MS based AbsoluteIDQ p180 Kit (Biocrates Life Sciences AG). All samples were processed according to manufacturer instruction and measurements were

performed with a UHPLC-MS/MS System (Shimadzu UHPLC and Sciex 5500 mass spectrometer). Multivariate data analysis was carried out by using the Umetrics SIMCA-P software.

2.10. Deep Sequencing

HCT116 cells were seeded in 12 well plates and treated for 24 h with either fluphenazine (5 µM) alone or with fluphenazine + DFO (1 mM) at 37 °C and 21 % O_2 (n = 4). Total RNA of each sample was extracted using the RNeasy Plus Mini Kit (Qiagen) according to manufacturer instructions. Subsequently, the TruSeq RNA Sample Preparation Kit v2 (Illumina) was used to convert the mRNA of each sample into a library of template molecules for DNA sequencing. Briefly, poly-A containing mRNA molecules were purified using oligo-dT attached magnetic beads. This was followed by mRNA fragmentation using divalent cations and subsequent first strand (reverse transcriptase and random primers) and second strand cDNA synthesis (DNA Polymerase I and RNase H). The synthesized cDNA fragments then went through an end repair process, the addition of a single 'A' base and ligation of the adapters.

Library quality was evaluated using the Agilent DNA 1000 Chip Kit and DNA quantity was determined using the KAPA Library Quantification Kit (Kappa Biosystems) according to manufacturer instructions. All libraries were pooled and adjusted to a final concentration of 10 nM before they were sequenced according to standard protocols for the Illumina HiSeq® 2500. Briefly, using the HiSeq SBS Reagent Kit v4 the sample cDNA library was denatured, mixed with HT1 and adjusted to 18 pM. The sample library was then mixed with a PhiX Library and applied to a HiSeq v4 flow cell (Illumina) which was subsequently clustered on a cBot (Illumina) using the HiSeq v4 PE cluster Kit (Illumina) before all samples were sequenced in the HiSeq® 2500 system. On average 39 ± 6 million clusters were sequenced per sample. Reads were mapped to the human genome (version hg19) using STAR aligner (version 2.4.2) and read counts were assigned to 20776 annotated genes (gencode v19).

Statistical analysis was performed using the R statistical programming environment version 3.1.2. The standard workflow implemented in the DESeq2 (Love et al., 2014) package version 1.6.3 was employed for identifying differentially expressed genes between samples treated with DFO and FP compared to samples treated only with DFO. Genes not expressed in any sample were removed before analysis. Genes were defined as differentially expressed if they showed a fold change greater than 2 in either of the conditions and had a Benjamini-Hochberg corrected p-value smaller than 0.05. Fisher's Exact test was used to identify Hallmark gene signatures from the Molecular

Signatures Database (Subramanian et al., 2005) version 5.1 overlapping with the list of genes significantly upregulated with treatment of DFO+FP compared to treatment with DFO alone. Hallmarks with a Benjamini-Hochberg corrected p-value below 0.05 were regarded as significantly overlapping.

2.11. Western Blot

Protein levels of HIF-1-α in HCT116 under various treatment conditions were obtained via Western Blotting. Briefly, HCT116 cells were either seeded in 6 well plates (2D growth) or on 384 well agarose coated plates for spheroid formation (4 days). After overnight incubation (2D) or 4 days of spheroid growth cells were treated with the compounds (DMSO control, fluphenazine 5 µM) under different conditions (Normoxia, Hypoxia or Normoxia + 1 mM DFO). After treatment, cells or spheroids were collected, lysed for 10 min with cold lysis buffer (0.5 M Tris-HCl. pH 7.4. 1.5 M NaCl. 2.5 % deoxycholic acid. 10 % NP-40. 10 mM EDTA; Merck Millipore) containing protease and phosphatase inhibitor (Thermo Fisher). The lysate was centrifuged for 10 min at 4 °C (14000 rpm) and the supernatant collected for determining the protein content of each probe using the Pierce™BCA protein assay kit with a BSA standard (Thermo Fisher) according to the manufacturer's instructions. Proteins were separated using 4-12 % Bis-Tris gels (Invitrogen) according to the manufacturer's instructions. Afterwards, the separated proteins were transferred to nitrocellulose membranes (Life Technologies) using an iBlot gel transfer device (Life Technologies). The membranes were blocked for 1 h in 5 % milk and afterwards wash with 1x TBST-Buffer (Carl Roth).

Following the blocking procedure, blots were incubated overnight at 4 °C with the primary antibodies, anti-HIF-1-α (Abcam ab51608) 1:200 and anti-beta-actin (Sigma Aldrich A5316) 1:3000. For quantification, blots were washed with TBST and the membranes were incubated with an IRDye® 680RD-anti-mouse IgG (Licor) or an IRDye® 800CW-anti-rabbit IgG (Licor). Blots were imaged using an Odyssey® CLx Imaging System (Licor). Quantification of bands was performed using Image Studio Lite Ver. 4 (Licor).

2.12. Immunofluorescence

After formaldehyde fixation with 4 % PFA, cells were permeabilized with 0.1 % Triton-X100 (Sigma) and unspecific binding sides were blocked using 1 % BSA. Rabbit anti-ASMase (Cell Signaling Technology #3687, 1:100), mouse anti-Lamp2 (Santa Cruz Biotechnology sc-18822, 1:200) and rabbit anti- Galectin 1 (Abcam ab25138, 1:250) were used as primary antibodies and appropriate secondary antibodies conjugated with

Alexa Fluor® 488 (Jackson ImmunoResearch) were used. Cell nuclei were stained with Hoechst 33342 (Life Technologies). Images were acquired by an Opera confocal spinning disc microscope system with a 40x water objective. Quantification of antibody staining was done with MetaXpress software (Molecular Devices).

2.13. LipidTOX™ Phospholipidosis assay

To visualize phospholipid accumulation in lysosomes, the LipidTOX™ Red Phospholipidosis Detection Reagent (Invitrogen, 1:2000) was added to the cells with compound treatment according to manufactures instructions. After 24 h incubation at standard cell culture conditions Hoechst 33342 (Life Technologies) was added to the cells at a final dilution of 1:5000. Images were acquired using the ImageXpress Micro widefield imaging system (Molecular Devices) with a 40x-magnification. Quantification of phospholipid accumulation (granules per cell and/or granules intensity) was done with MetaXpress software (Molecular Devices).

2.14. Lysotracker assay

After 24 h compound treatment, LysoTracker® Red DND-99 (Invitrogen) and Hoechst 33342 (Life Technologies) were added to the cells at a final dilution of 1:2000 and 1:5000. Cells were incubated with the staining reagent for 30 min at 37 °C bevor they were imaged using the ImageXpress Micro widefield imaging system (Molecular Devices) with a 40x-magnification. Quantification of lysosomes (granules per cell and/or granules intensity) was done with MetaXpress software (Molecular Devices).

2.15. Sphingosine kinase 1 activity assay

After 6.5 h compound treatment, HCT116 cells were lysed by performing multiple freeze-thaw cycles. The lysate was centrifuged for 10 min at 4 °C (14000 rpm) and the supernatant collected for determining the protein content of each probe using the Pierce™BCA protein assay kit with a BSA standard (Thermo Fisher) according to the manufacturer's instructions. Subsequently, the activity of sphingosine kinase 1 (SphK1) was measured using the Echelon sphingosine kinase 1 activity assay kit according to manufacturer's instructions. Briefly, 20 µg per 20 µl sample were incubated for 0.5 h at 37 °C in sphingosine kinase reaction buffer containing 0.02 U/ml active SphK1, 100 µM sphingosine and 5 µM ATP. The kinase reaction was stopped by adding the luminescence attached ATP detector. Subsequently, luminescence levels were determined using a Tecan Plate reader (Tecan Trading AG). The luminescent signal is inversely correlated with the kinase activity.

2.16. Acid Sphingomyelinase assay

After 24 h compound treatment, HCT116 cells were lysed by performing multiple freeze-thaw cycles. The lysate was centrifuged for 10 min at 4 °C (14000 rpm) and the supernatant collected for determining the protein content of each probe using the Pierce™BCA protein assay kit with a BSA standard (Thermo Fisher) according to the manufacturer's instructions. Subsequently, the activity of acid sphingomyelinase (ASMase) was measured using the Echelon Acid Sphingomyelinase Assay Kit according to the manufacturer's instructions. Briefly, 20 µg per 20 µl sample or diluted standards were added to a 96 well plate and mixed with 30 µl substrate buffer. Afterwards, 50 µl diluted fluorogenic ASMase specific substrate were added and the plate was incubated at 37 °C for 3 h with shaking before it was further diluted and incubated for 10 min with 50 µl stop buffer. Subsequently, fluorescence levels were determined using a Tecan Plate reader (Tecan Trading AG).

2.17. BODIPY® FL C12-Sphingomyelin

To visualize cellular sphingomyelin uptake and localization, the fluorescent reagent BODIPY® FL C12-Sphingomyelin (Thermo Fisher, 1 mM) was added to the cells with compound treatment. After 24 h incubation at standard cell culture conditions Hoechst 33342 (Life Technologies) was added to the cells at a final dilution of 1:5000. Additionally lysosomes were stained using LysoTracker® Red DND-99 (Thermo Fisher, 1:2000). Images were acquired by an Opera confocal spinning disc microscope system with a 40x water objective.

2.18. Hypoxia-Response Element (HRE)-Luciferase reporter assay

To study HIF signaling, a HCT116 reporter cell line was used which is transfected with a 598-pGL3-HIF-RE-Luc reporter plasmid that contains a luciferase gene expressed under the control of a VEGF promoter-derived hypoxia response element (HRE) (Ellinghaus. 2013). Cells were selected using 100 µg/ml Hygromycin B (Invitrogen). Luciferase activity was measured using the luminescence kit Steady-Glo® (Promega) and a luminescence plate reader (PHERAstar (BMG Labtech)) according to manufacturer's instructions. Briefly, HCT 116-HRE-Luc cells were plated at 3000 cells/5µl in white 384 well small volume plates (Greiner) using a liquid dispenser (Multidrop Combi, Thermo Scientific), 5 µl compounds were added and cells were either incubated in a normal incubator or in a hypoxia chamber at > 1 % O_2 for 16 to 24 h. 5 µl SteadyGlo (Promega) were then added to cells and incubated for 30 min in the dark. Subsequently, luminescence intensity was measured in a plate reader.

2.19. siRNA and shRNA transfection

siRNA: To generate ATF4 or ASMase knockdown cells, HCT116 cells were incubated with either ATF4 siRNA (Thermo Fisher s1703, 10 nM) or SMPD1 (ASMase encoding gene) siRNA (Dharmacon, ON-TARGETplus siRNA J006676-05 and J-006676-07, 10 nM) and Lipofectamine RNAiMAX (Thermo Fisher, 1:1000 in Opti-MEM (Gibco)) lipid or control (lipid only) in agarose coated 384 well plates and grown as spheroids for 3 days at 37 °C and 21 % O_2 (see Spheroid generation). To generate CITED2 knockdown cells, HCT116-HRE-Luc cells were incubated for 72 h with CITED2 siRNA (Thermo Fisher 114594, 10 nM) and Lipofectamine RNAiMAX (Thermo Fisher, 1:1000 in Opti-MEM (Gibco)) lipid or control (lipid only) in 384 well plates at 37 °C and 21 % O_2.

shRNA: To generate ATF4, HIF-1-α and EPAS1 knockdown cells, HCT116 cells were stably transfected with shRNA (Sigma Aldrich, TRCN0000013574, TRCN0000318674 and TRCN0000003803). Cells were selected using 0.6 µg/ml Puromycin (Sigma Aldrich) and subsequently grown to spheroids in agarose coated 384 well plates for 4 days at 37 °C and 21 % O_2.

2.20. Statistical analysis

For statistical analysis the Prism Scientific Presentation Software (GraphPad Software) was used. Values were compared by applying a two-tailed t-test with Welch's correction. The statistical significance between two levels is represented in stars (* = p-value between 0.01 and 0.05. ** = p-value between 0.001 and 0.01. *** = p-value between 0.0001 and 0.001 and **** = p-value smaller 0.0001). Error bars in graphs represent standard deviations (SD).

3. Results[1]

3.1. Evaluation of tumor spheroids as *in vitro* model for tumor hypoxia

The development of nutrient and oxygen gradients is a common feature of most solid tumors and significantly contributes to treatment failure. *In vitro* generated tumor spheroids mimic many aspects of the tumor microenvironment and represent an opportunity to discover novel therapeutic targets in hypoxic and nutrient depleted tumor regions. Therefore, it was aimed to characterize and evaluate multicellular spheroids as model system for tumor hypoxia and to establish a screening compatible system to identify small molecules that specifically target hypoxic cancer cells.

3.1.1. Tumor spheroid model for high-throughput screening

In order to generate spheroids for phenotypic high-throughput-screening (HTS), certain requirements need to be met, including the cost-effective generation of multiple uniform spheroids with reproducible morphology and composition that enables the comparison of different treatments. Additionally, the compatibility with multi-well plate formats (384- or 1536- well microplates), as well as an easy accessibility of spheroids for medium, compound or staining solution addition and automated imaging is a necessary prerequisite. To meet these criteria, the scaffold-free liquid overlay technique described by Wenzel et al. (2014) was used to generate multicellular spheroids in agarose coated 384-well microplates (a detailed description can be found under 2.3 Spheroid generation and 2.6 Image acquisition and analysis of spheroids). The basic principle of this method is visualized in Figure 3.

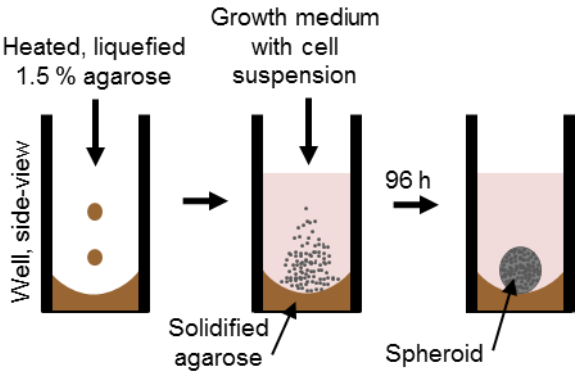

Figure 3: Principle scaffold-free liquid overlay- based generation of tumor spheroids. Imaging-compatible 384-well plates are coated with heated medium containing 1.5 % agarose using an automated dispensing system. After agarose solidification, tumor cells are seeded on top of the non-adherent agarose surface and one tumor spheroid per well is formed over a period of 96 h (adapted from Wenzel et al. (2014)).

[1] Results shown in this chapter are partially adapted from Klutzny et al. (2017). The usage of verbatim passages will not be marked separately as self-citation (see declaration pre-publication of the dissertation).

This setup led to the formation of one spheroid per well with high intra-well and intra-plate reproducibility (Figure 4). The generated multi-well spheroid plates can directly be used to assess compound effects by automated imaging and high-content based analysis without a transfer of spheroids. Tumor spheroids formed from a cell suspension of HCT116 colon cancer cells are characterized by a uniform size and shape and consist of viable cells. Moreover, when treating the cells with the general cytotoxic small molecule inhibitor staurosporine, the spheroids display an equal and reproducible cell death staining throughout the spheroid (Figure 4). Similar results were also obtained with other cell lines of different tissue origin, such as T47D (breast cancer), SUM149 (breast cancer), H460 (lung cancer) or LnCap (prostate cancer), (see Supplementary Figure 1).

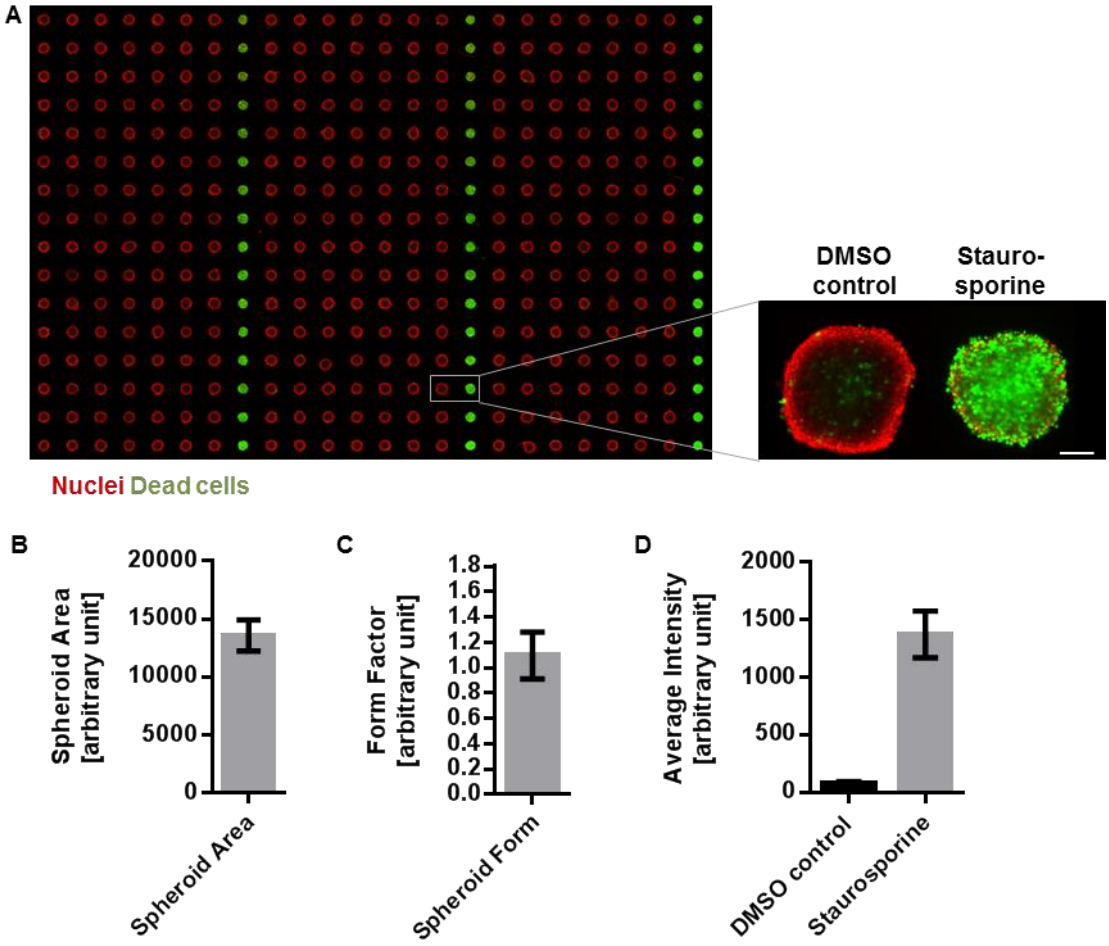

Figure 4: Tumor spheroid generation from single cell suspension in agarose-covered 384-well plates allows spheroid formation with high intra-well and intra-plate reproducibility. Single cell suspension of HCT116 cells was seeded in agarose-covered 384-well plates. Cells were incubated for 4 days to form spheroids, followed by 3 days incubation with either DMSO control (solvent control) or 10 µM staurosporine (cell death control). After 7 days spheroids were stained with Hoechst (red) and dead cells were stained with SytoxGreen (green). A) Overview 384-well spheroid plate. Scale bar 100 µm. B) Average spheroid area (n > 300, DMSO control). C) Average spheroid shape (n > 300, DMSO control), Form factor = ratio of spheroid length to its breadth (1 = round, 0 = unshapely). D) Average SytoxGreen cell death staining (n > 30). Bars show mean with SD. (adapted from Klutzny et al. (2017))

3.1.2. Characterization of tumor spheroids as *in vitro* model for tumor hypoxia

Owing to the fast growth of cancer cells and lagging neo-angiogenesis, large regions of a tumor can become hypoxic, especially parts located distal to supplying blood vessels (Wilson and Hay, 2011, Kyle et al., 2012). Indeed, this can also been seen in an *in vivo* tumor model of HCT116 colon cancer cells. Figure 5 A shows the distribution of hypoxic areas in HCT116 xenograft sections which were stained for the exogenous hypoxia marker pimonidazole (Hypoxyprobe), CD31 (a marker for blood vessels) and the nuclear marker Hoechst. Intensity profiling (Figure 5 B) shows that hypoxic regions increase with growing distance from supplying blood vessels.

In tumor spheroids this is mimicked by the increasing distance from surrounding medium. Accordingly, tumor spheroids or tissue discs show oxygen, nutrient and energy gradients from outer to inner spheroid regions and proliferation mainly occurs in the well-perfused outer regions (Kyle et al., 2012, Wenzel et al., 2014). In order to identify compounds that specifically target cells in hypoxic or anoxic tumor regions, it was aimed to establish conditions of severe hypoxia in HCT116 colon cancer tumor spheroids. Cryosections from HCT116 tumor spheroids cultured for 3 days under normoxic conditions show pimonidazole staining in the core region of the spheroid. This region expands to the outer spheroid cell layer in spheroids that were cultured for 3 days in hypoxic conditions (< 1 % oxygen), (Figure 5 C and hypoxia profile in Figure 5 D).

In tumor tissue, hypoxic gradients develop by cellular respiration of intervening cells and promote the development of hypoxic regions in cells distal from oxygen-supplying blood vessels (Kyle et al., 2012). Accordingly, pimonidazole staining of hypoxic regions in HCT116 tumor spheroids is diminished after addition of an inhibitor of cellular respiration (Figure 5 C and D), indicating that hypoxic gradients in spheroids are also established by cellular oxygen consumption.

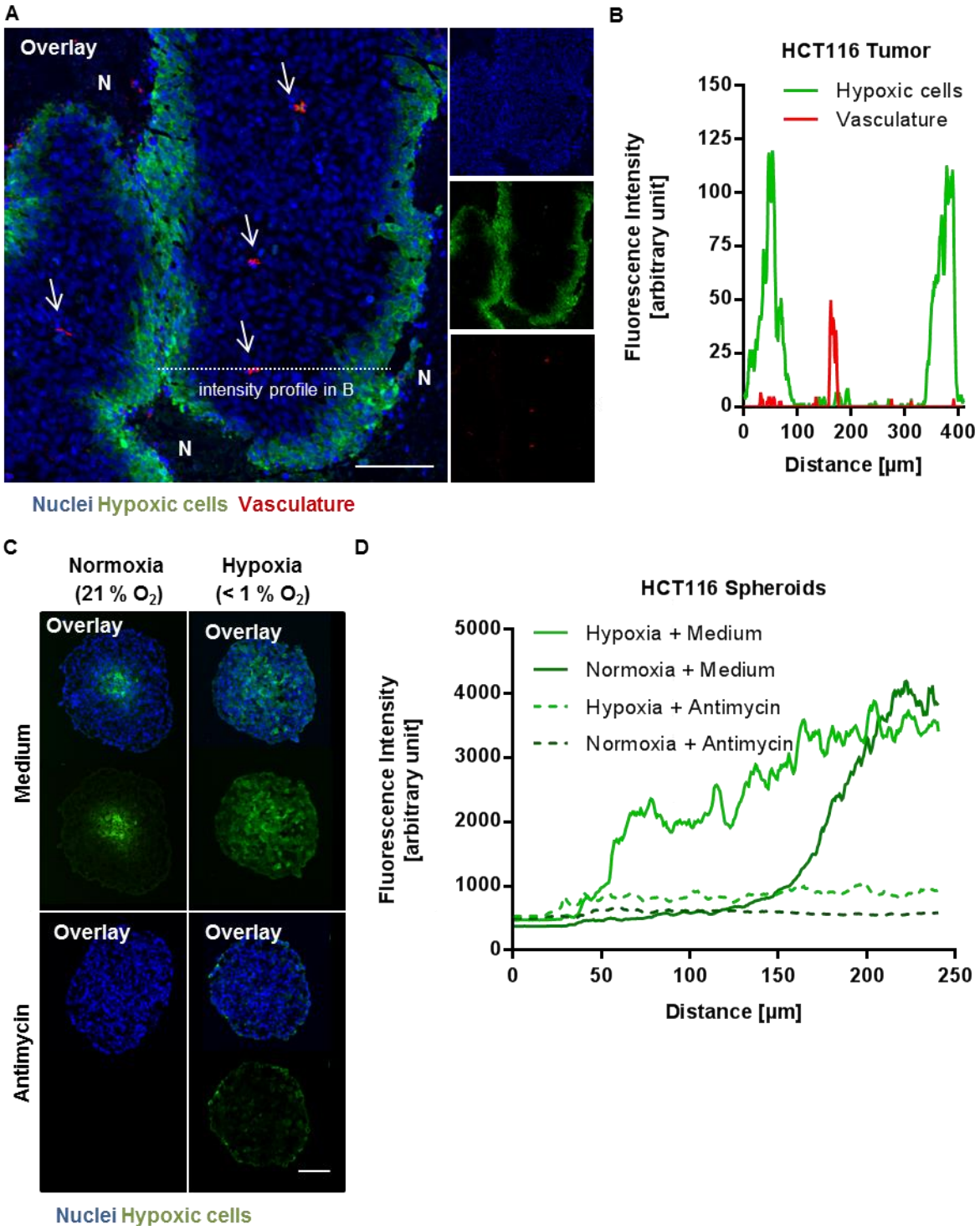

Figure 5: HCT116 spheroids incubated under reduced oxygen level mimic hypoxic tumor regions distal from blood vessels in HCT116 xenografts. A) IHC staining of HCT116 colon cancer xenograft tumor sections. Green: exogenous hypoxia marker pimonidazole (Hypoxyprobe), Red: vascular marker CD31, Blue: nuclear marker Hoechst. Arrows indicating blood vessels. N = Necrotic region. Dashed line: region for measuring intensity profile in B. Scale bar 100 µm. B) Line scan through HCT116 tumor section showing intensity profile of pimonidazole and CD31 staining. C) Cryosections of HCT116 spheroids. Spheroids were treated for 3 days in normoxia or hypoxia with or without the complex III inhibitor antimycin (200 nM). Nuclei were stained by Hoechst (blue) and hypoxic areas with anti-pimonidazole (green). Scale bar 100 µm. D) Intensity profile pimonidazole staining (n ≥ 5 spheroids) from spheroid border to spheroid core region. (adapted from Klutzny et al. (2017))

Additionally supporting the use of spheroids cultured under hypoxia as model system for hypoxic tumor regions, HIF-1-α, which is specifically stabilized in hypoxic conditions (Semenza, 2014), shows a strong accumulation in tumor spheroids cultured under severe hypoxia (< 1 % oxygen) while it is only faintly detected in normoxic conditions (Figure 6 A). Moreover, mRNA expression of hypoxia-induced stress response pathway genes, such as HIF-1 target genes (Figure 6 B) or UPR-induced genes (Figure 6 C) are upregulated in tumor spheroids cultured under hypoxia as compared to spheroids cultured under normoxia.

To further investigate the changes in HCT116 spheroids in response to severe hypoxia, a protein expression profile of over 600 proteins or protein modifications was created by quantitative Western blotting (DigiWest). In addition to a transcriptional upregulation of HIF-1 and UPR-signaling, hypoxic tumor spheroids show an accumulation of proteins involved in various other cellular survival pathways such as chromatin regulation and DNA damage response, as well as the regulation of translation and cell cycle checkpoint proteins (for a complete list of all upregulated proteins see Supplementary Table 1). Moreover, multiple proteins involved in mitogen-activated protein kinase (MAPK) signaling were found to be upregulated in tumor spheroids incubated under severe hypoxia (Supplementary Table 1). The MAPK pathway regulates various fundamental cellular processes, such as growth and apoptosis, in response to cellular stress (Zhang and Liu, 2002).

Taken together, these data show that HCT116 tumor spheroids cultured in reduced oxygen conditions are strongly hypoxic and activate hypoxia adaption pathways. Thus, they represent a suitable model system for the identification of compounds that target tumor hypoxia or anoxia.

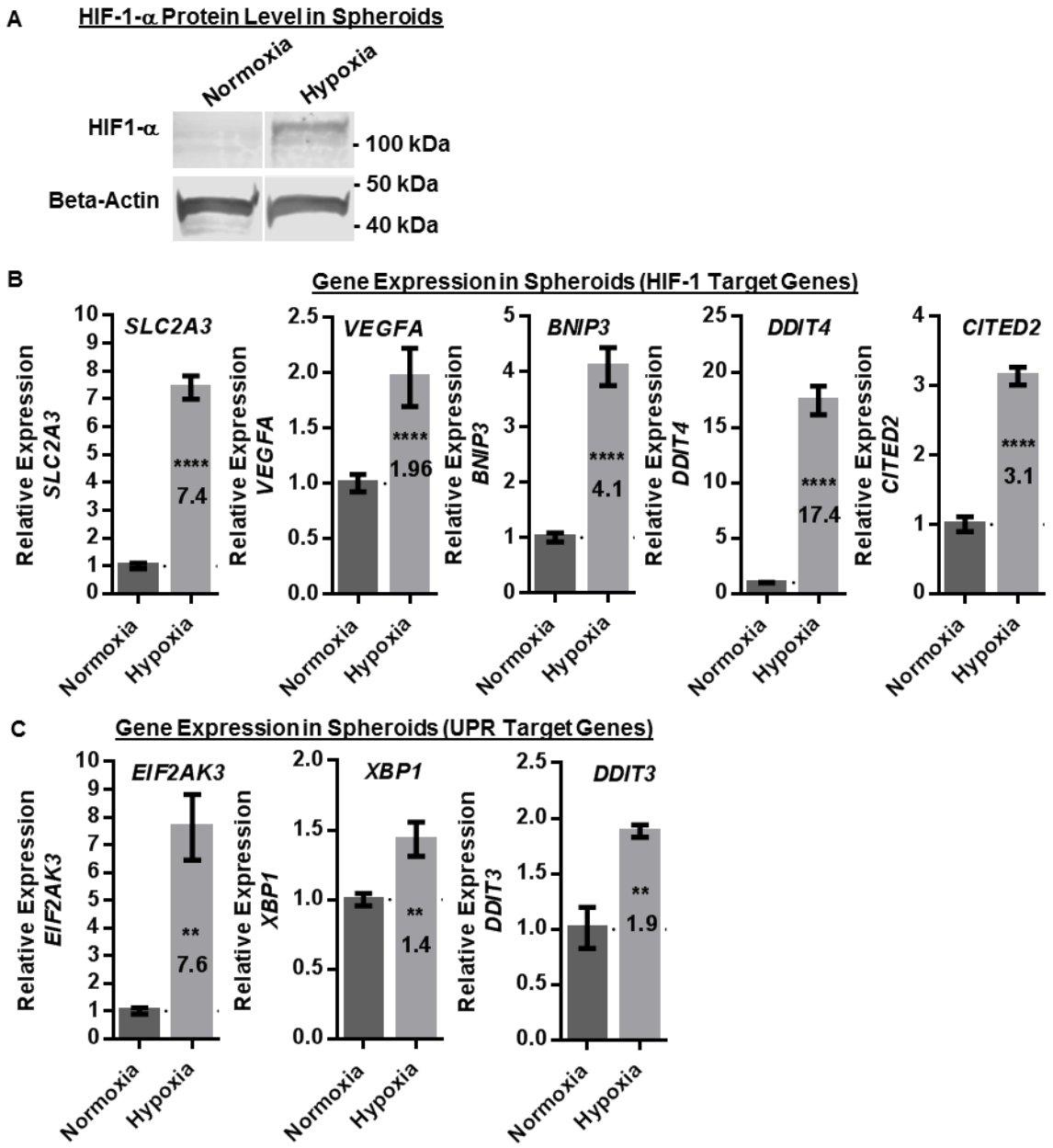

Figure 6: Tumor cells under severe hypoxic conditions in HCT116 tumor spheroids significantly upregulate hypoxia-dependent stress-response pathways. A) Western blot analysis of HIF-1-α protein expression in HCT116 spheroids incubated for 24 h in normoxia or hypoxia. Beta-Actin was used as internal control. Representative data of multiple experiments shown (n = 3). B-C) RT-qPCR gene expression analysis of B – HIF-1 target genes and C – UPR target genes in HCT116 spheroids incubated for 24 h in normoxia or hypoxia. Ct values of each sample were normalized with the internal control *RPL32* and normalized to the normoxia sample. Bars show mean with SD (n = 3). **** p-value < 0.0001, ** p-value < 0.01. (adapted from Klutzny et al. (2017))

3.2. Screen for the identification of compounds that induce hypoxia specific cell death

In order to identify hypoxia specific small molecule inhibitors, it was hypothesized that targeting hypoxia adaption pathways necessary for cellular survival should induce cell death in HCT116 tumor spheroids incubated under severe hypoxia (< 1 % oxygen), while showing less or no effect in spheroids cultured under normoxia. Therefore, the established HTS- and imaging-compatible 384-well spheroid plates were used to screen a drug library of known bioactive substances on HCT116 spheroids cultured under hypoxia or normoxia (n = 4 per compound). The general screening workflow is illustrated in Figure 7 and described in detail under 2.3, 2.5, 2.6.

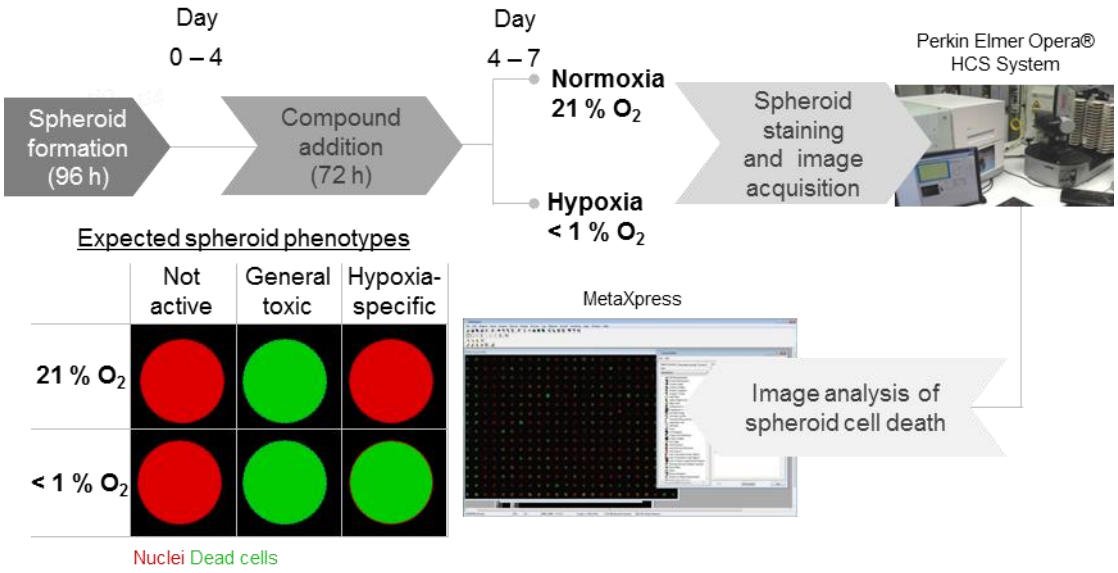

Figure 7: Screening workflow for the identification of compounds that induce hypoxia specific cell death. After spheroid generating in agarose-coated 384-well imaging plates, tumor spheroids are incubated with compounds for 72 h under hypoxia (< 1 % oxygen) or normoxia (21 % oxygen). Spheroid nuclei and dead cells are stained and spheroids are subjected to automatic imaging and subsequent image analysis to determine the spheroid phenotype.

From 468 tested compounds 43 induced a significant increase in staining for cell death under hypoxia (at least 50 % intensity of dead cell staining (dashed line in Figure 8) normalized to DMSO (0 %) and 10 µM staurosporine general cell death control (100 %)). For 16 of these compounds cell death staining (normalized to controls) was significantly stronger under hypoxia compared to spheroids cultured under normoxia (red dots in Figure 8). The pilot screen performance was characterized by a robust RZ`factor of 0.65, indicating excellent assay quality.

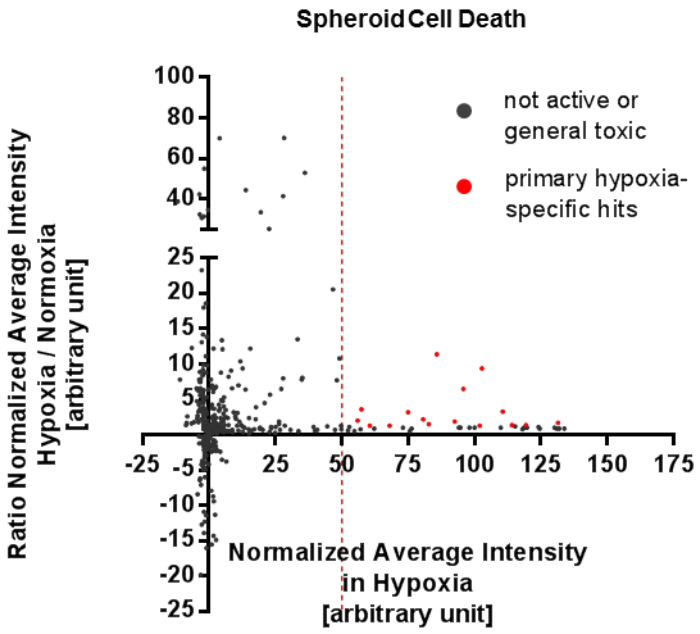

Figure 8: Scatter plot visualization of screened compounds. Normalized average intensity of cell death staining (n = 2-4, values normalized to DMSO (0) and 10 µM staurosporine (100)). Dashed line indicates threshold used for primary hit determination. Primary hypoxia-specific hits marked in red show at least 50 % increased cell death staining under hypoxia with significant higher values than under normoxic conditions.

All primary hits were retested and further validated by EC50 determination under hypoxic and normoxic conditions. 9 of the 16 hit compounds could be confirmed as hypoxia specific, showing concentration dependent cell death induction under hypoxia and no effects or effects only at significantly higher concentrations under normoxia (Table 1). Representative images of HCT116 spheroids treated with controls (DMSO or staurosporine) or trifluoperazine, the most potent hypoxia specific hit identified, are shown in Figure 9. To exclude cell-line specific effects, all confirmed hits were additionally profiled in T47D breast cancer tumor spheroids and showed similar effects (Supplementary Table 2).

Taken together, from 468 compounds of a known bioactives library, 9 compounds could be identified as hypoxia-sensitizing compounds, showing an increase in cell death staining specifically when incubated with tumor spheroids under hypoxia.

Table 1: EC50 generation of hypoxia specific hits in hypoxic and normoxic 3D tumor spheroids.
HCT116 spheroids were treated for 72 h in normoxic or hypoxic conditions. Dead cells were stained with SytoxGreen and fluorescent intensities in spheroids were measured. Values were normalized with DMSO control (0) and 10 µM staurosporine cell death control (100). EC50 values were determined in n≥3 experiments. (adapted from Klutzny et al. (2017))

Compound	**Proposed Mode of Action** (ENZO Screen-Well ICCB Known Bioactives library information)	**EC50 (cell death) in tumor spheroids [M]**	
		Hypoxia < 1% O_2	**Normoxia 21 % O_2**
Trifluoperazine	Dopamine receptor antagonist	**1.35E-06** (SD 7.2E-07)	> 1E-05
E6 berbamine	Calmodulin inhibitor	**2.09E-06** (SD 3.4E-07)	9.04E-06 (SD 9.4E-07)
Wiskostatin	N-WASP inhibitor	**2.16E-06** (SD 1.2E-07)	> 1E-05
Latrunculin B	Actin polymerization inhibitor	**2.67E-06** (SD 1.2E-06)	> 1E-05
ML9	MLCK inhibitor	**2.79E-06** (SD 2.0E-06)	> 1E-05
GF-109203X	PKC inhibitor	**3.39E-06** (SD 7.9E-07)	1.00E-05 (SD 1.5E-13)
Tamoxifen	Estrogen receptor antagonist	**3.44E-06** (SD 2.5E-06)	> 1E-05
ML7	MLCK inhibitor	**3.92E-06** (SD 1.6E-06)	> 1E-05
Cytochalasin B	Inhibitor of F actin capper	**5.67E-06** (SD 2.3E-06)	> 1E-05

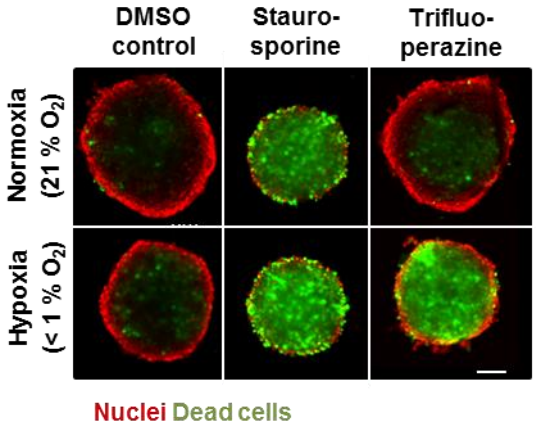

Figure 9: High-content screen on HCT116 spheroids identifies hypoxia-specific compounds. HCT116 spheroids were treated for 3 days in normoxic and hypoxic conditions with either DMSO control, 10 µM staurosporine (general cell death control) or 5 µM trifluoperazine. Spheroid nuclei were stained with Hoechst (red) and dead cells were stained with SytoxGreen (green). Representative images of multiple experiments shown (n≥3). Scale bar 100 µm. (adapted from Klutzny et al. (2017))

3.3. Mode of action identification of hypoxia specific hits

An advantage of phenotypic screening approaches is the unbiased identification of new drug candidates without prior knowledge of the drug-target. Moreover, phenotypic screens have the potential to identify novel targets which have not been described for a specific disease indication before (Swinney and Anthony, 2011). In order to better understand the adaptive mechanisms needed for cancer cells to survive severe hypoxia and to potentially identify novel targets for the treatment of hypoxic tumor regions, the next part of this work was aimed to elucidate the mode of action (MOA) of the identified hypoxia-specific hits.

3.3.1. GLUT or glycolysis inhibition induces hypoxia specific cell death

A major characteristic of cellular hypoxia is the repression of the respiratory chain, which forces cells to switch from cellular respiration to glycolysis for energy production. Therefore, it might be speculated that the identified hypoxia specific hits act by sensitizing cells to hypoxia by preventing glucose uptake or inhibiting glycolysis. Indeed, similar hypoxia specific effects could be observed when incubating HCT116 spheroids in medium with reduced glucose levels or with a known glycolysis inhibitor (2-Deoxy-D-glucose (2-DG)) (Figure 10).

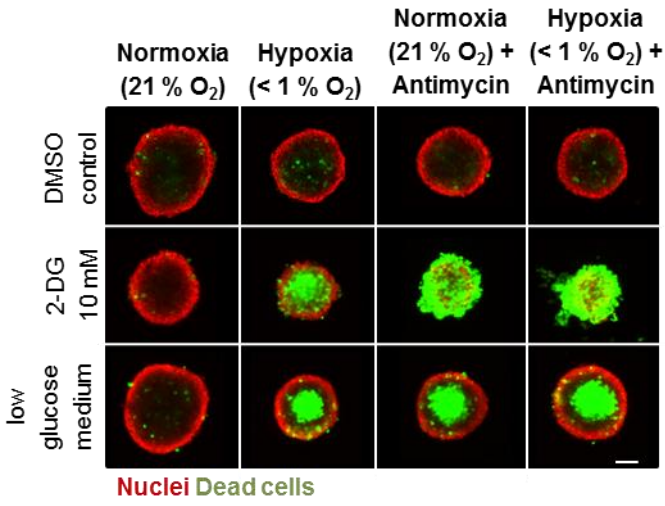

Figure 10: Glycolysis inhibition induces hypoxia specific cell death and induces synthetic lethality in normoxic spheroids when co-incubated with a respiratory chain inhibitor. HCT116 spheroids were treated for 3 days either in normoxia, hypoxia, normoxia + antimycin (200 nM) or hypoxia + antimycin (200 nM). For incubation with low glucose medium, spheroids were grown in normal culture medium, which was replaced after 4 days with medium without glucose. Spheroid nuclei were stained with Hoechst (red) and dead cells were stained with SytoxGreen (green). Representative images of multiple experiments shown (n≥3). Scale bar 100 µm. (adapted from Klutzny et al. (2017))

In order to determine hit compounds with a similar MOA, all hits were tested under normoxia in co-incubation with a respiratory chain inhibitor (Complex III inhibitor antimycin). Respiratory chain inhibition renders cells dependent on glycolysis for energy production and survival and co-incubation with a glucose transport (GLUT) or glycolysis inhibitor leads to synthetic lethality also under normoxia ((Ulanovskaya et al., 2011), see also Figure 10). Hence, similar to low glucose medium or 2-DG, only hypoxia-specific hits which act by interfering with glycolysis should increase cell death staining in normoxic tumor spheroids.

Two compounds from the hit list, cytochalasin B and E6 berbamine, showed synthetic lethality on HCT116 spheroids cultured under normoxia when incubated with antimycin (Figure 11 and Figure 12). While showing no or only minimal induction of cell death in normoxic spheroids, both compounds display a concentration dependent increase of cell death after antimycin addition (EC50 see Figure 11). Indeed, cytochalasin B is a long-known glucose transport (GLUT) inhibitor (Deves and Krupka, 1978), and hence confirms the initial hypothesis that cancer cells can be sensitized to cell death in hypoxic conditions by interfering with glycolysis.

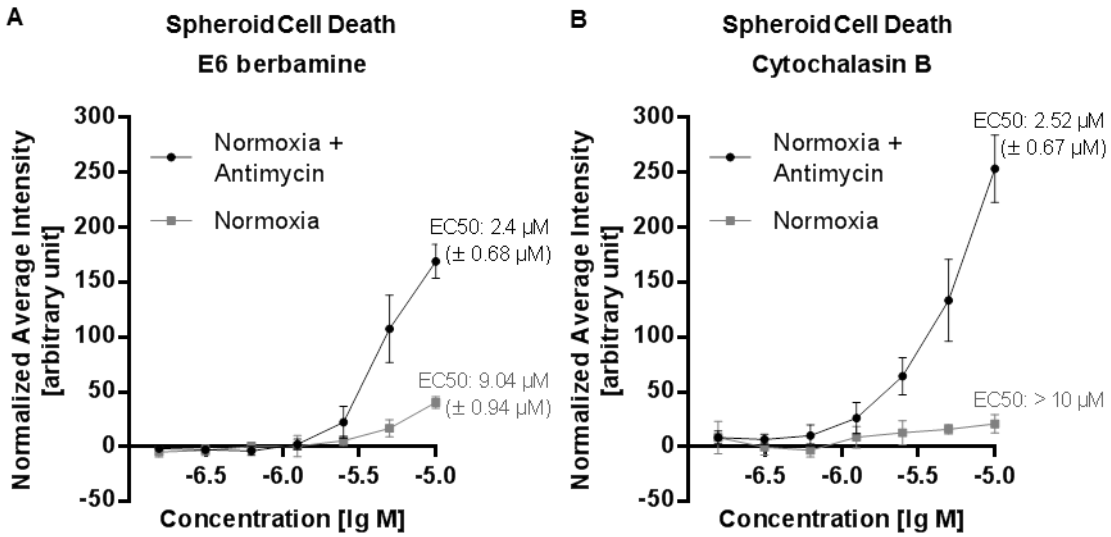

Figure 11: EC50 generation of E6 berbamine (A) and cytochalasin B (B) in normoxic tumor spheroids without or with a respiratory chain inhibitor. HCT116 spheroids were treated for 3 days either in normoxia or normoxia + antimycin (200 nM). Dead cells were stained with SytoxGreen and fluorescent intensities in spheroids were measured. Values were normalized with DMSO control (0) and 10 µM staurosporine cell death control (100). EC50 values were determined in n≥3 experiments. Graphs show mean with SD.

Taken together, these data indicate that limiting glucose supply or inhibition of glycolysis could be a treatment option to kill cancer cells in hypoxic tumor areas that are dependent on glycolysis for energy production. Nevertheless, a detailed analysis of GLUT inhibitors

for cancer therapy is covered elsewhere (Pelicano et al., 2006, Granchi et al., 2014, Barron et al., 2016) and this work concentrated on the remaining hits with a different and potential novel MOA.

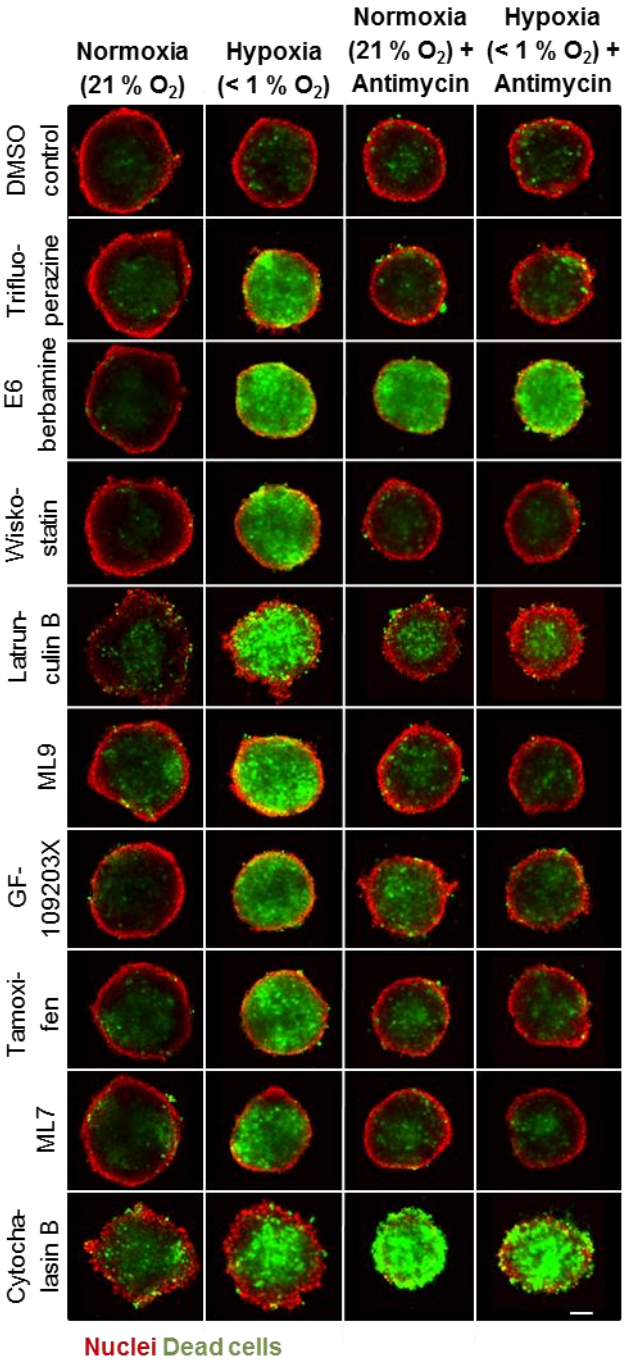

Figure 12: Co-incubation with a respiratory chain inhibitor identifies two hit compounds (E6 berbamine and cytochalasin B) that act via glycolysis inhibition. HCT116 spheroids were treated (5 µM compound) for 3 days either in normoxia, hypoxia, normoxia + antimycin (200 nM) or hypoxia + antimycin (200 nM). Spheroid nuclei were stained with Hoechst (red) and dead cells were stained with SytoxGreen (green). Representative images of multiple experiments shown (n≥3). Scale bar 100 µm. (adapted from Klutzny et al. (2017))

3.3.2. Hypoxia-selective and 3D specific hits act independent of their reported mode of action

Seven of the identified hits displayed a phenotype different from GLUT or Glycolysis inhibitors, showing no synthetic lethality in tumor spheroids when co-incubated with the respiratory chain inhibitor antimycin under normoxia (Figure 12). Strikingly, under hypoxic culture conditions co-incubation with antimycin almost completely prevented the induction of tumor spheroid cell death by these hit compounds (Figure 12). Therefore, it was speculated that these hits display a potential novel MOA to induce cell death specifically in hypoxic tumor spheroid regions.

Spheroids better mimic the physiological conditions and interactions found in a tumor than standard 2D cell culture conditions. In order to determine whether the MOA of the remaining hypoxia specific hit compounds is dependent on conditions found only in a complex 3D environment, HCT116 cells were also treated under 2D cell culture conditions (Table 2). While four compounds were highly specific for hypoxic tumor spheroids (colored in green), three hits, including Wiskostatin, Latrunculin B and GF-109203X, induced cell death or proliferation inhibition also in hypoxic or normoxic 2D culture conditions. Interestingly, also the two identified GLUT/glycolysis inhibitors, E6 berbamine and cytochalasin B, significantly affected cell numbers in 2D conditions (Table 2). Hence, for all following experiments only 3D cell culture specific hits with a potential novel MOA were further evaluated in the following studies. A summarizing hit classification is illustrated in Figure 13.

Table 2: EC50 generation of hypoxia specific hits under 2D cell culture conditions. HCT116 cells were treated for 72 h in normoxic or hypoxic conditions. Nuclei were stained with Hoechst and cell counts were determined by automated image analysis and normalized with DMSO control (0). EC50 values were determined in n≥3 experiments. 3D cell culture specific hits are colored in green. (adapted from Klutzny et al. (2017))

Compound	EC50 (cell count) in 2D in [M]	
	Hypoxia < 1 % O_2	Normoxia 21 % O_2
Trifluoperazine	> 1E-05	> 1E-05
E6 berbamine	2.83E-06 (SD 4.7E-07)	5.85E-06 (SD 9.2E-08)
Wiskostatin	4.77E-06 (SD 7.5E-07)	6.71E-06 (SD 3.3E-06)
Latrunculin B	8.82E-07 (SD 5.2E-07)	1.11E-06 (SD 2.1E-07)
ML9	> 1E-05	> 1E-05
GF-109203X	5.80E-06 (SD 2.1E-06)	7.32E-06 (SD 9.5E-07)
Tamoxifen	> 1E-05	> 1E-05
ML7	> 1E-05	> 1E-05
Cytochalasin B	1.94E-06 (SD 7.9E-08)	1.61E-06 (SD 1.8E-07)

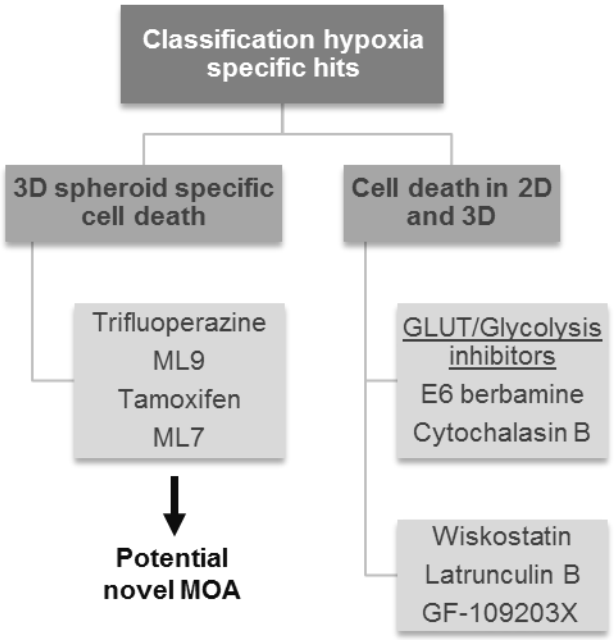

Figure 13: Classification of hypoxia specific hits.

The most potent compound of this novel class of hypoxia-selective and 3D specific hits is trifluoperazine (see Table 1), an antipsychotic of the phenothiazine class, compounds which are known to inhibit dopamine receptors (Seeman et al., 1997). However, while other phenothiazines such as fluphenazine, chlorpromazine or thioridazine showed similar hypoxia and 3D spheroid specific effects other structurally unrelated antipsychotics with activity against dopamine receptors, such as haloperidol, pimozide or fluspirilene (Galizzi et al., 1986, Fox et al., 1994, Karolewicz et al., 1996) showed no hypoxia specific effects (Figure 14 A). Therefore, it was speculated that these compounds specifically kill cells in hypoxic or anoxic tumor spheroid regions not via dopamine receptor inhibition but through a different MOA.

In addition to dopamine receptor inhibition, phenothiazines like trifluoperazine or fluphenazine have also been reported as calmodulin-inhibiting drugs (Weiss et al., 1980, Silver and Stull, 1983, Vandonselaar et al., 1994). Interestingly, the other three hit compounds, tamoxifen, ML7 and ML9, also affect calcium-calmodulin (Ca^{2+}-CaM) dependent signaling (Lopes et al., 1990, Matsumura et al., 1999). Moreover, Ca^{2+}-CaM dependent regulation of various protein kinases and phosphatases has been closely interlinked with hypoxia and HIF-1 stress signaling (Beitner-Johnson et al., 1998, Yuan et al., 2005, Hui et al., 2006, Jung et al., 2010). Thus, it was validated whether the hypoxia specific MOA of the remaining hits is mediated by interfering with cellular calcium and/or CaM signaling. However, neither the addition of other known CaM antagonists, such as W7 or ophiobolin A, nor the increase (e.g. by Ca2+ channel blockage) or decrease (e.g.

by Ca2+ chelation) of intracellular calcium levels showed similar hypoxia specific effects in HCT116 tumor spheroids (Figure 14 B).

In conclusion, since neither dopamine receptor- nor CaM-inhibition seem to be the pivotal MOA responsible for hypoxia specific induction of tumor spheroid cell death, it was hypothesized that the identified compounds act independently of their known biological function.

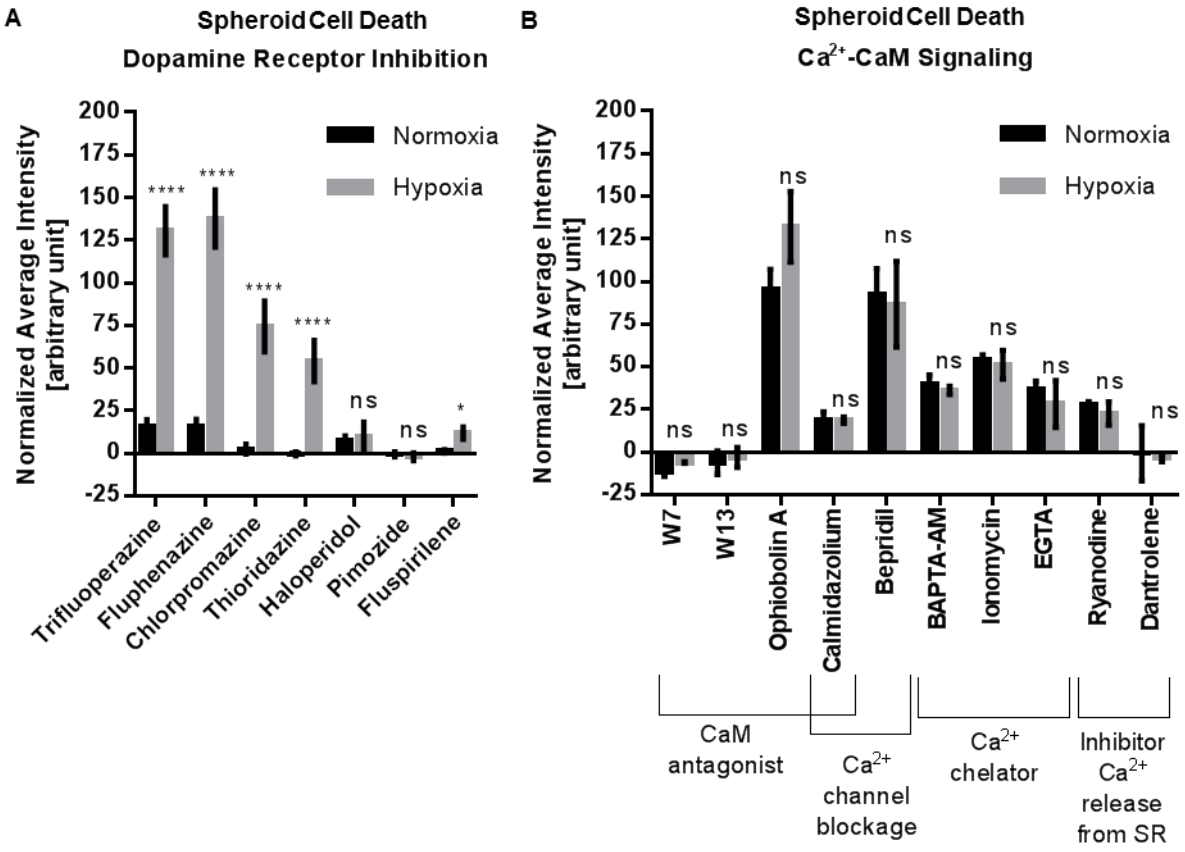

Figure 14: Hypoxia-selective and 3D specific hits act independent of their reported mode of action.
HCT116 spheroids were treated for 3 days either in normoxia or hypoxia with A) different dopamine receptor inhibitors (10 µM) and B) different Ca^{2+}-CaM modulating compounds (10 µM). Dead cells were stained with SytoxGreen and fluorescent intensities in spheroids were measured. Values were normalized with DMSO control (0) and 10 µM staurosporine cell death control (100). Bars show mean with SD (n ≥ 3). Statistical difference between normoxia and hypoxia was determined for each compound, **** p-value < 0.0001, * p-value < 0.05, ns – not significant.

3.3.3. The role of lysosomal sphingolipid metabolism in hypoxia specific tumor spheroid cell death

Fluphenazine impairs lysosomal function

The pharmacological effect of a drug is greatly influenced by its physicochemical properties. They affect not only how well a compound interacts with its target(s) but also its transport and processing within a tissue. Therefore, looking at the physicochemical characteristics of a compound can give valuable indications about characteristics and a potential MOA of a drug (Imming et al., 2006).

Interestingly, many of the identified hits show similar chemical properties, including a hydrophobic ring structure and a hydrophilic side chain with one or more charged cationic amine groups (Figure 15).

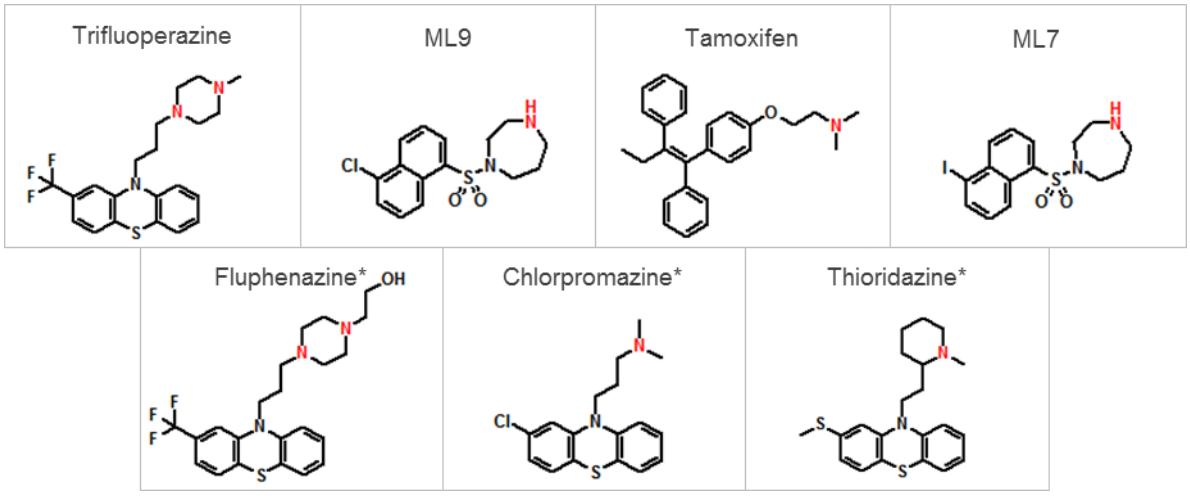

Figure 15: Chemical structure of hypoxia-selective and 3D specific hits. Red = basic center. * phenothiazine hit expansion. (adapted from Klutzny et al. (2017))

Based on these chemical groups, the compounds can be characterized as “cationic amphiphilic” drugs (CAD) (Halliwell, 1997). CADs can accumulate in lysosomes, can cause lysosomal stress and lysosome dysfunction and lysosome membrane permeabilization (LMP), (Petersen et al., 2013, Beckmann et al., 2014, Ellegaard et al., 2016), and have been associated with the induction of phospholipidosis (Halliwell, 1997, Petersen et al., 2013, Shayman and Abe, 2013). Accordingly, most identified hypoxia-sensitizing hits or compound classes have been reported as lysosomotropic or phospholipidosis inducing substances (Altan et al., 1999, Kasahara et al., 2006, Nadanaciva et al., 2011, Muehlbacher et al., 2012, Kondratskyi et al., 2014). Owing to the described similarities of hypoxia sensitizing compounds, further experiments were concentrated on fluphenazine as one of the most potent compounds with high hypoxia-

specificity in spheroids (EC50 1.63 µM under hypoxia, > 10 µM under normoxia, > 10 µM under normoxia/hypoxia + antimycin, no effect on 2D cell culture).

Because of its chemical characterization as CAD, the impact of fluphenazine treatment on lysosomes and lysosomal functions was investigated. By Lamp2 antibody staining, a lysosomal associated protein which lines the inner surface of the lysosomes, it was found that fluphenazine leads to an aggregation of lysosomes in HCT116 cells (Figure 16 A). Accordingly, fluphenazine treatment resulted in a dose-dependent accumulation of acidic vesicles in HCT116 cells as seen by Lysotracker staining at an EC50 of 3.8 µM (SD 360 nM), (Figure 16 B).

Lysosomes are a major site of cellular phospholipid metabolism. Lysosomal stress or damage induced by CADs can induce phospholipidosis, the accumulation of phospholipids in cells and tissue (Halliwell, 1997, Shayman and Abe, 2013). To test the effect of fluphenazine on lysosome functionality, the accumulation of lipids was measured using the LipidTOX™ phospholipidosis detection kit. Fluphenazine led to a dose-dependent accumulation (EC50 of 2.74 µM, SD 710 nM) of fluorescent phospholipids in HCT116 cells (Figure 16 C). Similar results were obtained for trifluoperazine, ML9, tamoxifen and ML7 (Supplementary Figure 2).

Taken together, these data indicate that fluphenazine impairs lysosomal functionality at similar concentrations required for induction of cell death in hypoxic spheroids.

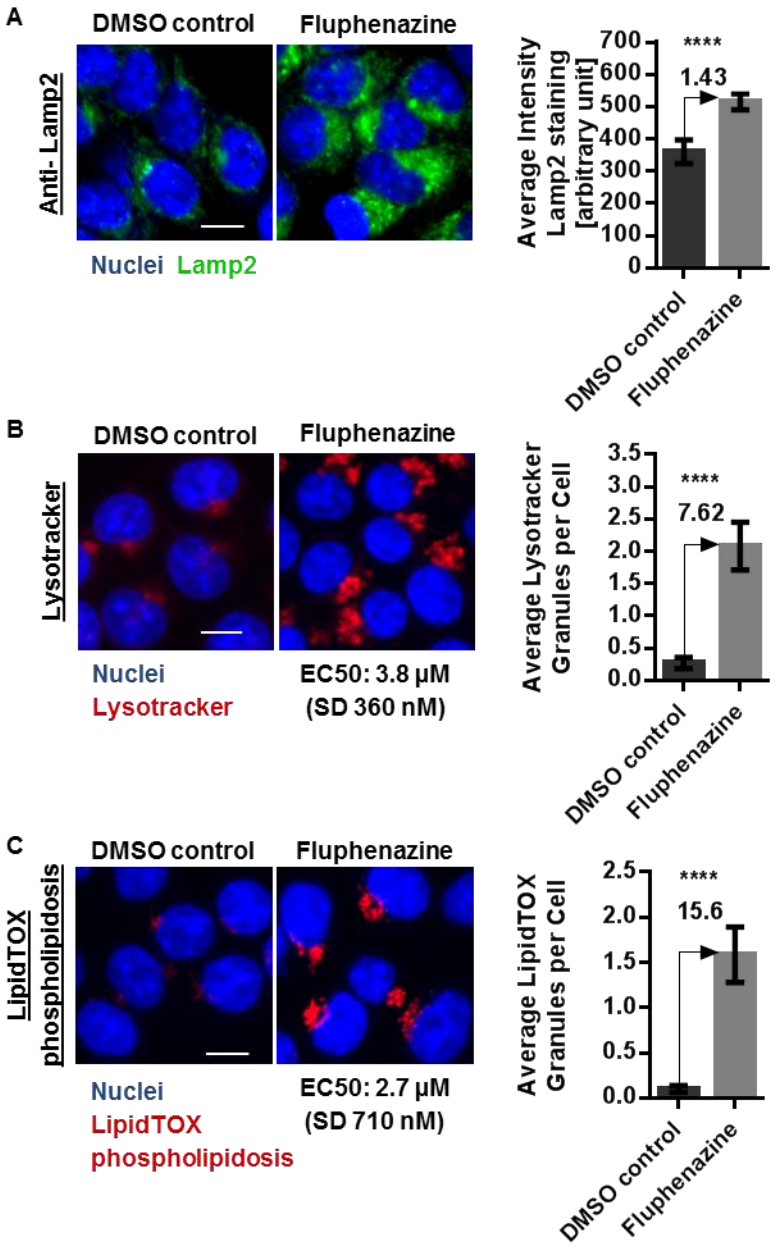

Figure 16: Fluphenazine impairs lysosomal function. HCT116 cells were treated for 24 h with either DMSO control or 5 µM fluphenazine. Cells were either stained for A) lysosome marker Lamp2 B) for acidic vesicles using Lysotracker or C) for the accumulation of undigested phospholipids using the LipidTOX phospholipidosis staining. Nuclei were stained with Hoechst. Representative images of multiple experiments shown (n = 3). Scale bar 10 µm. Quantification of stainings shown on right hand side. Bars show mean with SD (n = 3). **** p-value < 0.0001. (adapted from Klutzny et al. (2017))

Fluphenazine alters cellular lipid composition and functionally inhibits acid sphingomyelinase

To further investigate the observed effects on lysosomal metabolism, the metabolic signature of 188 metabolites, including several different lipids, was profiled by mass spectrometry of fluphenazine treated cells (overview see Supplementary Figure 3). Fluphenazine treatment led to a strong accumulation of lipids of the sphingolipid metabolism such as sphingomyelins (SM), phosphatidylcholines (PC) and lysophosphatidylcholines (lysoPC) (Figure 17).

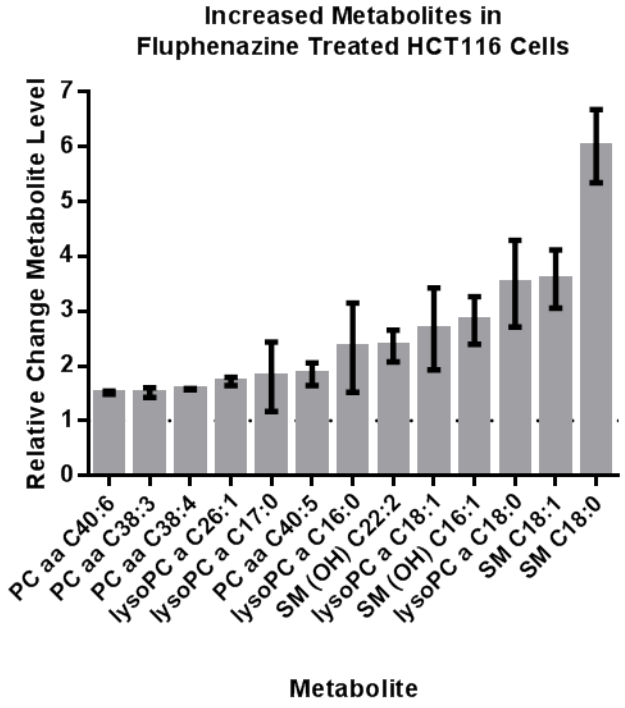

Figure 17: Fluphenazine alters cellular lipid composition. Metabolomics analysis of 188 endogenous metabolites identifies the accumulation of sphingomyelins in fluphenazine treated cells. For full profile see Supplementary Figure 3. HCT116 cells treated for 24 h with 5 µM fluphenazine (compared to DMSO control). Bars show mean with SD (n = 2, 4 replicates per experiment). PC: phosphatidylcholine, lysoPC: lysophosphatidylcholine, SM: sphingomyelin. (adapted from Klutzny et al. (2017))

Next to the ER, lysosomes are a primary side for sphingolipid metabolism. Complex sphingolipids are degraded to ceramide and subsequently to sphingosine which is phosphorylated in the cytoplasm by sphingosine kinases (SphKs) to sphingosine-1-phosphate (S1P). S1P is an important signaling molecule that regulates a broad variety of cellular functions such as proliferation, survival, migration, invasion or differentiation, and thus has been implicated in the development of different tumor types (Kunkel et al., 2013). Moreover, increasing evidence suggests S1P signaling as important mediator of cellular adaption to hypoxia (Ader et al., 2009). Indeed, blocking phosphorylation of sphingosine by SphK-1 inhibition induced hypoxia specific cell death in HCT116 tumor spheroids

(Figure 18 A). However, the induction of cancer cell death in hypoxic spheroids was much weaker with the two SphK-1 inhibitors PF-543 and SKI-II than with the endogenous metabolite of sphingosine N-N-Dimethylsphingosine (DMS) or with fluphenazine. Additionally, it was tested if medium supplementation with exogenous S1P could prevent cell death in fluphenazine treated spheroids (Figure 18 B). Only a minimal reduction of cell death staining could be observed in co-incubated hypoxic spheroids and cell death induction by fluphenazine remained significantly stronger in hypoxic conditions compared to normoxic conditions. Nevertheless, to further validate SphK as potential molecular target of fluphenazine, the activity of SphK-1 in fluphenazine treated cells was measured (Figure 18 C). Compared to the known SphK-1 inhibitor PF-543, fluphenazine did not affect SphK-1 enzyme activities.

In conclusion, although SphK-1 might be a potential therapeutic target in hypoxic tumors, these results do not indicate SphK-1 inhibition as molecular MOA of fluphenazine.

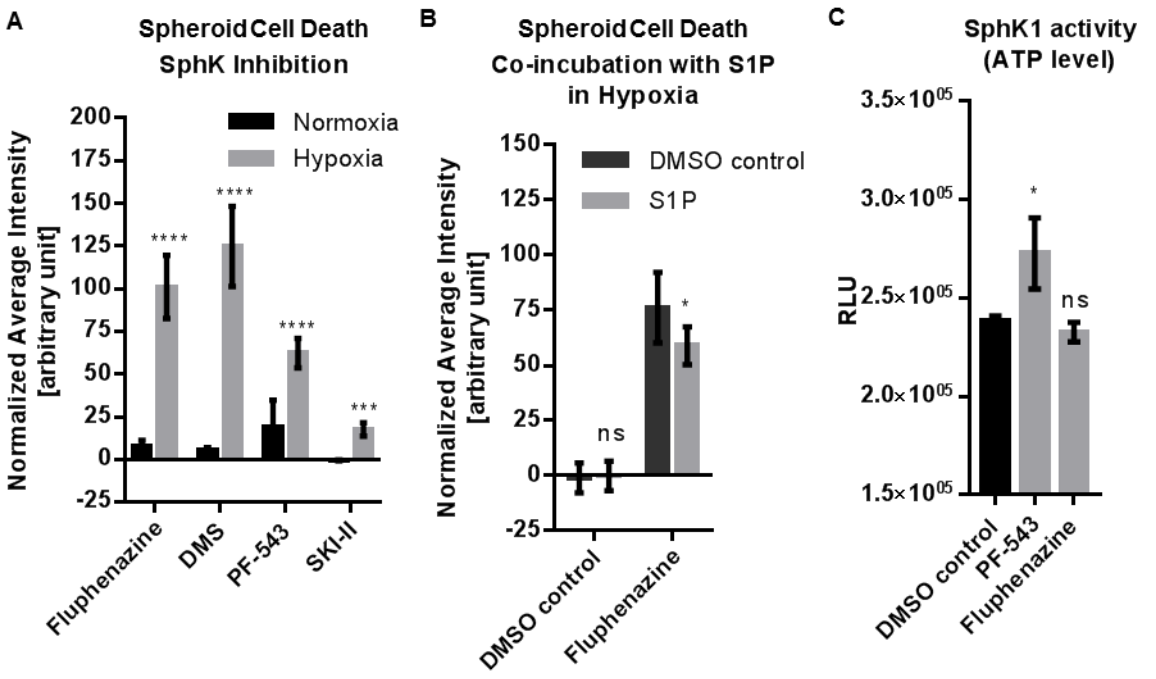

Figure 18: Fluphenazine does not affect SphK activity. A and B) HCT116 spheroids were treated for 3 days either with DMSO control, 10 µM staurosporine control, 5 µM fluphenazine or A) different SphK inhibitors (10 µM N-N-Dimethylsphingosine (DMS), 10 µM PF-543 or 20 µM SKI-II) under normoxia or hypoxia or B) co-treated with 20 µM S1P under hypoxia. Dead cells were stained with SytoxGreen and fluorescent intensities in spheroids were measured. Values were normalized with DMSO control (0) and staurosporine cell death control (100). Bars show mean with SD (n = 3). Statistical difference between A) normoxia and hypoxia or B) DMSO control and S1P treated spheroids was determined, **** p-value < 0.0001, *** p-value < 0.001, * p-value < 0.05, ns – not significant. C) SphK1 activity in HCT116 cells treated for 6.5 h with either DMSO control, 10 µM PF-543 or 5 µM fluphenazine. ATP consumption by SphK1 was measured by luminescence measurements. Luminescent signal (ATP level) inversely correlates with kinase activity. Bars show mean with SD (n = 3). * p-value < 0.05, ns – not significant.

It was speculated that cell death in hypoxic spheroids could be a consequence of accumulated lipids of the sphingolipid metabolism, such as SM, PC or ceramide. Indeed, multiple SMs and PCs were increased after fluphenazine treatment (Figure 17) and ceramide has been implicated as a potent pro-apoptotic bioactive lipid (Galadari et al., 2015). In order to test if hypoxia-specific cell death in spheroids could be a consequence of cellular sphingolipid accumulation, tumor spheroids were incubated with different concentrations of exogenously added SM, PC or ceramide under hypoxic and normoxic conditions. While, exogenous addition of N-Palmitoyl-D-Sphingomyelin (SM (18:1/ 16)) or SM mixture from bovine brain led to the induction of cell death in hypoxic, but not normoxic spheroids, the addition of different phosphocholines or ceramide showed no effect on cell death (Figure 19 A). Additionally, similar to fluphenazine treatment, co-treatment of sphingomyelin with a respiratory chain inhibitor led to a rescue of cell death induction in tumor spheroids (Figure 19 B). Therefore, it was speculated that hypoxia-specific induction of cell death in spheroids is caused by cellular SM accumulation. Supporting this hypothesis, exogenously added fluorescent SM showed a strong lysosomal accumulation after fluphenazine treatment (Figure 19 C).

SMs are a major component of cellular lipid membranes. In lysosomes they are converted to ceramide and phosphocholine by the lysosomal enzyme acid sphingomyelinase (ASMase). Therefore, it was tested if fluphenazine could increase SM level by interfering with ASMase function. Indeed, cell extracts of HCT116 cells treated for 24 h with fluphenazine before harvesting showed a strong reduction of ASMase activity (Figure 19 D). However, when cell extracts from untreated cells or recombinant acid sphingomyelinase were incubated with fluphenazine for 3 h, no reduction in ASMase activity was found (Figure 19 E). This indicates that fluphenazine is not a direct but a functional inhibitor of ASMase.

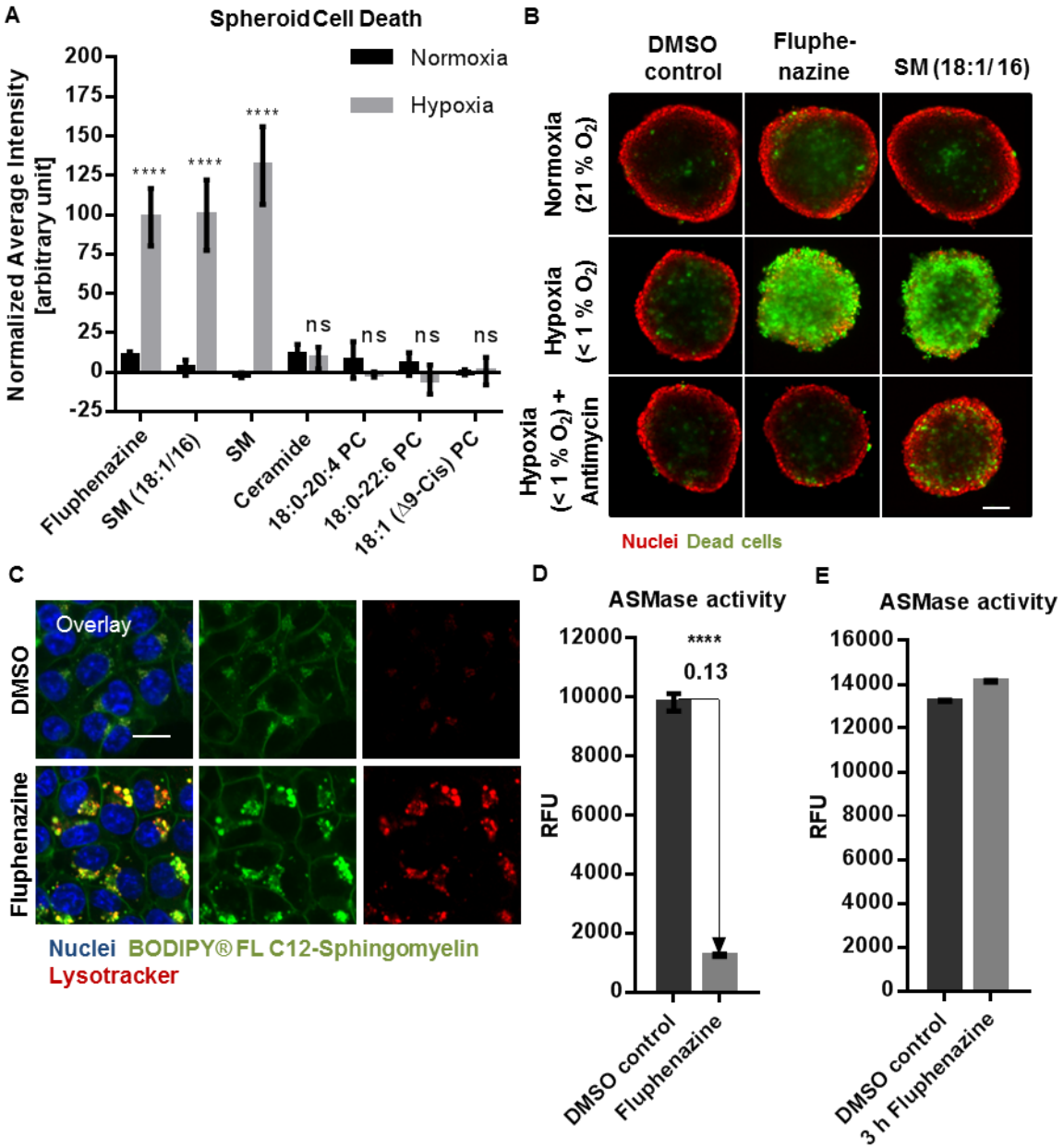

Figure 19: Fluphenazine increases cellular SM level by ASMase inhibition. A) HCT116 spheroids were treated for 3 days either in normoxia or hypoxia with DMSO control, 10 µM staurosporine control, 5 µM fluphenazine or different sphingolipids (100 µM (~70 µg/ml) SM (18:1/16), 200 µg/ml SM from bovine brain, 200 µg/ml Ceramide from bovine spinal cord, 60 µM 18:0-20:4 PC, 60 µM 18:0-22:6 PC or 200 µM 18:1 (Δ9-Cis) PC). Dead cells were stained with SytoxGreen and fluorescent intensities in spheroids were measured. Values were normalized with DMSO control (0) and staurosporine cell death control (100). Bars show mean with SD (n≥3). Statistical difference between normoxia and hypoxia was determined. B) HCT116 spheroids were treated for 3 days with either DMSO control, 5 µM fluphenazine or 100 µM SM (18:1/16) in normoxia, hypoxia or hypoxia + 200 nM antimycin. Spheroid nuclei were stained with Hoechst (red) and dead cells were stained with SytoxGreen (green). Representative images shown (n≥3). Scale bar 100 µm. C) HCT116 cells were co-incubated ON with either DMSO control or 5 µM fluphenazine and 1 µM BODIPY® FL C12-Sphingomyelin. Nuclei were stained with Hoechst and Lysosomes with Lysotracker. Representative images shown (n = 3). Scale bar 20 µm. D-E) ASMase activity in D) HCT116 cells treated for 24 h with either DMSO control or 5 µM fluphenazine or in E) untreated HCT116 cell extracts incubated for 3 h with either DMSO control or 5 µM fluphenazine. Bars show mean with SD (n = 3). **** p-value < 0.0001, ns – not significant. (adapted from Klutzny et al. (2017))

To validate ASMase as potential target for the development of novel hypoxia-specific anti-cancer drugs, it was tested if siRNA-based knockdown of the ASMase encoding gene *sphingomyelin phosphodiesterase 1* (*SMPD1*) phenocopies the effects of fluphenazine in tumor spheroids. For this, the spheroid generation protocol was adapted and a single cell suspension of HCT116 cells was co-seeded with SMPD1 siRNA into agarose-covered 384-well plates and grown to tumor spheroids (a detailed description can be found under 2.19 siRNA and shRNA transfection). Compared to fluphenazine treated HCT116 spheroids, cells grown to spheroids while incubated with SMPD1 siRNA showed neither in normoxia nor in hypoxia a strong increase in cell death staining (Figure 20 A). However, *SMPD1* mRNA level and ASMase antibody staining in siRNA transfected HCT116 cells indicate suboptimal knockdown efficacies and might be a reason for the lack of cell death induction in hypoxic spheroids (Figure 20 B and C).

Taken together, it can be concluded that fluphenazine induced hypoxia specific spheroid cell death is caused by a cellular accumulation of sphingomyelin which is a result of functional inhibition of ASMase activity. Whether ASMase on its own might be a potential anti-cancer target in hypoxic tumor regions remains to be shown and further studies are necessary to clarify the role of ASMase for cancer therapy.

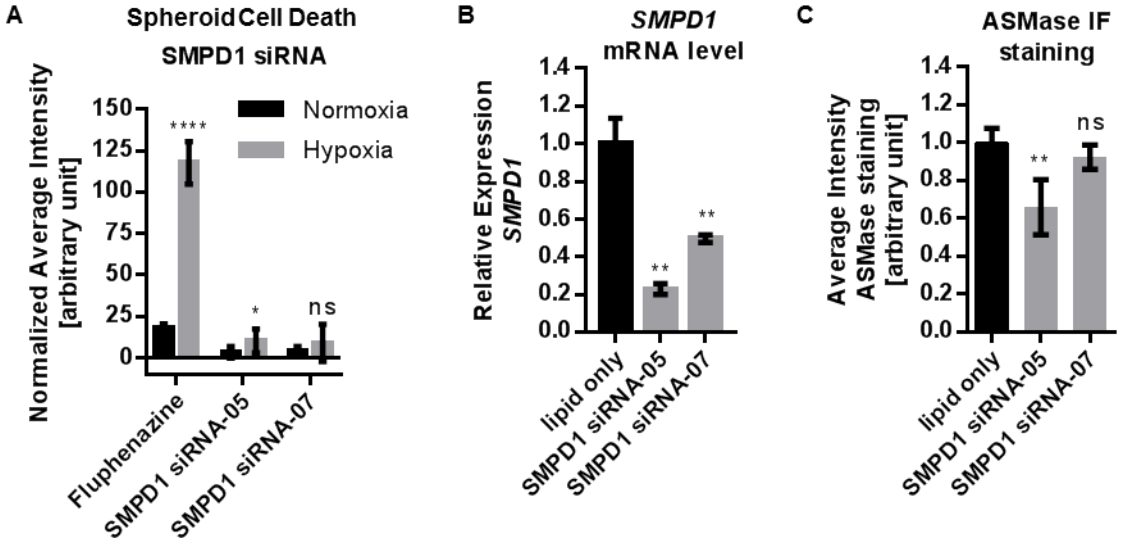

Figure 20: SMPD1 siRNA does not phenocopy fluphenazine induced cell death in hypoxic spheroids.
A) HCT116 cells were incubated with SMPD1 siRNA or lipid only control and grown as spheroids for 3 days. Afterwards spheroids were incubated for 72 h under hypoxia or normoxia and treated with DMSO control, 10 µM staurosporine or 5 µM fluphenazine. Dead cells were stained with SytoxGreen and fluorescent intensities in spheroids were measured. Values were normalized with DMSO control (0) and staurosporine cell death control (100). Statistical difference between normoxia and hypoxia was determined. B) Gene expression level of *SMPD1* in HCT116 cells (2D) incubated with SMPD1 siRNA or lipid only control. Ct values of each sample were normalized with the internal control *RPL32* and normalized to the lipid only control. C) ASMase protein levels were analyzed by IF antibody staining in HCT116 cells (2D) incubated with SMPD1 siRNA or lipid only control. Average intensity values were normalized to the lipid only control. Bars show mean with SD (n = 3). **** p-value < 0.0001, ** p-value < 0.01, * p-value < 0.05, ns – not significant.

Fluphenazine functionally inhibits ASMase distinct from known lysosomotropic substances

Interestingly, lysosomal membrane permeabilizing (LMP) compounds such as siramesine have also been shown to inhibit ASMase and have been proposed as anti-cancer drugs for the treatment of multidrug-resistant cancers (Ellegaard et al., 2013, Petersen et al., 2013). LMP inducing substances most likely generally affect lysosomal functions. By interfering with lysosomal membrane integrity and ASMase membrane localization they are thought to act as functional inhibitors of ASMase (Beckmann et al., 2014). However, as lysosomes are important organelles which cover a wide range of cellular functions, disrupting lysosomes in general will impair a variety of cellular functions and has been proposed to be generally cytotoxic to most cells (Aits and Jaattela, 2013). Hence, LMP-inducing compounds as well as V-ATPase inhibitors, which prevent lysosomal acidification and also generally disrupt lysosomal functions (Huss and Wieczorek, 2009), have been shown to unspecifically induce cell death in 2D culture conditions (Petersen et al., 2013).

Indeed, Table 3 and Figure 21 A show that the LMP inducing compound siramesine, as well as the V-ATPase inhibitor bafilomycin A1 do not act as hypoxia-selective and 3D spheroid specific compounds. Both substances induce cell death in spheroids or in 2D cell culture under hypoxia or normoxia alike. This strongly contrasts with fluphenazine, which is inactive in spheroids under normoxia and in 2D cell culture conditions (Table 3 and Figure 21 A).

Table 3: Siramesine and bafilomycin A1 induce tumor spheroid cell death independently of oxygen levels. HCT116 cells / spheroids were treated for 72 h in normoxic or hypoxic conditions. Tumor spheroids: Dead cells were stained with SytoxGreen and fluorescent intensities in spheroids were measured. Values were normalized with DMSO control (0) and 10 µM staurosporine cell death control (100). 2D cell culture: Nuclei were stained with Hoechst and cell counts were determined by automated image analysis and normalized with DMSO control (0). EC50 values were determined in n≥3 experiments. (adapted from Klutzny et al. (2017))

Compound	EC50 (cell death) in tumor spheroids [M]		EC50 (cell count) in 2D in [M]	
	Hypoxia < 1 % O_2	Normoxia 21 % O_2	Hypoxia < 1 % O_2	Normoxia 21 % O_2
Fluphenazine	1.63E-06 (SD 1.2E-06)	> 1E-05	> 1E-05	> 1E-05
Siramesine	1.84E-06 (SD 1.1E-07)	5.82E-06 (SD 2.4E-06)	3.35E-06 (SD 3.0E-07)	3.19E-06 (SD 5.2E-07)
Bafilomycin A1	< 1E-08	< 1.0E-08	< 1.0E-08	< 1.0E-08

Given the hypoxia-selective action of fluphenazine, it was speculated that fluphenazine induces lysosomal stress and targets ASMase by a different mechanism than LMP induction. Indeed, while siramesine and bafilomycin A1 lead to the formation of Galectin puncta at lysosomes, which is an indicator for LMP (Aits et al., 2015), this could not be detected in fluphenazine treated cells (Figure 21 B and C).

Therefore, it can be concluded that fluphenazine specifically targets lysosomal functions and ASMase activity without destabilizing lysosomal membranes and leads to hypoxia specific cell death in spheroids. This is in contrast to LMP inducing compounds and V-ATPase inhibitors, which generally disrupt lysosomal functionality and unselectively kill cancer cells.

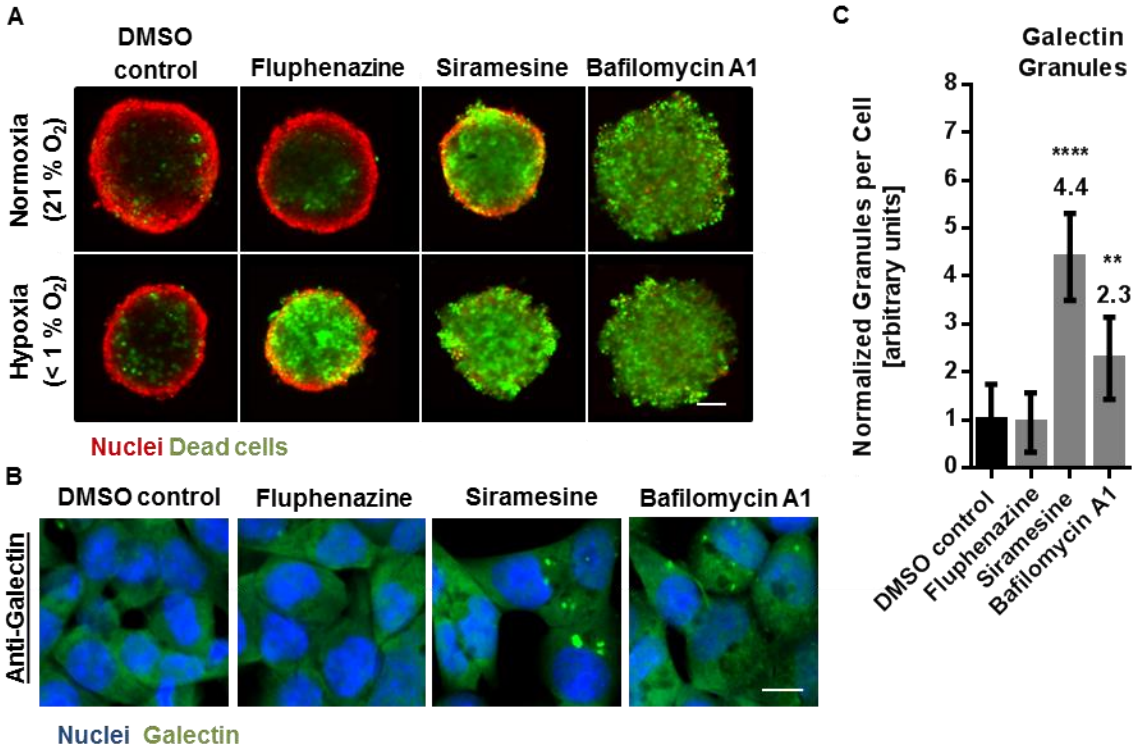

Figure 21: Fluphenazine induces lysosomal stress distinct from known lysosomotropic substances.
A) HCT116 spheroids were treated for 3 days with DMSO control, 5 µM fluphenazine, 5 µM siramesine or 200 nM bafilomycin A1 in normoxia or hypoxia. Spheroid nuclei were stained with Hoechst (red) and dead cells were stained with SytoxGreen (green). Representative images of multiple experiments shown (n≥3). Scale bar 100 µm. B) HCT116 cells were treated for 24 h with DMSO control, 5 µM fluphenazine, 5 µM siramesine or 200 nM bafilomycin A1. Cells were stained for Galectin. Representative images of multiple experiments shown (n≥3). Scale bar 10 µm. C) Quantification of Galectin puncta formation from B). Bars show mean with SD (n = 4). **** p-value < 0.0001, ** p-value < 0.01. (adapted from Klutzny et al. (2017))

3.3.4. Hypoxia stress response pathways

To ensure survival under reduced oxygen levels, hypoxic cancer cells activate different but partially overlapping stress response pathways. Therefore, it was aimed to identify how the effects of fluphenazine on lysosomal sphingolipid metabolism interfere with hypoxic adaption pathways to induce hypoxia specific tumor cell death.

Fluphenazine induces HIF overactivation in conditions of high HIF background levels

The transcription factor family of hypoxia inducible factors (HIF) is selectively stabilized under hypoxia and regulates the transcription of several genes important for a cellular response to low oxygen levels (Semenza, 2010). Hence, it was speculated that hypoxia-sensitizing compounds like fluphenazine could induce hypoxia specific cell death in tumor spheroids by interfering with HIF signaling.

For this, a HCT116 reporter cell line that expresses luciferase under the control of a VEGF promoter-derived hypoxia response element (HRE) (Ellinghaus et al., 2013) was used to measure HIF transcriptional activity by luminescence measurements in response to compound treatment (HRE-Luc assay; see 2.18 Hypoxia-Response Element (HRE)-Luciferase reporter assay). While the reporter shows no activity under normoxia (as HIF-α proteins are destabilized), the signal increases significantly under hypoxia or after inhibition of prolyl hydroxylase domain-containing (PHD) proteins by the hypoxia-mimetic Deferoxamine (DFO) (Jaakkola et al., 2001), (Figure 22 A). Interestingly, fluphenazine has no effect on the luminescence signal under normoxia but shows an approximately 2-fold stronger signal compared to controls in conditions of high HIF background activity, e.g. under hypoxia or in combination with DFO. Similar effects could be observed in the same cell line on *luciferase* mRNA level (Supplementary Figure 4 A), thus excluding luminescence measurement artefacts or interference with the luciferase protein. Moreover, HIF-1 target gene expression analysis in fluphenazine treated HCT116 cells showed an upregulation of pro-survival (*SLC2A3* and *VEGFA*) as well as pro-apoptotic HIF-1 target genes (*BNIP3*) in HIF stabilized conditions (DFO treatment). Additionally, no changes in mRNA expression levels were observed under normoxic growth conditions upon fluphenazine treatment (Figure 22 B).

In order to determine if the observed effects of fluphenazine on HIF-1 overactivity are mediated by ASMase inhibition and SM accumulation, the effects of SM supplementation on HRE-Luc reporter expression were tested. Indeed, similar to fluphenazine treatment exogenous SM led to 2.2-fold stronger luminescence signal compared to controls in

hypoxic conditions (Figure 22 C). Therefore, it can be concluded that fluphenazine induces HIF transcriptional overactivity in conditions of high HIF basal levels possibly by inducing cellular SM accumulation.

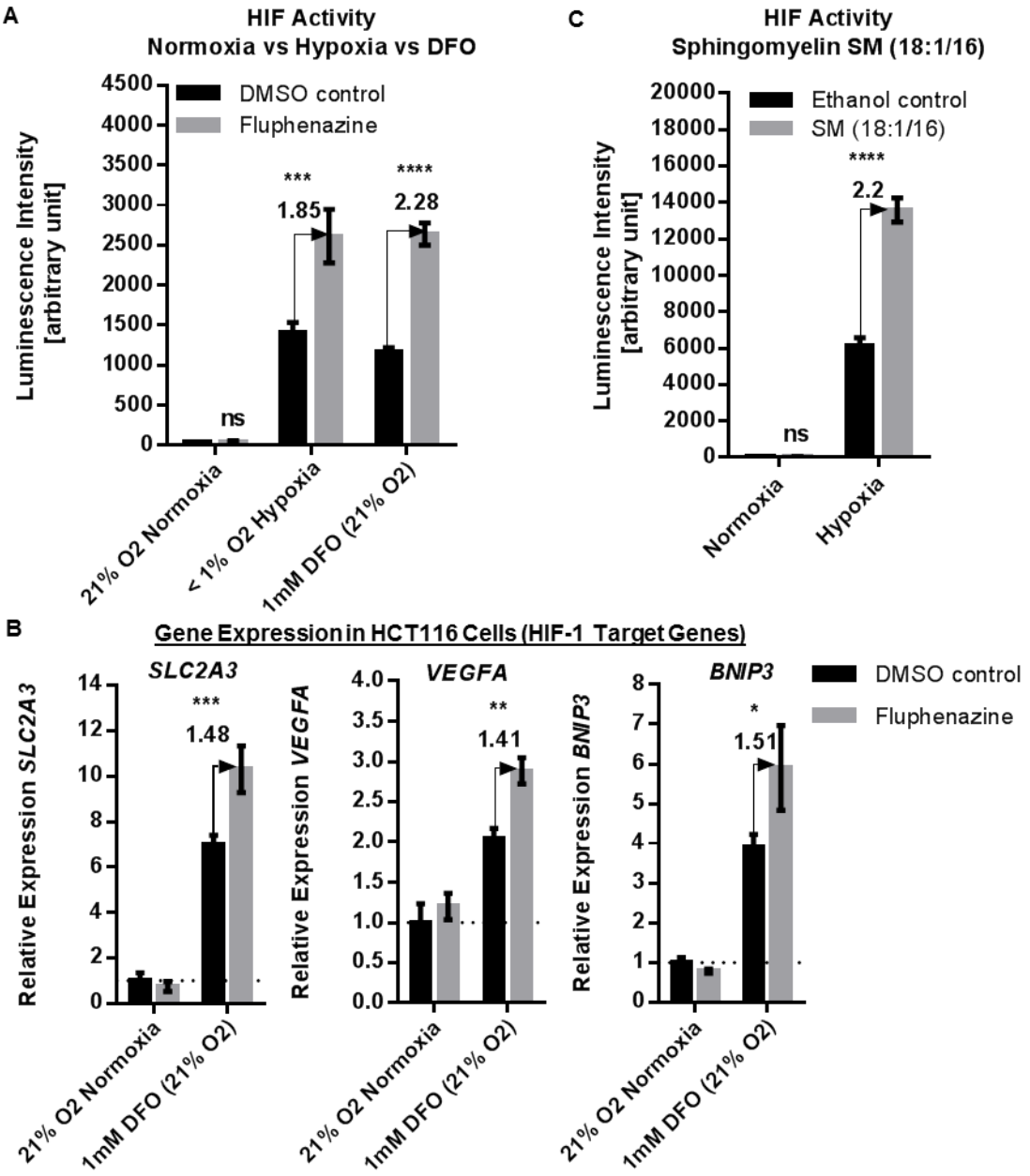

Figure 22: Fluphenazine induces HIF-1 overactivation in conditions of high HIF-1 background levels.
A) HCT116-HRE-Luc cells were treated with DMSO control or 10 µM fluphenazine and incubated for 16 h in normoxia, hypoxia or in normoxia with the DFO. After incubation, cells were lysed and luciferase activity was measured. Bars show mean with SD (n = 3). B) HCT116 cells were treated for 24 h with or without DFO (1 mM) and additionally with DMSO control or 5 µM fluphenazine. Gene expression analysis was performed for three HIF-1 target genes (*SLC2A3, VEGFA* and *BNIP3*) by RT-qPCR. *RPL32* was used as reference gene and relative expression level were normalized to the untreated control (no DFO, DMSO). Bars show mean with SD (n = 3). C) HCT116-HRE-Luc cells were treated with either ethanol control or 100 µM sphingomyelin SM (18:1/16) and incubated for 24 h either in normoxia or hypoxia. After incubation, cells were lysed and luciferase activity was measured (n = 3). **** p-value < 0.001, *** p-value < 0.001, ** p-value < 0.01, * p-value < 0.05. (adapted from Klutzny et al. (2017))

These results contrast with current treatment approaches in hypoxic tumor regions, which have been mainly focused on HIF-1 inhibition (Wilson and Hay, 2011, Semenza, 2012, Masoud and Li, 2015). However, while the two described HIF-1 inhibitors antimycin (Maeda et al., 2006) and BAY84-7296 (Helbig et al., 2014), that block HIF-1 activity via respiratory chain inhibition, significantly reduce the measured luminescence intensity in HCT116 HRE-Luc cells, they do not induce cell death in hypoxic tumor spheroids (Figure 23). On the contrary, they reduce fluphenazine induced HIF-1 overactivity and prevent cell death induction in fluphenazine treated hypoxic tumor spheroids. This rescue effect seems to be specific for hypoxia-sensitizing hits like fluphenazine, as cell death by a general cytotoxic compound like staurosporine cannot be prevented by co-incubation with antimycin or BAY84-7296 (Figure 23 B).

In summary, the identified hypoxia-sensitizing compound fluphenazine interferes with HIF-1 stress signaling specifically under HIF-1-α stabilized conditions (hypoxia or DFO treatment) by overactivating the transcriptional activity of HIF-1 most likely via SM accumulation. Both, cell death in hypoxic spheroids and HIF-1 overactivity, can be reduced by HIF-1 inhibition.

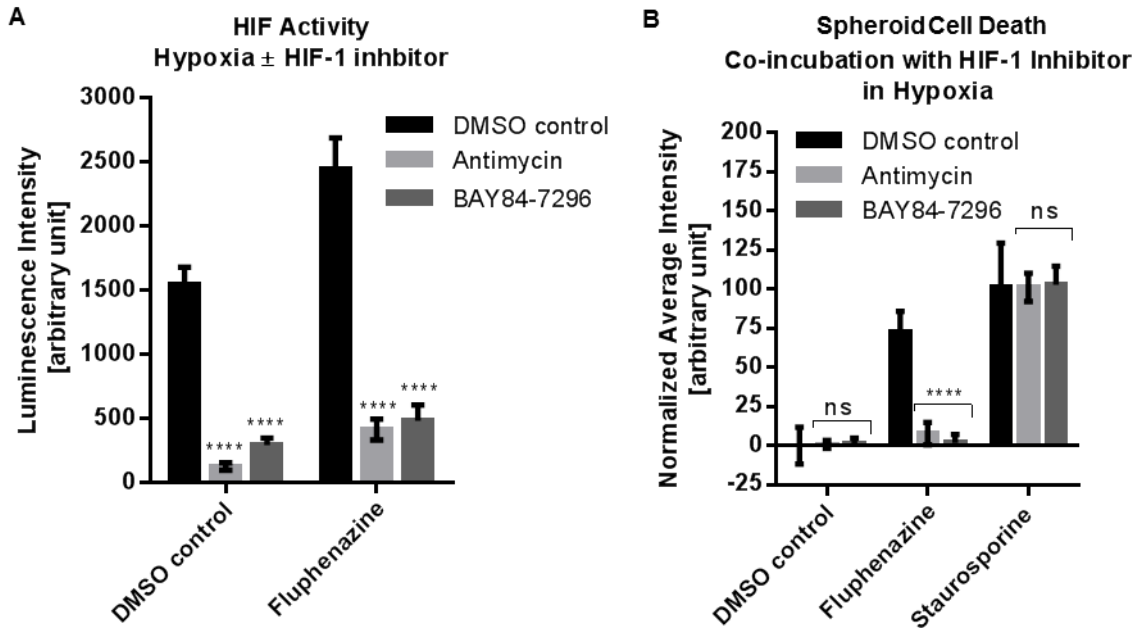

Figure 23: HIF-1 inhibition (via respiratory chain inhibition) reduces fluphenazine induced HIF-1 overactivity and spheroid cell death in hypoxia. A) DMSO control and fluphenazine (5 µM) treated HCT116-HRE-Luc cells were co-treated with DMSO control, 200 nM antimycin or 100 nM BAY84-7296 and incubated for 16 h in hypoxia. After incubation, cells were lysed and luciferase activity was measured. Bars show mean with SD (n = 3). B) HCT116 spheroids were treated for 3 days with DMSO control, 5 µM fluphenazine or 10 µM staurosporine and co-treated with either DMSO control, 200 nM antimycin or 100 nM BAY84-7296 in hypoxia. Dead cells were stained with SytoxGreen and fluorescent intensities in spheroids were measured. Values were normalized with DMSO/DMSO control (0) and staurosporine/DMSO cell death control (100). Bars show mean with SD (n = 3). **** p-value < 0.0001, ns – not significant.

Fluphenazine acts downstream of HIF-1-α protein stabilization or accumulation

HIF-1 is regulated at different levels, including translational, transcriptional control, protein stability and activity (Koh and Powis, 2012, Semenza, 2012). Therefore, it was aimed to identify the mechanism by which fluphenazine increases HIF-1 activity.

For this, mRNA as well as protein expression levels of the oxygen sensitive HIF-1-α subform were measured in response to fluphenazine treatment. Interestingly, fluphenazine did not lead to alterations in *HIF-1-α* transcript levels in hypoxic spheroids (Figure 24 A) and no differences in HIF-1-α protein levels in untreated or fluphenazine treated spheroids or in cells treated in 2D with DFO could be observed (Figure 24 B). Consequently, this suggests that fluphenazine leads to an activation of HIF-1-dependent transcription, downstream of HIF-1-α protein stabilization or accumulation, for example on the level of activity regulation by post-translational protein modification or interaction with transcriptional co-factors.

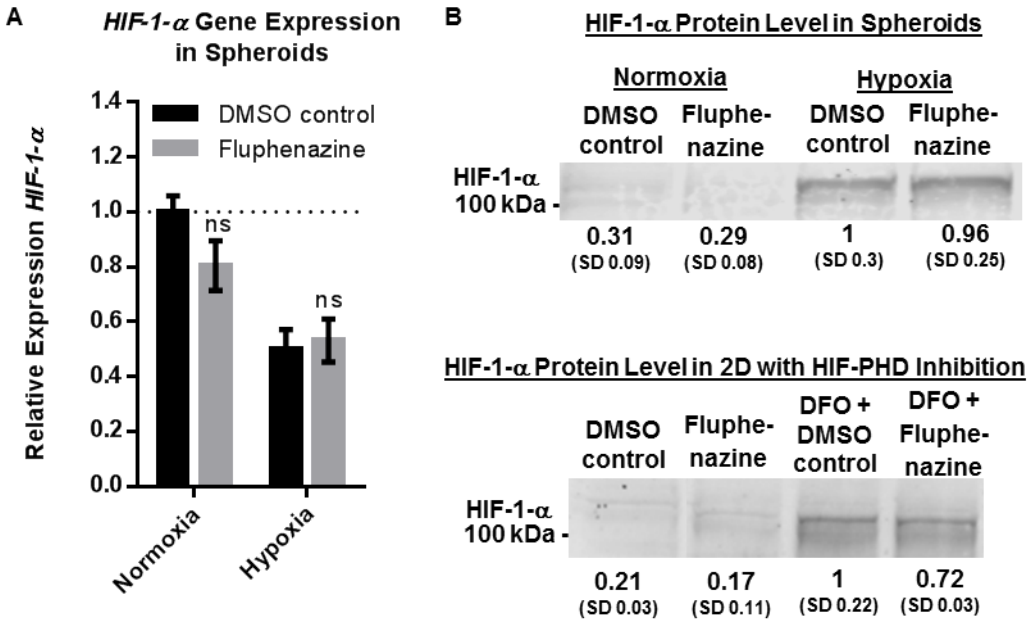

Figure 24: HIF-1-α gene and protein expression analysis. A) RT-qPCR analysis of *HIF-1-α* mRNA level of HCT116 spheroids treated for 24 h in normoxia or hypoxia with either DMSO control or 5 µM fluphenazine. *RPL32* was used as reference gene and relative expression level were normalized with the untreated control (Normoxia DMSO control). Bars show mean with SD (n = 3). ns –not significant. B) Western blot analysis of HIF-1-α protein expression in HCT116 spheroids or HCT116 cells grown in 2D which were treated for 24 h with either DMSO control or 5 µM fluphenazine under normoxia, hypoxia or normoxia + 1 mM DFO. Representative data of multiple experiments shown (n = 3). Intensity values were normalized to loading control and DMSO treated controls under hypoxia (upper row) or DMSO controls co-incubated with DFO (lower row). Beta-actin was used as internal control (not shown). (adapted from Klutzny et al. (2017))

Different co-regulatory pathways have been identified which fine-tune the activity of HIF-1 to balance pro-survival and pro-apoptotic functions. For example, the HIF-1 target gene *CITED2* has been shown to balance HIF-1 signaling via a regulatory feedback mechanism that involves the competitive binding of p300 (Yoon et al., 2011). CITED2 is stabilized by proteasome inhibition and reduces HIF-1 activity despite increased HIF-1 protein level under hypoxic conditions (Shin et al., 2008). This effect can also be observed in HCT116-HRE-Luc cells (Figure 25 A). Treatment with the proteasome inhibitor MG132 significantly decreases the luminescence level under HIF-1-α stabilized conditions (DFO treatment). Moreover, HIF-1 activity can be restored by CITED2 siRNA (Figure 25 A). Hence, it was speculated that SM accumulation by fluphenazine might inhibit a CITED2-mediated feedback mechanism and this way induce HIF-1 overactivity in HIF-1-α stabilized conditions (hypoxia or DFO treatment). However, despite the knockdown of *CITED2* gene expression (knockdown efficacy see Supplementary Figure 4 B), the relative increase of HIF activity upon fluphenazine treatment was similar in control cells (incubated with lipid only) and CITED2 siRNA cells (Figure 25 B). These results suggest, that fluphenazine induced HIF-1 overactivity is not primarily mediated by CITED2.

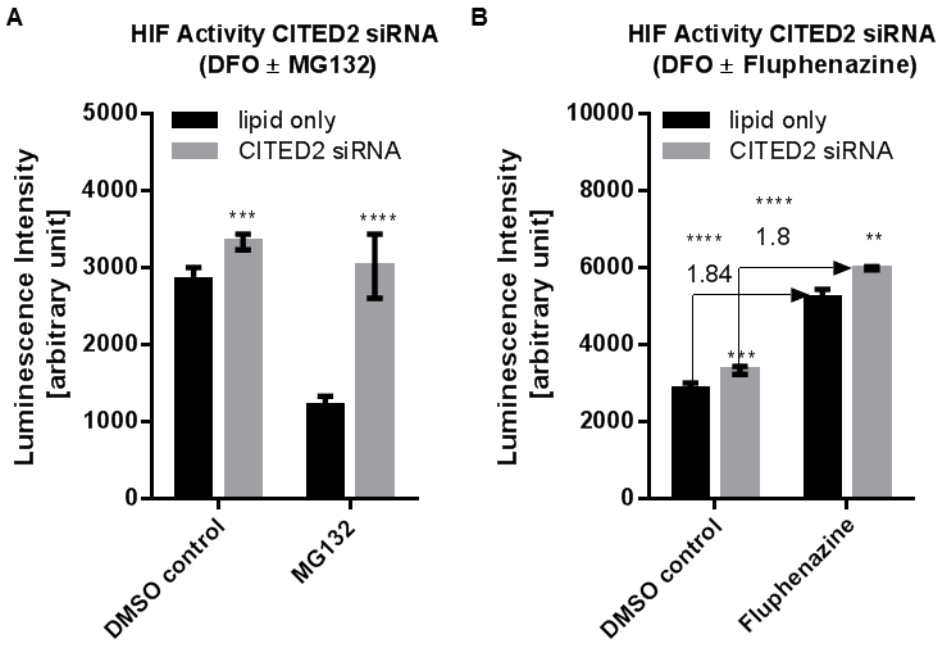

Figure 25: Effect of CITED2 knockdown on HIF activity. HCT116-HRE-Luc cells were transfected with either lipid only control or CITED2 siRNA for 72 h and subsequently treated with DMSO control, A) 500 nM MG132 or B) 5 µM fluphenazine and incubated for 16 h in normoxia, hypoxia or in normoxia with the DFO (1 mM). After incubation, cells were lysed and luciferase activity was measured. Bars show mean with SD (n = 3). **** p-value < 0.0001, *** p-value < 0.001, ** p-value < 0.01.

In addition to CITED2 feedback mechanism, the interference of mTOR inhibition with HIF-1 activity was investigated. While mTOR signaling is also one of the key adaptive pathways to hypoxia, it overlaps with HIF signaling and has been shown to stabilize HIF-1-α and its transcriptional activity (Land and Tee, 2007). Therefore, it was hypothesized that fluphenazine induced HIF-1 overactivity is mediated by enhanced mTOR signaling. Consequently, incubation with an mTOR inhibitor should prevent fluphenazine induced cell death in hypoxic tumor spheroids and reduce luciferase expression in HCT116-HRE-Luc cells. Indeed, incubation of hypoxic tumor spheroids with AZD8055 partially restored the viability in fluphenazine treated spheroids (Figure 26 A, similar results with rapamycin and temsirolimus (see Supplementary Figure 5)). Moreover, mTOR inhibition by AZD8055 reduced HIF-1 activity in DFO and DFO + fluphenazine treated HCT116-HRE-Luc cells (Figure 26 B). Nevertheless, mTOR inhibition by AZD8055 alone seems not to be sufficient to fully prevent the HIF-1 overactivating-effect of fluphenazine treatment, as the relative increase of HIF activity upon fluphenazine treatment is similar in DMSO control and AZD8055 incubated cells (Figure 26 B).

In conclusion, the generated results indicate that fluphenazine mediates the elevation of HIF-1-dependent transcription downstream of HIF-1-α protein stabilization or accumulation by interfering with multiple co-regulatory mechanisms of HIF-1 activity.

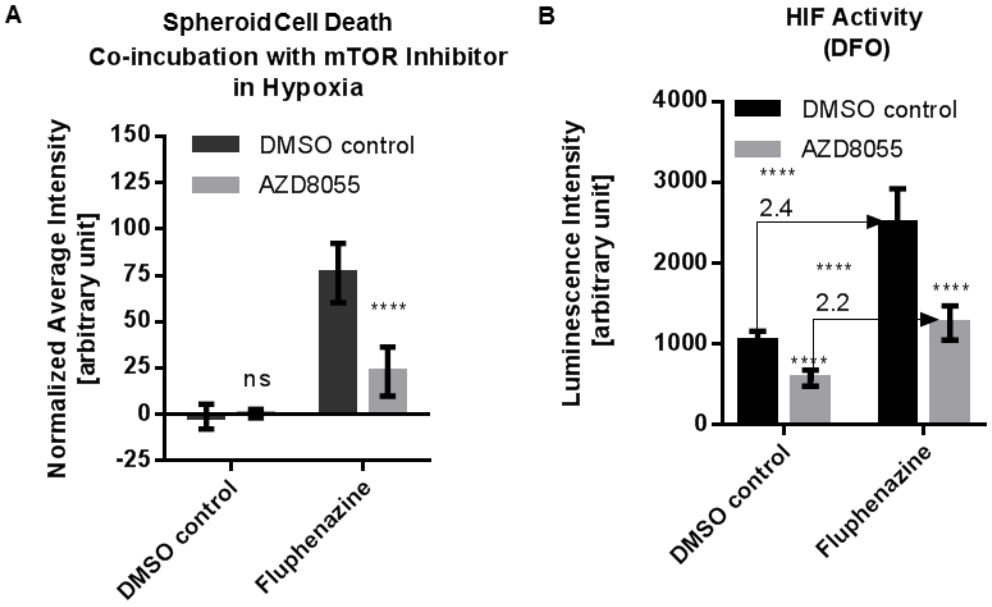

Figure 26: Effect of mTOR inhibition on spheroid cell death and HIF activity. A) HCT116 spheroids were treated for 3 days with DMSO control, 5 µM fluphenazine or 10 µM staurosporine and co-treated with either DMSO control or 1 µM AZD8055 under hypoxic conditions. Dead cells were stained with SytoxGreen and fluorescent intensities in spheroids were measured. Values were normalized with DMSO/DMSO control (0) and staurosporine/DMSO cell death control (100). Bars show mean with SD (n≥3). B) DMSO control and fluphenazine (5 µM) treated HCT116-HRE-Luc cells were co-treated with DMSO control or 1 µM AZD8055 and incubated for 16 h in Normoxia + 1 mM DFO. After incubation, cells were lysed and luciferase activity was measured. Bars show mean with SD (n = 3). **** p-value < 0.0001, ns – not significant.

Fluphenazine induces ATF4 mediated stress response signaling

To further investigate the effect on HIF-1 activity and to obtain a broader picture of transcriptional regulation induced by fluphenazine, the transcript level of all protein-encoding genes (~ 20.000 genes) was determined by deep sequencing of HCT116 cells treated with either DFO or DFO together with fluphenazine. As expected, among 559 significantly upregulated transcripts (> 2-fold increased expression and adjusted p-value < 0.05, see volcano plot Supplementary Figure 6) several known HIF-1 target genes were identified (Supplementary Table 3), including both pro-survival as well as pro-apoptotic genes such as *ANGPT2, VEGF, CTGF, SLC2A3, BNIP3* or *REDD1 (Regazzetti et al., 2010, Dengler et al., 2014)*.

Interestingly, in addition to HIF-1 target genes, a significant number of upregulated transcripts could be assigned to ATF4/CHOP dependent stress response pathway (Figure 27 A), (Wang and Kaufman, 2014). Strikingly, many central components of the ATF4 and CHOP dependent pro-apoptotic stress response pathway such as *ATF4*, *DDIT3* (CHOP), *PPP1R15A* (GADD34), *ATF3*, *HERPUD1* and *GADD45A* (Marciniak et al., 2004, Jiang et al., 2007, Kim et al., 2008, Han et al., 2013) are amongst the hits which show the highest upregulation after fluphenazine-DFO cotreatment. Accordingly, similar results were obtained in hypoxic tumor spheroids treated with fluphenazine. The two ATF4 dependent pro-apoptotic target genes *PPP1R15A* (GADD34) and *DDIT3* (CHOP) show a strong hypoxia-specific upregulation upon fluphenazine treatment (Figure 27 B).

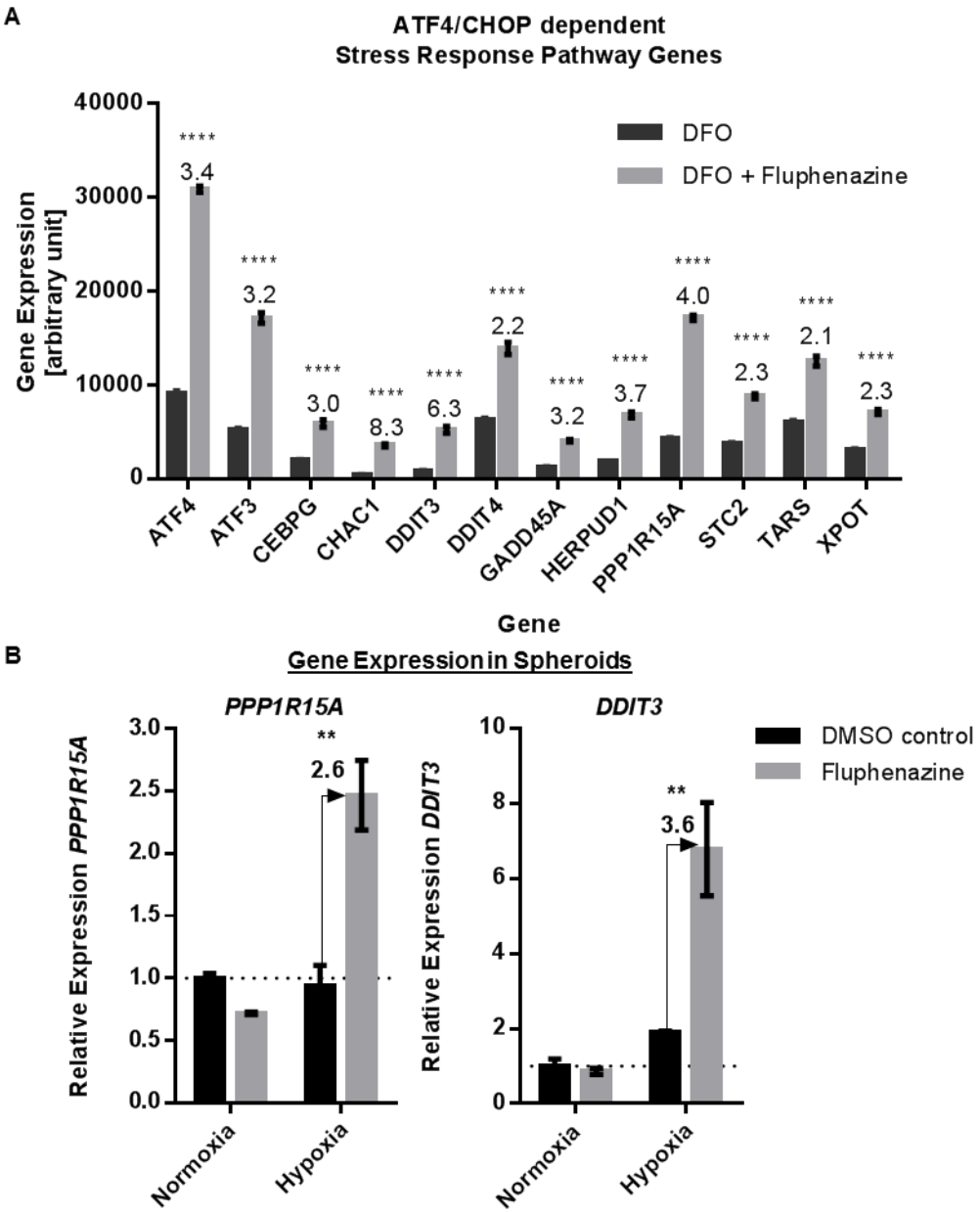

Figure 27: Fluphenazine induces ATF4 overactivation. A) Deep sequencing analysis of HCT116 cells treated for 24 h with either 1 mM DFO or 1 mM DFO + 5 µM fluphenazine (see also Supplementary Figure 6) showed upregulation of ATF4/CHOP dependent stress response pathway upon fluphenazine and DFO cotreatment. Bars show mean with SD (n = 1, median of 4 replicates). B) Gene expression analysis (RT-qPCR) of ATF4 pro-apoptotic target genes in HCT116 spheroids treated for 24 h in normoxia or hypoxia with DMSO control or 5 µM fluphenazine. Ct values of each sample were normalized with the internal control *RPL32* and normalized to the normoxia DMSO control. Bars show mean with SD (n = 3).). **** p-value < 0.0001, ** p-value < 0.01. (adapted from Klutzny et al. (2017))

Hypoxia or cellular stress pathways such as the HIF-1 or ATF4/CHOP dependent pathway have been shown to activate pro-survival as well as pro-apoptotic pathways, which are balanced to determine cellular fate depending on the amount of stress received (Greijer and van der Wall, 2004, Kim et al., 2008, Han et al., 2013, Wang and Kaufman, 2014). HCT116 tumor spheroids showed a significant upregulation of multiple HIF-1 and ATF4 dependent pro-apoptotic genes in response to fluphenazine treatment. Therefore, it was speculated that fluphenazine could shift the balance of hypoxia and cellular stress response signaling pathways to a pro-apoptotic response in hypoxic spheroids. To assess this hypothesis, the contribution of ATF4 or HIF signaling pathways to the induction of cell death in hypoxic spheroids was investigated by gene specific knockdown. For this, it was tested if either *ATF4*, *HIF-1-*α or *HIF-2-*α gene knockdown was sufficient to rescue fluphenazine induced cell death (knockdown efficacies in HCT116 spheroids see Supplementary Figure 7). Knockdown of *ATF4* significantly reduced fluphenazine-mediated overactivation of ATF4 pro-apoptotic target genes *DDIT3* (CHOP) and *PPP1R15A* (GADD34) under hypoxia (Figure 28). Additionally, knockdown of *ATF4* but not *HIF-1-*α or *HIF-2-*α partially rescued fluphenazine or sphingomyelin (SM d18:1) induced cell death in hypoxic spheroids (Figure 28, similar but smaller effects with ATF4 shRNA due to weaker gene knockdown (see Supplementary Figure 7)). This indicates that hypoxia-specific cell death induced by fluphenazine is dependent on ATF4.

Taken together, these data suggest that SM accumulation by fluphenazine increases the activity of hypoxia stress response pathways and induces spheroid cell death in hypoxic conditions by potentiating the pro-apoptotic response of ATF4-dependent ER stress signaling.

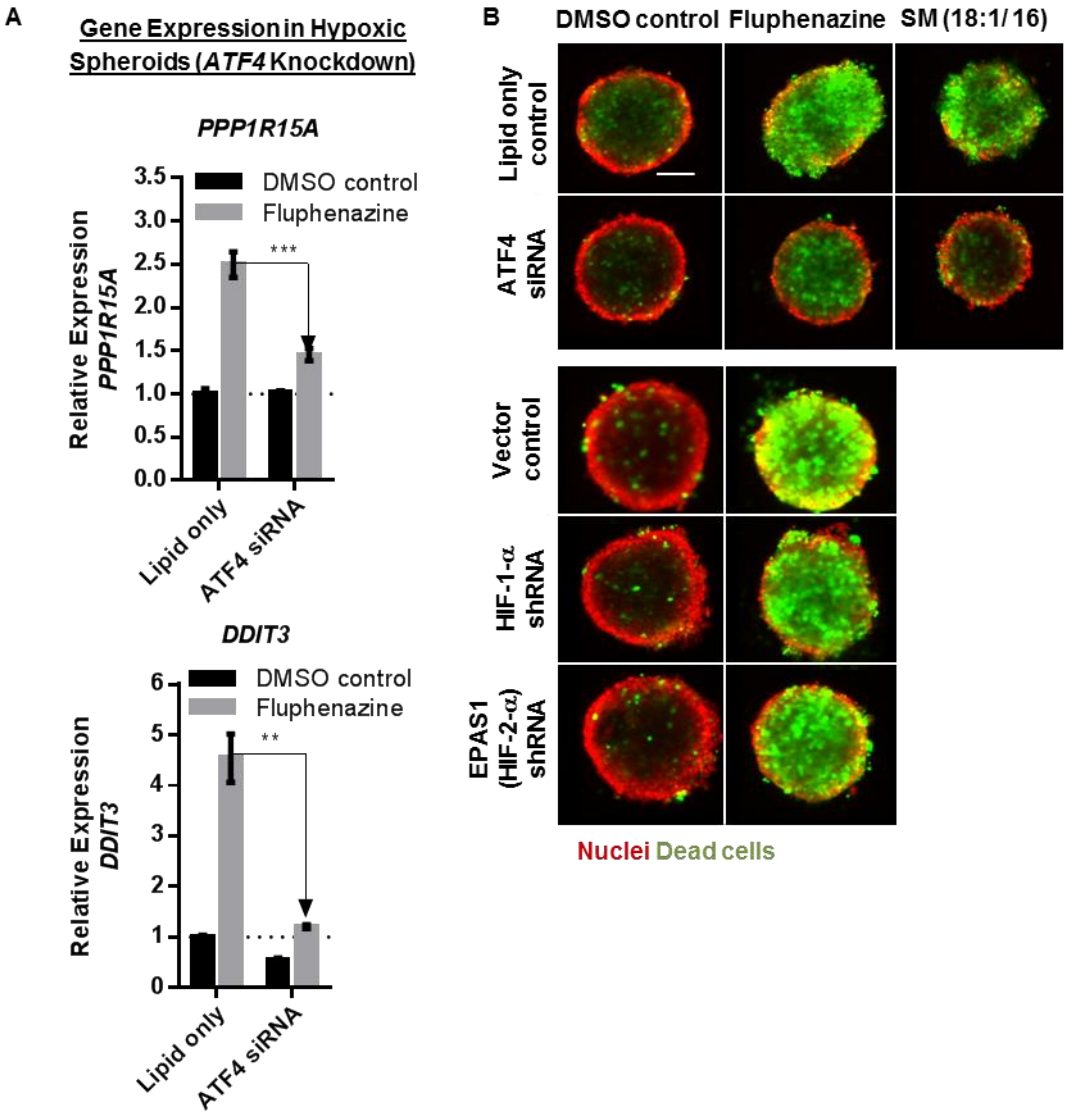

Figure 28: *ATF4* gene knockdown reduces fluphenazine or SM induced cell death under hypoxia.
A) HCT116 cells were incubated with ATF4 siRNA or lipid only control and grown as spheroids for 3 days under normoxic conditions. Afterwards spheroids were incubated for 24 h under hypoxia with DMSO control or 5 µM fluphenazine. Gene expression level for ATF4 target genes *PPP1R15A* and *DDIT3* were determined using RT-qPCR. Ct values of each sample were normalized with the internal control *RPL32* and the hypoxia lipid only control sample. Bars show mean with SD (n = 3). *** p-value < 0.001, ** p-value < 0.01. B) siRNA treated cells grown as spheroids (for *ATF4*) or spheroids from HCT116 cells stably transfected with HIF shRNA were treated with either DMSO control or fluphenazine (3 µM) (or 100 µM sphingomyelin (SM d18:1 /16)) for 3 days under hypoxia. Spheroid nuclei were stained with Hoechst (red) and dead cells were stained with SytoxGreen (green). Representative images of multiple experiments shown (n = 3). Scale bar 100 µm. (adapted from Klutzny et al. (2017))

4. Discussion[1]

Cancer therapy has come a long way since its beginnings in the early 20th century. While for a long time radical surgery was the only treatment option for most cancer patients, novel approaches such as targeted and immune cancer therapy have significantly improved the overall survival of tumor patients (DeVita and Rosenberg, 2012). Moreover, new diagnostic and research tools, like ctDNA or gene manipulation studies using RNAi, have increased our knowledge of cancer development, drug response and resistance development.

Nevertheless, cancer continues to be one of the leading causes of death worldwide and most drug treatments can only prolong the life of patients (Sudhakar, 2009, who.int, 2017). One of the major reasons for this is the development of treatment resistance. Through a variety of resistance mechanisms cancer cells adapt their metabolism and cellular signaling to evade the effects of an anti-cancer drug, leading to tumor relapse even after an initial positive drug response (Holohan et al., 2013). The tumor microenvironment (TME) is a key driver for resistance development and greatly affects cancer cell characteristics (Holohan et al., 2013, Barker et al., 2015, Sun, 2016). Among the variety of complex TME features, hypoxia is one of the leading causes of tumor resistance and substantially contributes to treatment failure (Vaupel and Mayer, 2007, Sullivan et al., 2008, Rohwer and Cramer, 2011, Wilson and Hay, 2011, Rebucci and Michiels, 2013, Multhoff et al., 2014, Semenza, 2014). Targeting cells in hypoxic tumor areas is therefore an important strategy for cancer treatment.

4.1. Tumor spheroids as *in vitro* model for tumor hypoxia

Despite significant advances in understanding the complexity of cancer biology and huge investments into anti-cancer drug research and development, more than 90 % of potential oncological drugs fail to show effectiveness in human patients when entering clinical trials (Thomas et al., 2016). One reason for this failure is the use of inadequate preclinical models. 2D cell culture methods using established cancer cell lines grown in a monolayer setting have been the most popular model for *in vitro* cancer research in the past. 2D cell culture approaches like cytotoxicity and proliferation assays have significantly advanced our knowledge of cancer biology and contributed to the development of potent anti-cancer drugs. However, with the increasing understanding of cancer complexity and the factors that contribute to tumor development, 2D cancer models display important limitations that may partially contribute to the high rate of clinical trial failures. Therefore, 3D cell culture

[1] Parts of the discussion are adapted from Klutzny et al. (2017). The usage of verbatim passages will not be marked separately as self-citation (see declaration pre-publication of the dissertation).

models are increasingly used to better reflect the complex physiological conditions found in *in vivo* tumors, including different nutrient and oxygen gradients, cell-cell and cell-matrix interactions (Thoma et al., 2014). Indeed, various studies demonstrated significant differences in drug response between 2D and 3D cell culture models (Herrmann et al., 2014, Wenzel et al., 2014). Moreover, 3D models have contributed to the understanding of adaption and resistance mechanisms developed, for example, in hypoxic tumor cells (Kim et al., 2011, Teppo et al., 2013). Therefore, in this work a 3D tumor spheroid based assay was adapted to mimic tumor hypoxia and to develop a screening compatible system for the identification of compounds that selectively kill cells in hypoxic tumor spheroid regions.

The developed spheroid system shows similar characteristics as found in hypoxic tumor regions. For example, visualization of hypoxia in spheroid cryosections shows a strong staining especially in spheroid core regions which are distal to the surrounding medium (see Figure 5). Similar, solid tumors which often lack a sufficient neo-angiogenesis also develop hypoxic regions especially in areas that are further away from nutrient- and oxygen-supplying blood vessels (Kyle et al., 2012).

Importantly, both severity and length of hypoxia greatly influence response mechanisms applied by cancer cells to survive, and thus have different clinical implications (Koumenis and Wouters, 2006). For example, it has been observed that hypoxic tumors with a significantly low oxygen level (down to less than 0.1 %) are more resistant to irradiation than cancer cells under mild hypoxia (> 1 % O_2). Moreover, many hypoxia adaption pathways do not become fully activated until severe oxygen levels are reached (Koumenis and Wouters, 2006, Vaupel et al., 2011, Prabhakar and Semenza, 2012, Yang et al., 2013). Indeed, increasing the extent and severity of hypoxia in tumor spheroids by an additionally cultivation under reduced oxygen levels (< 1 % O_2) significantly increases the accumulation HIF-1-α proteins and enhances the expression of hypoxia-induced stress response pathway genes, such as HIF-1 target genes or UPR-induced genes (see Figure 6). Both pathways belong to the key response mechanisms activated during hypoxia and initiate pro-survival signaling e.g. to promote angiogenesis in order to restore oxygen supply (Wouters and Koritzinsky, 2008). Accordingly, tumor spheroids incubated under severe hypoxia show a strong upregulation of the angiogenic factor *VEGFA* and the endothelial cell proliferation inducing protein *XBP1* (Zeng et al., 2013), (see Figure 6). Increased expression of both factors has been linked to tumor progression, metastasis development and poor patient survival (Niu and Chen, 2010, Koong et al., 2014).

Moreover, several other pathways that have been correlated with cancer cell survival under increased stress conditions display an enhanced activation in spheroids incubated

under severe hypoxic conditions. Thus, for example, stress activated MAPK pathway proteins like p38 or JNK show an accumulation in hypoxic tumor spheroids and have been shown to mediate important cellular processes like proliferation and survival that contribute to tumorigenesis (Wagner and Nebreda, 2009). Moreover, p38-MAPK is implicated specifically in the survival of hypoxic cancer cells through HIF-1 activation (Emerling et al., 2005).

However, hypoxic tumor spheroids do not only increase pro-survival signaling, but also show an enhanced expression of pro-apoptotic pathway genes such as *BNIP3* or *DDIT3* (see Figure 6). Indeed, hypoxic signaling by the key response pathways, HIF and UPR induced ER-stress signaling, is a tightly balanced network that regulates both pro-survival as well as pro-apoptotic responses depending on the severity of hypoxia and the amount of stress received (Harris, 2002, Wouters and Koritzinsky, 2008). Thus, in regions of anoxia or prolonged severe hypoxia HIF signaling can also result in hypoxia-induced cell death (Greijer and van der Wall, 2004).

Many of the signaling changes found in hypoxic tumor regions in response to severe stress are regulated by chromatin structure changes that modulate gene expression (Tsai and Wu, 2014). Accordingly, tumor spheroids with regions of severe hypoxia display multiple histone modifications compared to spheroids cultured under normoxia (see Supplementary Table 1).

Summarizing these results, the here adapted tumor spheroid model mimics several important parameters found in hypoxic tumor regions, and thus represents a suitable system to screen for compounds that specifically target tumor hypoxia.

However, although the here used spheroid model was tailored to represent the crucial characteristics found in a hypoxic tumor environment, certain limitations remain including the lack of an angiogenic structure or co-stimulatory signals from CAFs or immune cells. These limitations might be overcome by co-culturing spheroids with e.g. endothelial cells or fibroblasts (Upreti et al., 2011, Teppo et al., 2013, Wenzel et al., 2015). Moreover, a more complex and dense ECM structure such as multicomponent hydrogels (Herrmann et al., 2014) could be used to create a more diverse microenvironment. Nevertheless, these adaptions make the system not only more complex, but also more difficult to handle, time-consuming and reduce the imaging- and screening-compatibility. Therefore, those systems are more appropriate once a lead compound has been identified to investigate other avenues like drug delivery or clearance and before proceeding to even more time-consuming and expensive *in vivo* systems.

4.2. Glycolysis inhibition as hypoxia specific anti-tumor strategy

Next to oxidative phosphorylation, glycolysis is one of the two main energy producing pathways in cells. In hypoxic tumor regions respiration is suppressed by the lack of oxygen and cells are rendered dependent on glycolysis for energy production and survival (Pelicano et al., 2006). Accordingly, incubating hypoxic tumor spheroids with a known glycolysis inhibitor or in low glycose medium induced hypoxia specific cell death (see Figure 10). This effect could be mimicked by co-incubating tumor spheroids under normoxia with a respiratory chain inhibitor. This way, two compounds, cytochalasin B and E6 berbamine, were identified in a small-molecule-screen that specifically kill cells in hypoxic tumor spheroid regions most likely by glycolysis inhibition.

In addition to its primary mode of action as actin polymerization inhibitor, cytochalasin B is also known to block glucose transport (Deves and Krupka, 1978). Glucose is the primary source for glycolysis but can only pass through the lipid bilayer of the plasma membrane by an active transport via glycose transporter (GLUT). Hence, GLUT inhibition by cytochalasin B significantly reduces intracellular level of glycose and prevents energy production by glycolysis thereby inducing cell death in hypoxic cells (Deves and Krupka, 1978). Although cytochalasin B has predominantly been used to study cell structure and movement, it has also been investigated as anticancer drug in various tumor types and has demonstrated enhanced anti-tumor effects in co-treatment with chemotherapeutic agents *in vitro* (Trendowski, 2015). Therefore, GLUT inhibition by cytochalasin B could be a potential treatment strategy to specifically kill cancer cells in oxygen depleted tumor regions that depend on glycolysis for survival.

In contrast to cytochalasin B, little is known about the pharmacological effect of E6 berbamine on glycolysis. E6 berbamine has been reported as calmodulin inhibitor that decreases CaM-dependent MLCK activity (Hu et al., 1992). But in contrast to other hits with similar reported MOA, such as ML9 or ML7, only E6 berbamine was synthetic lethal in normoxic tumor spheroids incubated with the respiratory chain inhibitor antimycin (see Figure 12). Furthermore, other tested CaM inhibitors did not show hypoxia specific cell death effects when tested in tumor spheroids (see Figure 14), suggesting that E6 berbamine might have another so far unknown MOA related to glycolysis. Berbamine is a natural Chinese medicine that has been used for centuries to treat inflammatory diseases and other illnesses. Nevertheless, some berbamine derivatives have also demonstrated anti-cancer properties in various tumor types such as leukemia, breast or lung cancer, both *in vitro* and *in vivo* (Xu, 2016). However, the exact mechanism by which berbamine derivatives act to kill cancer cells is not well understood. Therefore, the here presented

results, which indicate a connection of E6 berbamine and glycolysis inhibition, could significantly contribute to exploring the therapeutic potential of berbamine in cancer.

In conclusion, the identification of glycolysis inhibitors validates the use of tumor spheroids incubated under reduced oxygen conditions as model system for the identification of compounds that specifically kill cells in hypoxic tumor regions. Both hit compounds, cytochalasin B and E6 berbamine, have reported anti-cancer properties in different tumor types, and might be even more effective when specifically applied to hypoxic tumors that depend on glycolysis for survival. Moreover, the glycolysis inhibitor 2-DG which also exhibited highly hypoxia specific effects in tumor spheroids (see Figure 10) has shown promising results *in vivo* and in first clinical trials by sensitizing cancer cells to chemotherapeutic treatment (Maschek et al., 2004, Raez et al., 2012). However, despite the clear potential of glycolysis inhibition as anti-cancer strategy, high toxicity in highly glucose-dependent tissues like the brain, retina or testes have been identified as a major challenge of this approach (Wilson and Hay, 2011, Ganapathy-Kanniappan and Geschwind, 2013). The development of glycolytic inhibitors with high target specificity and advances in tumor-side-specific delivery might overcome these undesirable side effects.

4.3. Identification of hypoxia sensitizing compounds with novel mode of action

In addition to GLUT and glycolysis inhibitors, further hypoxia-sensitizing hits were identified that displayed a different and potential novel MOA to induce hypoxia specific tumor spheroid cell death (see Figure 13 - hypoxia and 3D spheroid specific hits). While those remaining hits induced hypoxia specific cell death, they were insensitive to respiratory chain inhibition under normoxia and showed no effects in 2D cell culture (see Figure 12 and Table 2). Interestingly, in contrast to GLUT or glycolysis inhibitors, suppression of the respiratory chain completely prevented cell death induction by these compounds in hypoxic spheroids (see Figure 12). This could be attributed to the observation that respiratory chain inhibition prevents the establishment of hypoxic gradients in spheroids cultured under hypoxic conditions (see Figure 5 and Kyle et al. (2012)).

Within this group of novel hypoxia-selective compounds the phenothiazine trifluoperazine was identified as the most potent substance. Likewise, other structurally related phenothiazines such as fluphenazine demonstrated similar or even higher potencies in hypoxic tumor spheroids. Both drugs, trifluoperazine and fluphenazine, have been used in the clinic predominantly to treat psychosis by inhibiting the dopamine receptor D2 (Seeman et al., 1997, Wu et al., 2016). In recent years multiple studies have associated

cancer cell survival with increased dopamine receptor expression and have investigated dopamine receptor targeting as potential approach for cancer treatment (Sachlos et al., 2012, Pornour et al., 2015, Borcherding et al., 2016). Nevertheless, since neither of the other remaining hit compounds (ML9, ML7 and tamoxifen) have a reported effect on dopamine receptor activity and other known potent dopamine antagonists displayed no hypoxia-specific effects in spheroids, it was speculated that trifluoperazine and fluphenazine kill cells in hypoxic or anoxic tumor spheroid regions independently of their function as dopamine receptor inhibitor.

Indeed, it is not uncommon for drugs to act through a diversity of molecular mechanisms and interact with multiple targets (Talevi, 2015). Accordingly, several phenothiazine drugs have been reported to have diverse biological activities (Wu et al., 2016). Thus, for example, trifluoperazine also displays inhibitory effects on calmodulin (CaM)-dependent enzymes. Interestingly, trifluoperazine has recently also been shown to exert anti-cancer effects by this additional function (Wu et al., 2016). Since fluphenazine and the other hit compounds, tamoxifen, ML7 and ML9 have similar reported effects on CaM signaling (Weiss et al., 1980, Silver and Stull, 1983, Lopes et al., 1990, Vandonselaar et al., 1994), it could be likely that hypoxia specific cell death in tumor spheroids is a consequence of CaM inhibition. However, other known CaM inhibitors like W7 or W13 did not induce cell death in tumor spheroids or were hypoxia unspecific (Ophiobolin A), (see Figure 14). Calmodulin interacts with a diversity of different target enzymes and therefore has a highly flexible binding structure (Tidow and Nissen, 2013). Due to this flexibility, CaM antagonists can bind calmodulin at distinct sides and this way inhibit the interaction with different CaM-dependent enzymes. Indeed, distinct binding mechanisms of W7 and trifluoperazine to CaM binding pockets have been demonstrated (Osawa et al., 1998) and might explain the different effects on spheroid cell death. However, further detailed binding studies would be needed to determine a clear connection between CaM inhibition by the identified screening hits and cancer cell death in hypoxic conditions. Nevertheless, since CaM activity is dependent on calcium (Ca^{2+}) binding, modulating cellular Ca^{2+} levels should significantly alter spheroid cell death in hypoxic condition, independent of which CaM-target enzyme interaction is blocked by the hit compounds. But neither the increase nor the reduction of intracellular calcium levels showed hypoxia specific effects in tumor spheroids (see Figure 14).

Therefore, it can be concluded that inhibition of Ca^{2+}-CaM signaling is most likely not the key MOA which induces hypoxia specific cancer cell killing. Hence, it is possible that this group of hypoxia-sensitizing compounds possesses another, so far unknown biological activity which is responsible for the observed effects in hypoxic tumor spheroids.

4.3.1. Sphingomyelin metabolism as target in hypoxic tumor cells

Besides similarities in some of their reported biological functions, all of the identified hypoxia-sensitizing compounds show similar “cationic amphiphilic” structural features (see Figure 15). These structural properties are characteristic for compounds that accumulate in lysosomes as consequence of protonation of their basic center in the acidic lysosome environment and interfere with the lysosomal physiology (Halliwell, 1997, Ellegaard et al., 2016). Accordingly, fluphenazine and the four hit compounds lead to a strong accumulation of lysosomes and impair lysosomal functions such as the metabolism of phospholipids (see Figure 16 and Supplementary Figure 2). More specifically, fluphenazine elevates sphingomyelin (SM) levels and functionally inhibits the lysosomal enzyme acid sphingomyelinase (ASMase).

Fluphenazine targets hypoxic cells by sphingomyelin accumulation

Sphingomyelin levels are controlled by both synthetic and catabolic pathways. On the one hand SM can be synthesized from ceramide and phosphocholine by sphingomyelin synthase and on the other hand SM is catabolized by sphingomyelinase. Based on the results that identify fluphenazine as functional inhibitor of ASMase (see Figure 19) it can be assumed that SM levels increase in fluphenazine treated cells primarily via decreasing SM degradation and not increasing SM synthesis.

Importantly, exogenous addition of SM to the cell culture medium phenocopies the effect of fluphenazine and therefore suggests SM accumulation as primary reason for the observed hypoxia specific cell death. In addition to spheroid and hypoxia selective induction of cancer cell death, SM treated hypoxic spheroids show a complete rescue of cell death upon inhibition of the respiratory chain (see Figure 19). Moreover, compared to fluphenazine treatment, exogenous addition of SM exhibits similar effects on hypoxia stress response pathways (see Figure 22). Consequently, these findings propose SM metabolism as target pathway of fluphenazine treatment.

Sphingolipids like SM are a major component of many cellular membranes and thus play an important role in signal transduction. Accordingly changes in SM membrane composition have been correlated with cancer cell adhesion and migration (Murai, 2012, Eich et al., 2016). Moreover, decreased SM levels have been associated with tumorigenesis in glioma cells (Barceló-Coblijn et al., 2011) and the malignant state of different human tumors (Hendrich and Michalak, 2003). This highlights the important role of SMs in cancer and proposes the induction of SM accumulation as potential treatment strategy in hypoxic tumors with decreased SM levels.

Acid sphingomyelinase (ASMase) inhibition by fluphenazine

This study identifies fluphenazine as functional inhibitor of acid sphingomyelinase. Firstly, fluphenazine treated cells show a significant reduction of ASMase activity and secondly, display a strong lysosomal accumulation of sphingomyelin, the substrate of ASMase (see Figure 19). However, fluphenazine seems to act differently than known inducers of lysosomal dysfunction, such as bafilomycin A1 or siramesine. In contrast to the hypoxia-specific effects of fluphenazine, these compounds induce cytotoxicity in spheroids and 2D cell culture independently of oxygen levels (see Table 3). Moreover, bafilomycin A1 and siramesine but not fluphenazine destabilize lysosomes by lysosomal membrane permeabilization (LMP) (see Figure 21), which could be the reason for their broader cytotoxic activity and hypoxia independent killing of cancer cells. Therefore, it can be concluded that fluphenazine acts differently from lysosome disrupting compounds by functionally inhibiting ASMase without inducing LMP.

ASMase becomes fully active when bound via electrostatic forces to the inner lysosomal membrane (Beckmann et al., 2014). Therefore, it might be speculated that fluphenazine interferes with this binding and thereby decreases ASMase activity. Due to its amphiphilic properties (see chemical structure Figure 15) fluphenazine is likely to interact with the lysosomal lipid membrane via its lipophilic part. In the acidic lysosome environment the basic group of fluphenazine is protonated and changes the inner membrane charge (Beckmann et al. 2014). This might disrupt the electrostatic forces that bind ASMase to the lysosomal membrane. Indeed, the antidepressant desipramine, which displays similar cationic amphiphilic characteristics as fluphenazine, has been shown to prevent ASMase membrane binding and to cause its proteolytic degradation (Kölzer et al., 2004). Similar to fluphenazine, desipramine does not show lysosome disrupting characteristics or general cytotoxicity (Kölzer et al., 2004, Taniguchi et al., 2015), (see also Supplementary Figure 8). Moreover, desipramine also acts as hypoxia-sensitizer in tumor spheroids (see Supplementary Figure 8). Hence, these data propose that fluphenazine functionally inhibits ASMase activity by interfering with the electrostatic forces that bind ASMase to the inner lysosomal membrane.

Nevertheless, the role of ASMase in cancer is controversial. On the one hand lysosome-based target strategies have been proposed as attractive treatment approaches in cancer therapy (Fehrenbacher et al., 2004) and functional ASMase inhibitors have demonstrated an anti-cancer function (Petersen et al., 2013). On the other hand, ASMase expression has been inversely correlated with tumor progression and metastasis (Bizzozero et al., 2013, Osawa et al., 2013) and treatment with recombinant ASMase has shown to sensitize tumor cells to radiation and chemotherapy (Grammatikos et al., 2007, Smith and

Schuchman, 2008). Furthermore, ASMase gene knockdown in HCT116 cells and spheroids led to inconclusive results. While it was expected that deletion of the ASMase encoding gene *SMPD1* mimics the effects of fluphenazine, no spheroid cell death could be observed (see Figure 20). This can be partly explained by suboptimal knockdown efficacies. Nevertheless, the potential use of ASMase inhibitors in cancer therapy remains to be investigated. Since cationic amphiphilic drugs like fluphenazine are known to alter the biophysical properties of cellular membranes, the mode of action of fluphenazine could also be mediated by several parallel effects in addition to ASMase inhibition. However, the identification of direct ASMase inhibitors may help to clarify the role of ASMase in cancer and will be facilitated by the recent availability of ASMase crystal structures (Gorelik et al., 2016).

4.3.2. Sphingomyelin accumulation shifts hypoxic stress signaling towards a pro-apoptotic response

Changes in cellular membrane lipid compositions, for example caused by impaired sphingomyelin metabolism, induce lipid stress which leads to the activation of ER stress pathways including ATF4 or XBP1 signaling (Volmer and Ron, 2015). Fluphenazine significantly alters cellular sphingolipid level (see Figure 17). Accordingly, deep sequencing analysis demonstrated an upregulation of *ATF4* transcripts and ATF4 target genes after fluphenazine treatment (see Figure 27).

Next to the stabilization of hypoxia-inducible transcription factors (HIF), the activation of ER stress signaling is one of the main cellular responses to hypoxia (Wouters and Koritzinsky, 2008). Both signaling pathways are partially overlapping (Köditz et al., 2007, Wouters and Koritzinsky, 2008, Chen et al., 2014, Pereira et al., 2014) and are balanced to either mediate a pro-survival or a pro-apoptotic response, depending on the severity of stress received (Harris, 2002, Zhou et al., 2006, Kim et al., 2008, Han et al., 2013, Pakos-Zebrucka et al., 2016). Fluphenazine treatment or sphingomyelin supplementation lead to an overinduction of the hypoxia response, including both HIF-1 and ATF4 transcriptional overactivity, specifically in HIF-1 stabilized cells or hypoxic spheroids (see Figure 22 and Figure 27). Importantly, not only pro-survival genes but also pro-apoptotic targets of both transcription factors are increased by fluphenazine treatment. Therefore, a possible explanation for the observed hypoxia specific induction of cell death in spheroids could be that the simultaneous induction of hypoxia- as well as lipid- stress lead to an imbalance of hypoxia stress signaling, tipping the balance from a pro-survival to a pro-apoptotic stress response.

Potentiation of HIF-1 and ATF4 activity as novel therapeutic strategy in hypoxic tumors

So far, most approaches to target hypoxic tumor cells have focused to a great extent on the inhibition of HIF signaling (Semenza, 2012). This has been owed to the fact that *HIF-1* is over-expressed in a large number of human tumors and correlates with poor prognosis and treatment failure (Semenza, 2003). Nevertheless, to date there is no clear clinical evidence of antitumor activity due to HIF-1 inhibition (Wilson and Hay, 2011) and no specific HIF-1 inhibitor has been clinically approved (Burroughs et al., 2013). Likewise, targeting ER stress signaling in cancer has mainly focused on the inhibition of downstream effectors and not the overactivation of ER pro-apoptotic signaling (Garg et al., 2015, Corazzari et al., 2017). Similar to HIF target strategies, this is based on the observation that ER stress induced UPR activation contributes to survival and resistance development in multiple human cancers through a persistent activation of pro-survival signaling (Corazzari et al., 2017). Thus, for example, upregulation of *ATF4* expression during severe hypoxic conditions has been correlated with cancer cell migration and survival (Nagelkerke et al., 2013, Pike et al., 2013). Nevertheless, inhibiting ER stress pathways is still a relatively new anti-cancer strategy with yet no clinical approved drugs (Garg et al., 2015, Corazzari et al., 2017).

In contrast to inhibiting hypoxia stress pathways as treatment approach, the here presented data suggest a novel, yet unexplored, mechanism in which induction of lipid stress could potentially lead to an overactivation of HIF-1 and ATF4 stress signaling and thereby promote their pro-apoptotic functions to specifically kill cells in hypoxic tumor areas. However, the question remains how HIF-1 and ATF4 are overactivated by fluphenazine.

Under hypoxic conditions HIF-1 becomes activated due to the decreased hydroxylation of HIF-1-α by PHD. Therefore, it could be speculated that fluphenazine overactivates HIF-1 activity by inhibiting PHD. However, compared to known PHD inhibitors like DFO fluphenazine acts only under conditions of high HIF-1 basal levels (hypoxia or co-incubation with DFO) and not under normoxic conditions (see Figure 22). Moreover, while PHD inhibition results in the accumulation of HIF-1-α proteins, fluphenazine does not affect HIF-1-α protein level (see Figure 24). Therefore, it can be concluded that fluphenazine does not act as PHD inhibitor and most likely increases HIF-1 activity downstream of protein stabilization e.g. by interfering with regulatory feedback mechanisms or by interacting with transcriptional co-factors.

Indeed, CITED2 as well as mTOR signaling, which both have been proposed to regulate HIF-1 activity by feedback inhibition (Land and Tee, 2007, Yoon et al., 2011), affect HIF-1 activity in HCT116 cancer cells. Nevertheless, inhibition of either factor cannot prevent HIF-1 overactivation by fluphenazine (see Figure 25 and Figure 26). mTOR is also an important mediator of autophagy, an intracellular recycling process that prevents apoptosis and confers treatment resistance (Sui et al., 2013). mTOR inhibition results in an increased level of autophagy and enhances cell viability (Wouters and Koritzinsky, 2008, Kapuy et al., 2014), which might explain the reduced cell death induction in fluphenazine treated hypoxic spheroids (see Figure 26). Hence, this suggests that mTOR inhibition by AZD8055 partially rescues fluphenazine induced spheroid cell death not by decreasing HIF-1 activity but by increasing cell survival via autophagy induction. However, on the other hand mTOR inhibition and autophagy induction have also been proposed as anti-cancer treatment (White, 2012, Zaytseva et al., 2012). This dual role in cancer seems to be highly context-dependent (e.g. dependent on cancer type or additional stress stimuli).Therefore, further studies would be needed to clarify the exact mechanism by which mTOR inhibition increases the viability in fluphenazine treated hypoxic spheroids.

Interestingly, it has been reported that ATF4 signaling also behaves as a co-regulatory mechanism and potentiates HIF-1 transcriptional activity under hypoxia (Pereira et al., 2014). Therefore, sphingomyelin accumulation might function as an additional stress stimulus that activates ER stress signaling via ATF4 and this way potentiates HIF-1 activity. Since the decision of cell survival or death highly depends on stress magnitude and duration (Corazzari et al., 2017), this additional stress stimulus might be sufficient to shift the cellular stress response under hypoxia towards apoptosis. Indeed, *ATF4* gene knockdown can reduce the overactivated pro-apoptotic signal in fluphenazine treated cells under hypoxia and prevent cell death in hypoxic tumor spheroids (see Figure 28). In contrast, knockdown of *HIF-1-*α or *HIF-2-*α is not sufficient to reduce cell death in fluphenazine treated hypoxic spheroids. Therefore, it can be concluded that the overactivation of cellular stress signaling and induction of hypoxia-specific spheroid cell death by fluphenazine is dependent on ATF4.

Based on these findings a mode of action model for fluphenazine induced hypoxia specific cell death can be proposed that is illustrated in Figure 29. Briefly, fluphenazine induces sphingomyelin accumulation by functionally inhibiting acid sphingomyelinase. Elevated sphingomyelin levels (also achieved by addition of exogenous SM) in turn induce lipid stress which activates ER stress signaling via ATF4 (Volmer and Ron, 2015). Combining both, lipid stress and hypoxic stress, shifts the balance of cellular stress signaling to an ATF4 dependent pro-apoptotic response and drives cells into apoptosis specifically in

highly stressed hypoxic tumor cells. In contrast, fluphenazine or hypoxia treatment alone is not sufficient to induce cell death and triggers a pro-survival response.

To sum up, the presented model presents a novel, yet unexplored mechanism in which induction of sphingolipid stress leads to the overactivation of hypoxia stress response pathways and thereby promotes their pro-apoptotic tumor suppressor functions to specifically kill cells in hypoxic tumor areas.

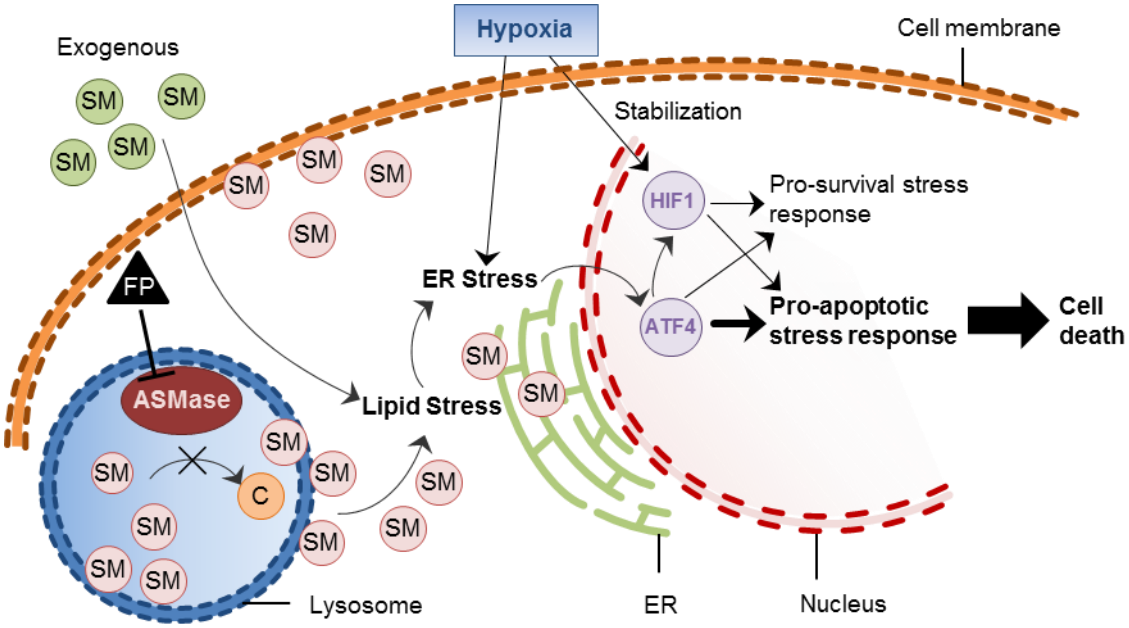

Figure 29: Model for fluphenazine induced hypoxia specific cell death by potentiating the pro-apoptotic path of cellular stress response pathways. Fluphenazine impairs lysosomal functions by interfering with ASMase activity. Sphingomyelin accumulation induces lipid stress and activates ER signaling via ATF4. Incubation under hypoxia induces additional stress response and additionally activates HIF-1 transcriptional activity. Both transcription factors, ATF4 and HIF-1, express pro-survival as well as pro-apoptotic genes which must be balanced to determine cellular fate depending on the amount of stress received. Together, fluphenazine and hypoxia treatment shift the cells stress response towards apoptosis and cell death. However, either of these treatments alone is not sufficient to induce cell death and favors the pro-survival stress response pathway. FP: fluphenazine; SM: sphingomyelin; C: ceramide; ASMase: acid sphingomyelinase; ER: endoplasmic reticulum. (adapted from Klutzny et al. (2017))

4.3.3. Translation into *in vivo* activity and strategies for combinational treatments

In contrast to current hypoxia-targeting treatment approaches, the here identified mode of action of hypoxia-sensitizer fluphenazine suggests the overactivation of hypoxia stress signaling pathways as potential novel strategy to specifically kill hypoxic tumor cells. However the question remains if this novel approach can be translated into anti-tumor activity *in vivo*.

One of the major advantages of the identified compounds is their hypoxia-selectivity. Only the combination of lipid stress and severe hypoxia induced cell death in tumor spheroids. This might significantly reduce off-target effects in normoxic tissue *in vivo*. The tumor spheroid assay was adapted to identify only compounds that act under severe hypoxic conditions (< 1 % O_2). Hence, hypoxia-selective hits like fluphenazine should also show a higher therapeutic window than current approaches which also target areas of mild hypoxia (between 1 and 5 % O_2) that are also present in healthy tissue regions, such as the brain or joints (Koumenis and Wouters, 2006). An additional advantage of drugs like fluphenazine and trifluoperazine is that they have already been approved by the FDA and used in humans for several years (accessdata.fda.gov., 2017). Moreover, trifluoperazine has already demonstrated anti-tumor efficacy in *in vivo* mouse models (Yeh et al., 2012, Wu et al., 2016).

Nevertheless, cationic amphiphilic drugs such as fluphenazine or trifluoperazine are known to alter the biophysical properties of cellular membranes and therefore could also affect other pathways and show unwanted side effects especially when used at higher concentrations. Since the concentrations required to induce cell death in hypoxic tumor spheroid regions *in vitro* (> 1 µM) are higher than the dosage used to treat patients with psychosis (accessdata.fda.gov., 2017), an increase of side effects in cancer studies might be expected. Indeed, concentrations needed for trifluoperazine to reduce the tumor size in mice demonstrated a considerable toxicity after longer incubation (Wu et al., 2016). Therefore, a direct use of the identified hypoxia-sensitizing compounds to target hypoxic tumor cells *in vivo* is rather unlikely and an application as lead compound to develop drugs with improved antitumor efficacy and reduced toxicity might be more probable. Moreover, improving *in vivo* models, for example by using cancer cells that are more likely to form hypoxic tumors and/or show reduced levels of SM compared to non-tumor cells (Hendrich and Michalak, 2003, Barceló-Coblijn et al., 2011) could enhance the effectiveness of these treatments. Additionally, combination studies with cytostatic drugs that target proliferating cells in non-hypoxic tumor areas could be beneficial (Yeh et al., 2012). On the other hand, co-treatment with mTOR inhibitors, that have also been used

as anti-cancer treatment (Zaytseva et al., 2012), should be avoided as the here presented findings demonstrate a rescue instead of an increase of hypoxia-specific cell death by fluphenazine (see Figure 26 and Supplementary Figure 5). Alternatively, hypoxia-selective compounds might be combined with anti-angiogenic therapies like VEGF inhibitors to prevent neo-vascularization and to increase the extent of hypoxic tumor regions (Ellis and Hicklin, 2008). However, a challenge of this approach will be the limited penetration of drugs through tumor tissue that will result from a reduced vascularization. Another strategy, that has been proven useful in targeted cancer therapy and could be used to reduce systemic toxicity of hypoxia-sensitizing drugs, is the linkage of small molecule inhibitors to tumor surface marker specific antibodies (Panowski et al., 2014, Chudasama et al., 2016). The distinct expression of hypoxia-regulated proteins (Harris, 2002) provides a good opportunity for this approach and could possibly reduce side effects by decreasing the concentration needed for *in vivo* efficacy.

5. Conclusion and outlook

Hypoxia is a characteristic of many solid tumors that contributes to resistance development and treatment failure. However, the availability of specific and effective drugs and physiologically-relevant *in vitro* screening models is limited. This study validated the use of tumor spheroids incubated under reduced oxygen conditions as an *in vitro* model for tumor hypoxia and identified in a small-molecule-screen hypoxia-selective hits that induce cancer cell death only in hypoxic but not normoxic conditions. Two of these hits were found to impact glucose uptake and glycolysis which is consistent with previous literature on glycolysis inhibition as treatment strategy for tumor hypoxia. Moreover, the study identified a group of compounds that act via a novel, yet unreported mode of action. Among those compounds the antipsychotic phenothiazine drug fluphenazine was identified as functional inhibitor of the lysosomal enzyme acid sphingomyelinase and induces cancer cell death in hypoxic tumor spheroids by elevating sphingomyelin levels. Furthermore, it was found that sphingomyelin accumulation by fluphenazine treatment overactivates the hypoxia response pathways HIF-1 and ATF4-dependent ER stress signaling and thereby promotes their pro-apoptotic tumor suppressor functions. Moreover, gene knockdown studies evaluated ATF4 as driver for the induction of hypoxia specific tumor spheroid cell death.

These results provide further insight into the survival of cancer cells in hypoxic tumor regions and propose the inhibition of sphingomyelin metabolism as potential novel target approach that could contribute to the development of new hypoxia specific anti-cancer drugs. Future studies developing direct inhibitors need to clarify the role of acid sphingomyelinase inhibition in tumor hypoxia and its potential as anti-cancer approach.

Moreover, the here validated spheroid hypoxia model might be used for larger lead finding approaches using bigger screening libraries. Indeed, this study formed the basis for a large compound screen at Bayer AG covering more than half a million small-molecule-inhibitors and led to the identification of hypoxia-specific compounds with significantly higher *in vitro* potency than fluphenazine. Additionally, the results from this work substantially contributed to the target deconvolution of these hits. Subsequent *in vivo* studies need to address the clinical potential of the newly identified hypoxia sensitizing compounds and clarify their future prospect as anti-cancer drug.

6. Highlights

- Established and validated a 3D tumor spheroid model to mimic tumor hypoxia

- First-ever reported high-content screen on hypoxic tumor spheroids to identify hypoxia-sensitizing compounds that specifically induce cell death in hypoxic tumor spheroid regions

- Small-molecule-screen confirmed GLUT and glycolysis inhibition as potential treatment strategy in hypoxic tumors and identified the antipsychotic drug fluphenazine and other structurally related phenothiazines as hypoxia-selective compounds

- Discovered a novel, yet unreported mode of action for the hypoxia-sensitizer fluphenazine as functional inhibitor of the lysosomal enzyme acid sphingomyelinase that induces lipid stress by cellular sphingomyelin accumulation

- Proposed sphingomyelin accumulation as potential novel treatment strategy in hypoxic tumors that potentiates ATF4 dependent signaling and shifts the balance of cellular stress pathways to a pro-apoptotic response specifically in severe hypoxic conditions

References

Accessdata.Fda.Gov. 2017. *Drugs@FDA: FDA Approved Drug Products* [Online]. Available: https://www.accessdata.fda.gov/scripts/cder/daf/ [Accessed 26. August 2017].

Ader, I., Malavaud, B. & Cuvillier, O. 2009. When the sphingosine kinase 1/sphingosine 1-phosphate pathway meets hypoxia signaling: new targets for cancer therapy. *Cancer Res,* 69**,** 3723-6.

Aebersold, D. M., Burri, P., Beer, K. T., Laissue, J., Djonov, V., Greiner, R. H., et al. 2001. Expression of hypoxia-inducible factor-1alpha: a novel predictive and prognostic parameter in the radiotherapy of oropharyngeal cancer. *Cancer Res,* 61.

Aits, S. & Jaattela, M. 2013. Lysosomal cell death at a glance. *J Cell Sci,* 126**,** 1905-12.

Aits, S., Kricker, J., Liu, B., Ellegaard, A. M., Hamalisto, S., Tvingsholm, S., et al. 2015. Sensitive detection of lysosomal membrane permeabilization by lysosomal galectin puncta assay. *Autophagy,* 11**,** 1408-24.

Alizadeh, A. A., Eisen, M. B., Davis, R. E., Ma, C., Lossos, I. S. & Rosenwald, A. 2000. Distinct types of diffuse large B-cell lymphoma identified by gene expression profiling. *Nature,* 403**,** 9.

Altan, N., Chen, Y., Schindler, M. & Simon, S. M. 1999. Tamoxifen inhibits acidification in cells independent of the estrogen receptor. *Proc. Natl. Acad. Sci. USA,* 96**,** 4432–4437.

Arora, V. K., Schenkein, E., Murali, R., Subudhi, S. K., Wongvipat, J., Balbas, M. D., et al. 2013. Glucocorticoid receptor confers resistance to antiandrogens by bypassing androgen receptor blockade. *Cell,* 155**,** 1309-22.

Barceló-Coblijn, G., Martin, M. L., De Almeida, R. F., Noguera-Salvà, M. A., Marcilla-Etxenike, A., Guardiola-Serrano, F., et al. 2011. Sphingomyelin and sphingomyelin synthase (SMS) in the malignant transformation of glioma cells and in 2-hydroxyoleic acid therapy. *Proc Natl Acad Sci U S A,* 108**,** 6.

Barker, H. E., Paget, J. T., Khan, A. A. & Harrington, K. J. 2015. The tumour microenvironment after radiotherapy: mechanisms of resistance and recurrence. *Nat Rev Cancer,* 15**,** 409-25.

Barron, C. C., Bilan, P. J., Tsakiridis, T. & Tsiani, E. 2016. Facilitative glucose transporters: Implications for cancer detection, prognosis and treatment. *Metabolism,* 65**,** 124-39.

Beckmann, N., Sharma, D., Gulbins, E., Becker, K. A. & Edelmann, B. 2014. Inhibition of acid sphingomyelinase by tricyclic antidepressants and analogons. *Front Physiol,* 5**,** 331.

Beitner-Johnson, D., Leibold, J. & Millhorn, D. E. 1998. Hypoxia regulates the cAMP- and Ca2+/calmodulin signaling systems in PC12 cells. *Biochem Biophys Res Commun,* 242**,** 61-6.

Bi, M., Naczki, C., Koritzinsky, M., Fels, D., Blais, J., Hu, N., et al. 2005. ER stress-regulated translation increases tolerance to extreme hypoxia and promotes tumor growth. *EMBO J,* 24**,** 12.

Bizzozero, L., Cazzato, D., Cervia, D., Assi, E., Simbari, F., Pagni, F., et al. 2013. Acid sphingomyelinase determines melanoma progression and metastatic behaviour via the microphtalmia-associated transcription factor signalling pathway. *Cell Death and Differentiation,* 21**,** 507-520.

Bonadonna, G., Brusamolino, E., Valagussa, P., Rossi, A., Brugnatelli, L., Brambilla, C., et al. 1976. Combination chemotherapy as an adjuvant treatment in operable breast cancer. *N Engl J Med,* 294**,** 6.

Borcherding, D. C., Tong, W., Hugo, E. R., Barnard, D. F., Fox, S., Lasance, K., et al. 2016. Expression and therapeutic targeting of dopamine receptor-1 (D1R) in breast cancer. *Oncogene,* 35**,** 3103-13.

Boveri, T. 1914. *Zur Frage der Entwicklung maligner Tumoren.,* Jena, Gustav Fischer-Verlag.

Bristow, R. G. & Hill, R. P. 2008. Hypoxia and metabolism. Hypoxia, DNA repair and genetic instability. *Nat Rev Cancer,* 8**,** 180-92.

Burroughs, S. K., Kaluz, S., Wang, D., Wang, K., Van Meir, E. G. & Wang, B. 2013. Hypoxia inducible factor pathway inhibitors as anticancer therapeutics. *Future Med Chem,* 5**,** 553-72.

Cairns, R. A., Harris, I. S. & Mak, T. W. 2011. Regulation of cancer cell metabolism. *Nat Rev Cancer,* 11**,** 85-95.

Cancer Genome Atlas, N. 2012. Comprehensive molecular portraits of human breast tumours. *Nature,* 490**,** 61-70.

Chang, T. T. & Hughes-Fulford, M. 2009. Monolayer and spheroid culture of human liver hepatocellular carcinoma cell line cells demonstrate distinct global gene expression patterns and functional phenotypes. *Tissue Eng Part A,* 15**,** 9.

Chen, X., Iliopoulos, D., Zhang, Q., Tang, Q., Greenblatt, M. B., Hatziapostolou, M., et al. 2014. XBP1 promotes triple-negative breast cancer by controlling the HIF1alpha pathway. *Nature,* 508**,** 103-7.

Chouaib, S., Noman, M. Z., Kosmatopoulos, K. & Curran, M. A. 2016. Hypoxic stress: obstacles and opportunities for innovative immunotherapy of cancer. *Oncogene*.

Chudasama, V., Maruani, A. & Caddick, S. 2016. Recent advances in the construction of antibody–drug conjugates. *Nature Chemistry*.

Corazzari, M., Gagliardi, M., Fimia, G. M. & Piacentini, M. 2017. Endoplasmic Reticulum Stress, Unfolded Protein Response, and Cancer Cell Fate. *Front Oncol,* 7**,** 78.

Cutts, J. H., Beer, C. T. & Noble, R. L. 1960. Biological properties of Vincaleukoblastine, an alkaloid in Vinca rosea Linn, with reference to its antitumor action. *Cancer Res,* 20**,** 10.

Davis, M. E., Zuckerman, J. E., Choi, C. H., Seligson, D., Tolcher, A., Alabi, C. A., et al. 2010. Evidence of RNAi in humans from systemically administered siRNA via targeted nanoparticles. *Nature,* 464**,** 1067-70.

Dengler, V. L., Galbraith, M. D. & Espinosa, J. M. 2014. Transcriptional regulation by hypoxia inducible factors. *Crit Rev Biochem Mol Biol,* 49**,** 1-15.

Deves, R. & Krupka, R. M. 1978. Cytochalasin B and the kinetics of inhibition of biological transport *Biochimica et Biophysica Acta,* 510**,** 339-48.

Devita, V. T. J. & Rosenberg, S. A. 2012. Two hundred years of cancer research. *N Engl J Med,* 366**,** 8.

Doll, R. & Hill, A. B. 1956. Lung cancer and other causes of death in relation to smoking: a second report on the mortality of British doctors. *BMJ,* 233**,** 11.

Dragani, T. A., Castells, A., Kulasingam, V., Diamandis, E. P., Earl, H., Iams, W. T., et al. 2016. Major milestones in translational oncology. *BMC Med,* 14**,** 110.

Ehrlich, P. 1909. Über den jetzigen stand der karzinomforschung. *Ned Tijdschr Geneeskd.,* 5**,** 18.

Eich, C., Manzo, C., De Keijzer, S., Bakker, G. J., Reinieren-Beeren, I., Garcia-Parajo, M. F., et al. 2016. Changes in membrane sphingolipid composition modulate dynamics and adhesion of integrin nanoclusters. *Sci Rep,* 6**,** 20693.

Ellegaard, A. M., Dehlendorff, C., Vind, A. C., Anand, A., Cederkvist, L., Petersen, N. H., et al. 2016. Repurposing Cationic Amphiphilic Antihistamines for Cancer Treatment. *EBioMedicine,* 9**,** 130-9.

Ellegaard, A. M., Groth-Pedersen, L., Oorschot, V., Klumperman, J., Kirkegaard, T., Nylandsted, J., et al. 2013. Sunitinib and SU11652 inhibit acid sphingomyelinase, destabilize lysosomes, and inhibit multidrug resistance. *Mol Cancer Ther,* 12**,** 2018-30.

Ellinghaus, P., Heisler, I., Unterschemmann, K., Haerter, M., Beck, H., Greschat, S., et al. 2013. BAY 87-2243, a highly potent and selective inhibitor of hypoxia-induced gene activation has antitumor activities by inhibition of mitochondrial complex I. *Cancer Med,* 2**,** 611-24.

Ellis, L. M. & Hicklin, D. J. 2008. VEGF-targeted therapy: mechanisms of anti-tumour activity. *Nat Rev Cancer,* 8**,** 579-91.

Emerling, B. M., Platanias, L. C., Black, E., Nebreda, A. R., Davis, R. J. & Chandel, N. S. 2005. Mitochondrial reactive oxygen species activation of p38 mitogen-activated protein kinase is required for hypoxia signaling. *Mol Cell Biol,* 25**,** 4853-62.

Engelman, J. A., Zejnullahu, K., Mitsudomi, T., Song, Y., Hyland, C., Park, J. O., et al. 2007. MET amplification leads to gefitinib resistance in lung cancer by activating ERBB3 signaling. *Science,* 316**,** 4.

Farber, S. & Diamond, L. K. 1948. Temporary remissions in acute leukemia in children produced by folic acid antagonist, 4-aminopteroyl-glutamic acid. *N Engl J Med,* 328**,** 7.

Fehrenbacher, N., Gyrd-Hansen, M., Poulsen, B., Felbor, U., Kallunki, T., Boes, M., et al. 2004. Sensitization to the lysosomal cell death pathway upon immortalization and transformation. *Cancer Res,* 64**,** 11.

Fisher, B., Redmond, C., Fisher, E. R., Bauer, M., Wolmark, N., Wickerham, D. L., et al. 1985. Ten-year results of a randomized clinical trial comparing radical mastectomy and total mastectomy with or without radiation. *N Engl J Med,* 312**,** 8.

Fox, C. A., Mansour, A. & Watson, S. J. J. 1994. The effects of haloperidol on dopamine receptor gene expression. *Exp Neurol.,* 130**,** 288-303.

Fuchs, B. C., Fujii, T., Dorfman, J. D., Goodwin, J. M., Zhu, A. X., Lanuti, M., et al. 2008. Epithelial-to-mesenchymal transition and integrin-linked kinase mediate sensitivity to epidermal growth factor receptor inhibition in human hepatoma cells. *Cancer Res,* 68**,** 2391-9.

Galadari, S., Rahman, A., Pallichankandy, S. & Thayyullathil, F. 2015. Tumor suppressive functions of ceramide: evidence and mechanisms. *Apoptosis,* 20**,** 689-711.

Galizzi, J. P., Fosset, M., Romey, G., Laduron, P. & Lazdunski, M. 1986. Neuroleptics of the diphenylbutylpiperidine series are potent calcium channel inhibitors. *Proc. Natl. Acad. Sci. USA,* 83**,** 7513-7517.

Ganapathy-Kanniappan, S. & Geschwind, J. F. 2013. Tumor glycolysis as a target for cancer therapy: progress and prospects. *Mol Cancer,* 12**,** 11.

Garg, A. D., Maes, H., Van Vliet, A. R. & Agostinis, P. 2015. Targeting the hallmarks of cancer with therapy-induced endoplasmic reticulum (ER) stress. *Mol Cell Oncol,* 2**,** e975089.

Gavande, N. S., Vandervere-Carozza, P. S., Hinshaw, H. D., Jalal, S. I., Sears, C. R., Pawelczak, K. S., et al. 2016. DNA repair targeted therapy: The past or future of cancer treatment? *Pharmacol Ther,* 160**,** 65-83.

Giampietri, C., Petrungaro, S., Conti, S., Facchiano, A., Filippini, A. & Ziparo, E. 2015. Cancer Microenvironment and Endoplasmic Reticulum Stress Response. *Mediators Inflamm,* 2015**,** 417281.

Giang, I., Boland, E. L. & Poon, G. M. 2014. Prodrug applications for targeted cancer therapy. *AAPS J,* 16**,** 899-913.

Girard, Y. K., Wang, C., Ravi, S., Howell, M. C., Mallela, J., Alibrahim, M., et al. 2013. A 3D fibrous scaffold inducing tumoroids: a platform for anticancer drug development. *PLoS One,* 8**,** 11.

Gorelik, A., Illes, K., Heinz, L. X., Superti-Furga, G. & Nagar, B. 2016. Crystal structure of mammalian acid sphingomyelinase. *Nat Commun,* 7**,** 12196.

Gotwals, P., Cameron, S., Cipolletta, D., Cremasco, V., Crystal, A., Hewes, B., et al. 2017. Prospects for combining targeted and conventional cancer therapy with immunotherapy. *Nat Rev Cancer,* 17**,** 286-301.

Grammatikos, G., Teichgraber, V., Carpinteiro, A., Trarbach, T., Weller, M., Hengge, U. R., et al. 2007. Overexpression of acid sphingomyelinase sensitizes glioma cells to chemotherapy. *Antioxid Redox Signal,* 9**,** 1449-56.

Granchi, C., Fancelli, D. & Minutolo, F. 2014. An update on therapeutic opportunities offered by cancer glycolytic metabolism. *Bioorg Med Chem Lett,* 24**,** 4915-25.

Greijer, A. E. & Van Der Wall, E. 2004. The role of hypoxia inducible factor 1 (HIF-1) in hypoxia induced apoptosis. *J Clin Pathol,* 57**,** 1009-14.

Halliwell, W. H. 1997. Cationic Amphiphilic Drug-Induced Phospholipidosis. *Toxicologic Pathology,* 25**,** 53-60.

Ham, S. L., Joshi, R., Thakuri, P. S. & Tavana, H. 2016. Liquid-based three-dimensional tumor models for cancer research and drug discovery. *Exp Biol Med (Maywood),* 241**,** 939-54.

Han, J., Back, S. H., Hur, J., Lin, Y. H., Gildersleeve, R., Shan, J., et al. 2013. ER-stress-induced transcriptional regulation increases protein synthesis leading to cell death. *Nat Cell Biol,* 15**,** 481-90.

Hannon, G. J. 2002. RNA interference. *Nature,* 18**,** 8.

Harper, D. M., Vierthaler, S. L. & Santee, J. A. 2010. Review of Gardasil. *J Vaccines Vaccin,* 1.

Harris, A. L. 2002. Hypoxia--a key regulatory factor in tumour growth. *Nat Rev Cancer,* 2**,** 38-47.

Harris, W. P., Mostaghel, E. A., Nelson, P. S. & Montgomery, B. 2009. Androgen deprivation therapy: progress in understanding mechanisms of resistance and optimizing androgen depletion. *Nature Clinical Practice Urology,* 6**,** 76-85.

Helbig, L., Koi, L., Bruchner, K., Gurtner, K., Hess-Stumpp, H., Unterschemmann, K., et al. 2014. Hypoxia-inducible factor pathway inhibition resolves tumor hypoxia and improves local tumor control after single-dose irradiation. *Int J Radiat Oncol Biol Phys,* 88**,** 159-66.

Hendrich, A. B. & Michalak, K. 2003. Lipids as a Target for Drugs Modulating Multidrug Resistance of Cancer

Cells. *Curr Drug Targets,* 4**,** 8.

Henze, A.-T. & Acker, T. 2014. Feedback regulators of hypoxia-inducible factors and their role in cancer biology. *Cell Cycle,* 9**,** 2821-2835.

Herrmann, D., Conway, J. R., Vennin, C., Magenau, A., Hughes, W. E., Morton, J. P., et al. 2014. Three-dimensional cancer models mimic cell-matrix interactions in the tumour microenvironment. *Carcinogenesis,* 35**,** 1671-9.

Hirschhaeuser, F., Menne, H., Dittfeld, C., West, J., Mueller-Klieser, W. & Kunz-Schughart, L. A. 2010. Multicellular tumor spheroids: an underestimated tool is catching up again. *J Biotechnol,* 148**,** 3-15.

Holohan, C., Van Schaeybroeck, S., Longley, D. B. & Johnston, P. G. 2013. Cancer drug resistance: an evolving paradigm. *Nat Rev Cancer,* 13**,** 714-26.

Housman, G., Byler, S., Heerboth, S., Lapinska, K., Longacre, M., Snyder, N., et al. 2014. Drug resistance in cancer: an overview. *Cancers (Basel),* 6**,** 1769-92.

Hsu, C. W., Huang, R., Khuc, T., Shou, D., Bullock, J., Grooby, S., et al. 2016. Identification of approved and investigational drugs that inhibit hypoxia-inducible factor-1 signaling. *Oncotarget,* 7**,** 12.

Hu, Z. Y., Gong, Y. S. & Huang, W. L. 1992. Interaction of berbamine compound E6 and calmodulin-dependent myosin light chain kinase. *Biochem Pharmacol,* 44**,** 5.

Huebner, R. J. & Todaro, G. J. 1969. Oncogenes of RNA tumor viruses as determinants of cancer. *Proc. Natl Acad. Sci. USA,* 64**,** 8.

Hui, A. S., Bauer, A. L., Striet, J. B., Schnell, P. O. & Czyzyk-Krzeska, M. F. 2006. Calcium signaling stimulates translation of HIF-alpha during hypoxia. *FASEB J,* 20**,** 466-75.

Huss, M. & Wieczorek, H. 2009. Inhibitors of V-ATPases: old and new players. *J Exp Biol,* 212**,** 341-6.

Imming, P., Sinning, C. & Meyer, A. 2006. Drugs, their targets and the nature and number of drug targets. *Nat Rev Drug Discov,* 5**,** 15.

Jaakkola, P., Mole, D. R., Tian, Y. M., Wilson, M. I., Gielbert, J., Gaskell, S. J., et al. 2001. Targeting of HIF-α to the von Hippel-Lindau Ubiquitylation Complex by O2-Regulated Prolyl Hydroxylation. *Science,* 292**,** 468-72.

Jeong, S. Y., Lee, J. H., Shin, Y., Chung, S. & Kuh, H. J. 2016. Co-Culture of Tumor Spheroids and Fibroblasts in a Collagen Matrix-Incorporated Microfluidic Chip Mimics Reciprocal Activation in Solid Tumor Microenvironment. *PLoS One,* 11**,** e0159013.

Jiang, H. Y., Jiang, L. & Wek, R. C. 2007. The eukaryotic initiation factor-2 kinase pathway facilitates differential GADD45a expression in response to environmental stress. *J Biol Chem,* 282**,** 3755-65.

Johansson, A. C., Ansell, A., Jerhammar, F., Lindh, M. B., Grenman, R., Munck-Wikland, E., et al. 2012. Cancer-associated fibroblasts induce matrix metalloproteinase-mediated cetuximab resistance in head and neck squamous cell carcinoma cells. *Mol Cancer Res,* 10**,** 1158-68.

Johnke, R. M., Sattler, J. A. & Allison, R. R. 2014. Radioprotective agents for radiation therapy: future trends. *Future Oncol,* 10**,** 13.

Johnston, P. G. & Kaye, S. 2001. Capecitabine: a novel agent for the treatment of solid tumors. *Anticancer Drugs,* 12**,** 8.

Jung, H. J., Kim, J. H., Shim, J. S. & Kwon, H. J. 2010. A novel Ca2+/calmodulin antagonist HBC inhibits angiogenesis and down-regulates hypoxia-inducible factor. *J Biol Chem,* 285**,** 25867-74.

Kanasty, R. L., Whitehead, K. A., Vegas, A. J. & Anderson, D. G. 2012. Action and reaction: the biological response to siRNA and its delivery vehicles. *Mol Ther,* 20**,** 513-24.

Kapuy, O., Vinod, P. K. & Banhegyi, G. 2014. mTOR inhibition increases cell viability via autophagy induction during endoplasmic reticulum stress - An experimental and modeling study. *FEBS Open Bio,* 4**,** 704-13.

Karantanos, T., Corn, P. G. & Thompson, T. C. 2013. Prostate cancer progression after androgen deprivation therapy: mechanisms of castrate resistance and novel therapeutic approaches. *Oncogene,* 32**,** 5501-11.

Karolewicz, B., Antkiewicz-Michaluk, L., Michaluk, J. & Vetulani, J. 1996. Different effects of chronic administration of haloperidol and pimozide on dopamine metabolism in the rat brain. *Eur J Pharmacol,* 313**,** 181-6.

Kasahara, T., Tomita, K., Murano, H., Harada, T., Tsubakimoto, K., Ogihara, T., et al. 2006. Establishment of an in vitro high-throughput screening assay for detecting phospholipidosis-inducing potential. *Toxicol Sci,* 90**,** 133-41.

Kim, I., Xu, W. & Reed, J. C. 2008. Cell death and endoplasmic reticulum stress: disease relevance and therapeutic opportunities. *Nat Rev Drug Discov,* 7**,** 1013-30.

Kim, J. W., Ho, W. J. & Wu, B. M. 2011. The role of the 3D environment in hypoxia-induced drug and apoptosis resistance. *Anticancer Res.,* 31**,** 9.

Klutzny, S., Lesche, R., Keck, M., Kaulfuss, S., Schlicker, A., Christian, S., et al. 2017. Functional inhibition of acid sphingomyelinase by Fluphenazine triggers hypoxia-specific tumor cell death. *Cell Death Dis,* 8**,** e2709.

Kobayashi, S., Boggon, T. J., Dayaram, T., Jänne, P. A., Kocher, O., Meyerson, M., et al. 2005. EGFR mutation and resistance of non-small-cell lung cancer to gefitinib. *N Engl J Med,* 352**,** 7.

Köditz, J., Nesper, J., Wottawa, M., Stiehl, D., Camenisch, G., Franke, C., et al. 2007. Oxygen-dependent ATF-4 stability is mediated by the PHD3 oxygen sensor. *Blood,* 110**,** 3610-7.

Koh, M. Y. & Powis, G. 2012. Passing the baton: the HIF switch. *Trends Biochem Sci,* 37**,** 364-72.

Köhler, G. & Milstein, C. 1975. Continuous cultures of fused cells secreting antibody of predefined specificity. *Nature,* 256**,** 3.

Kölzer, M., Werth, N. & Sandhoff, K. 2004. Interactions of acid sphingomyelinase and lipid bilayers in the presence of the tricyclic antidepressant desipramine. *FEBS Letters,* 559**,** 96-98.

Kondratskyi, A., Yassine, M., Slomianny, C., Kondratska, K., Gordienko, D., Dewailly, E., et al. 2014. Identification of ML-9 as a lysosomotropic agent targeting autophagy and cell death. *Cell Death Dis,* 5**,** e1193.

Koong, A. C., Chauhan, V. & Romero-Ramirez, L. 2014. Targeting XBP-1 as a novel anti-cancer strategy. *Cancer Biology & Therapy,* 5**,** 756-759.

Koumenis, C. & Wouters, B. G. 2006. "Translating" tumor hypoxia: unfolded protein response (UPR)-dependent and UPR-independent pathways. *Mol Cancer Res,* 4**,** 423-36.

Kroemer, G. & Pouyssegur, J. 2008. Tumor cell metabolism: cancer's Achilles' heel. *Cancer Cell,* 13**,** 472-82.

Ku, S. Y., Rosario, S., Wang, Y., Mu, P., Seshadri, M., Goodrich, Z. W., et al. 2017. Rb1 and Trp53 cooperate to suppress prostate cancer lineage plasticity, metastasis, and antiandrogen resistance. *Science,* 355**,** 6.

Kunkel, G. T., Maceyka, M., Milstien, S. & Spiegel, S. 2013. Targeting the sphingosine-1-phosphate axis in cancer, inflammation and beyond. *Nat Rev Drug Discov,* 12**,** 688-702.

Kwon, H. C., Roh, M. S., Oh, S. Y., Kim, S. H., Kim, M. C., Kim, J. S., et al. 2007. Prognostic value of expression of ERCC1, thymidylate synthase, and glutathione S-transferase P1 for 5-fluorouracil/oxaliplatin chemotherapy in advanced gastric cancer. *Ann Oncol,* 18**,** 504-9.

Kyle, A. H., Baker, J. H. & Minchinton, A. I. 2012. Targeting quiescent tumor cells via oxygen and IGF-I supplementation. *Cancer Res,* 72**,** 801-9.

Lagory, E. L. & Giaccia, A. J. 2016. The ever-expanding role of HIF in tumour and stromal biology. *Nature Cell Biology,* 18**,** 356-65.

Land, S. C. & Tee, A. R. 2007. Hypoxia-inducible factor 1alpha is regulated by the mammalian target of rapamycin (mTOR) via an mTOR signaling motif. *J Biol Chem,* 282**,** 20534-43.

Leksell, L. 1983. Stereotactice radiasurgery. *J Neurol Neurosurg Psychiatry,* 46**,** 7.

Liu, W., Shen, S. M., Zhao, X. Y. & Chen, G. Q. 2012. Targeted genes and interacting proteins of hypoxia inducible factor-1. *Int J Biochem Mol Biol,* 3**,** 14.

Lohmueller, J. J., Sato, S., Popova, L., Chu, I. M., Tucker, M. A., Barberena, R., et al. 2016. Antibodies elicited by the first non-viral prophylactic cancer vaccine show tumor-specificity and immunotherapeutic potential. *Sci Rep,* 6**,** 31740.

Lopes, M. C., Vale, M. G. & Carvalho, A. P. 1990. Ca2(+)-dependent binding of tamoxifen to calmodulin isolated from bovine brain. *Cancer Res,* 50**,** 6.

Love, M. I., Huber, W. & Anders, S. 2014. Moderated estimation of fold change and dispersion for RNA-seq data with DESeq2. *Genome Biol,* 15**,** 550.

Maeda, M., Hasebe, Y., Egawa, K., Shibanuma, M. & K., N. 2006. Inhibition of angiogenesis and HIF-1alpha activity by antimycin A1. *Biol Pharm Bull,* 29**,** 5.

Marciniak, S. J., Yun, C. Y., Oyadomari, S., Novoa, I., Zhang, Y., Jungreis, R., et al. 2004. CHOP induces death by promoting protein synthesis and oxidation in the stressed endoplasmic reticulum. *Genes Dev. ,* 18**,** 3066-77.

Maschek, G., Savaraj, N., Priebe, W., Braunschweiger, P., Hamilton, K., Tidmarsh, G. F., et al. 2004. 2-deoxy-D-glucose increases the efficacy of adriamycin and paclitaxel in human osteosarcoma and non-small cell lung cancers in vivo. *Cancer Res,* 64**,** 4.

Masoud, G. N. & Li, W. 2015. HIF-1alpha pathway: role, regulation and intervention for cancer therapy. *Acta Pharm Sin B,* 5**,** 378-89.

Matsumura, C., Kuwashima, H. & Kimura, T. 1999. Myosin light chain kinase inhibitors and calmodulin antagonist inhibit Ca(2+)- and ATP-dependent catecholamine secretion from bovine adrenal chromaffin cells. *J Auton Pharmacol,* 19**,** 7.

Mcintyre, A. & Harris, A. L. 2015. Metabolic and hypoxic adaptation to anti-angiogenic therapy: a target for induced essentiality. *EMBO Mol Med,* 7**,** 368-79.

Mi, Y., Shao, Z., Vang, J., Kaidar-Person, O. & Wang, A. Z. 2016. Application of nanotechnology to cancer radiotherapy. *Cancer Nanotechnol,* 7**,** 11.

Molina, M. A., Codony-Servat, J., Albanell, J., Rojo, F., Arribas, J. & Baselga, J. 2001. Trastuzumab (herceptin), a humanized anti-Her2 receptor monoclonal antibody, inhibits basal and activated Her2 ectodomain cleavage in breast cancer cells. *Cancer Res,* 61**,** 6.

Monographs.Iarc.Fr. 2017. *Agents Classified by the IARC Monographs* [Online]. Available: http://monographs.iarc.fr/ENG/Classification/ [Accessed 24. July 2017].

Mu, P., Zhang, Z., Benelli, M., Karthaus, W. R., Hoover, E., Chen, C. C., et al. 2017. SOX2 promotes lineage plasticity and antiandrogen resistance in TP53- and RB1-deficient prostate cancer. *Science,* 355**,** 5.

Muehlbacher, M., Tripal, P., Roas, F. & Kornhuber, J. 2012. Identification of drugs inducing phospholipidosis by novel in vitro data. *ChemMedChem,* 7**,** 1925-34.

Multhoff, G., Radons, J. & Vaupel, P. 2014. Critical role of aberrant angiogenesis in the development of tumor hypoxia and associated radioresistance. *Cancers (Basel),* 6**,** 813-28.

Murai, T. 2012. The role of lipid rafts in cancer cell adhesion and migration. *Int J Cell Biol,* 2012**,** 763283.

Nadanaciva, S., Lu, S., Gebhard, D. F., Jessen, B. A., Pennie, W. D. & Will, Y. 2011. A high content screening assay for identifying lysosomotropic compounds. *Toxicol In Vitro,* 25**,** 715-23.

Nagelkerke, A., Bussink, J., Mujcic, H., Wouters, B. G., Lehmann, S., Sweep, F. C., et al. 2013. Hypoxia stimulates migration of breast cancer cells via the PERK/ATF4/LAMP3-arm of the unfolded protein response. *Breast Cancer Res,* 15.

Nagy, J. A., Chang, S. H., Dvorak, A. M. & Dvorak, H. F. 2009. Why are tumour blood vessels abnormal and why is it important to know? *Br J Cancer,* 100**,** 865-9.

Neto, A. I., Correia, C. R., Oliveira, M. B., Rial-Hermida, M. I., Alvarez-Lorenzo, C., Reis, R. L., et al. 2015. A novel hanging spherical drop system for the generation of cellular spheroids and high throughput combinatorial drug screening. *Biomater. Sci.,* 3**,** 581-585.

Ni Chonghaile, T., Sarosiek, K. A., Vo, T. T., Ryan, J. A., Tammareddi, A., Moore Vdel, G., et al. 2011. Pretreatment mitochondrial priming correlates with clinical response to cytotoxic chemotherapy. *Science,* 334**,** 1129-33.

Nirenberg, M. W. & Matthaei, J. H. 1961. The dependence of cell-free protein synthesis in E. coli upon naturally occurring or synthetic polyribonucleotides. *Proc Natl Acad Sci USA,* 47**,** 15.

Niu, G. & Chen, X. 2010. Vascular endothelial growth factor as an anti-angiogenic target for cancer therapy. *Curr Drug Targets,* 11**,** 18.

Olive, P. L., Banáth, J. P. & Durand, R. E. 2002. The Range of Oxygenation in SiHa Tumor Xenografts. *Radiation Research,* 158**,** 8.

Oppermann, H., Levinson, A. D., Varmus, H. E., Levintow, L. & Bishop, J. M. 1979. Uninfected vertebrate cells contain a protein that is closely related to the product of the avian sarcoma virus transforming gene (src). *Proc. Natl Acad. Sci. USA,* 76**,** 5.

Osawa, M., Swindells, M. B., Tanikawa, J., Tanaka, T., Mase, T., Furuya, T., et al. 1998. Solution structure of calmodulin-W-7 complex: the basis of diversity in molecular recognition. *J Mol Biol,* 276**,** 12.

Osawa, Y., Suetsugu, A., Matsushima-Nishiwaki, R., Yasuda, I., Saibara, T., Moriwaki, H., et al. 2013. Liver acid sphingomyelinase inhibits growth of metastatic colon cancer. *J Clin Invest,* 123**,** 10.

Paget, S. 1889. The distribution of secondary growths in cancer of the breast. *Lancet,* 1**,** 3.

Pakos-Zebrucka, K., Koryga, I., Mnich, K., Ljujic, M., Samali, A. & Gorman, A. M. 2016. The integrated stress response. *EMBO Rep,* 17**,** 1374-1395.

Panowski, S., Bhakta, S., Raab, H., Polakis, P. & Junutula, J. R. 2014. Site-specific antibody drug conjugates for cancer therapy. *MAbs,* 6**,** 34-45.

Pao, W., Miller, V. A., Politi, K. A., Riely, G. J., Somwar, R., Zakowski, M. F., et al. 2005. Acquired resistance of lung adenocarcinomas to gefitinib or erlotinib is associated with a second mutation in the EGFR kinase domain. *PLoS Med,* 2**,** 11.

Parker, R. C., Varmus, H. E. & Bishop, J. M. 1984. Expression of v-src and chicken c-src in rat cells demonstrates qualitative differences between pp60v-src and pp60c-src. *Cell,* 37**,** 9.

Pelicano, H., Martin, D. S., Xu, R. H. & Huang, P. 2006. Glycolysis inhibition for anticancer treatment. *Oncogene,* 25**,** 4633-46.

Pereira, E. R., Frudd, K., Awad, W. & Hendershot, L. M. 2014. Endoplasmic reticulum (ER) stress and hypoxia response pathways interact to potentiate hypoxia-inducible factor 1 (HIF-1) transcriptional activity on targets like vascular endothelial growth factor (VEGF). *J Biol Chem,* 289**,** 3352-64.

Petersen, N. H., Olsen, O. D., Groth-Pedersen, L., Ellegaard, A. M., Bilgin, M., Redmer, S., et al. 2013. Transformation-associated changes in sphingolipid metabolism sensitize cells to lysosomal cell death induced by inhibitors of acid sphingomyelinase. *Cancer Cell,* 24**,** 379-93.

Pike, L. R., Singleton, D. C., Buffa, F., Abramczyk, O., Phadwal, K., Li, J. L., et al. 2013. Transcriptional up-regulation of ULK1 by ATF4 contributes to cancer cell survival. *Biochem J,* 449**,** 389-400.

Pinto, M. L., Rios, E., Silva, A. C., Neves, S. C., Caires, H. R., Pinto, A. T., et al. 2017. Decellularized human colorectal cancer matrices polarize macrophages towards an anti-inflammatory phenotype promoting cancer cell invasion via CCL18. *Biomaterials,* 124**,** 211-224.

Pornour, M., Ahangari, G., Hejazi, S. H. & Deezagi, A. 2015. New perspective therapy of breast cancer based on selective dopamine receptor D2 agonist and antagonist effects on MCF-7 cell line. *Recent Pat Anticancer Drug Discov,* 10**,** 10.

Prabhakar, N. R. & Semenza, G. L. 2012. Adaptive and maladaptive cardiorespiratory responses to continuous and intermittent hypoxia mediated by hypoxia-inducible factors 1 and 2. *Physiol Rev,* 92**,** 39.

Prates, C., Sousa, S., Oliveira, C. & Ikram, S. 2011. Prostate metastatic bone cancer in an Egyptian Ptolemaic mummy, a proposed radiological diagnosis. *In J of Paleopathology,* 1**,** 6.

Raez, L. E., Papadopoulos, K., Ricart, A. D., Chiorean, E. G., Dipaola, R. S., Stein, M. N., et al. 2012. A phase I dose-escalation trial of 2-deoxy-d-glucose alone or combined with docetaxel in patients with advanced solid tumors. *Cancer Chemotherapy and Pharmacology,* 71**,** 523-530.

Rautio, J., Kumpulainen, H., Heimbach, T., Oliyai, R., Oh, D., Järvinen, T., et al. 2008. Prodrugs: design and clinical applications. *Nature Reviews Drug Discovery,* 7**,** 255-270.

Rebucci, M. & Michiels, C. 2013. Molecular aspects of cancer cell resistance to chemotherapy. *Biochem Pharmacol,* 85**,** 1219-26.

Regazzetti, C., Bost, F., Le Marchand-Brustel, Y., Tanti, J. F. & Giorgetti-Peraldi, S. 2010. Insulin induces REDD1 expression through hypoxia-inducible factor 1 activation in adipocytes. *J Biol Chem,* 285**,** 5157-64.

Rodu, B. & Cole, P. 2002. Impact of the American anti-smoking campaign on lung cancer mortality. *Int J Cancer,* 97**,** 804-6.

Rohwer, N. & Cramer, T. 2011. Hypoxia-mediated drug resistance: novel insights on the functional interaction of HIFs and cell death pathways. *Drug Resist Updat,* 14**,** 191-201.

Romero-Ramirez, L., Cao, H., Nelson, D., Hammond, E., Lee, A. H., Yoshida, H., et al. 2004. XBP1 is essential for survival under hypoxic conditions and is required for tumor growth. *Cancer Res,* 64**,** 5.

Rosenberg, B., Vancamp, L., Trosko, J. E. & Mansour, V. H. 1969. Platinum compounds: a new class of potent antitumour agents. *Nature,* 222**,** 2.

Rosenberg, S. A., Mulé, J. J., Spiess, P. J., Reichert, C. M. & Schwarz, S. L. 1985. Regression of established pulmonary metastases and subcutaneous tumor mediated by the systemic administration of high-dose recombinant interleukin 2. *J Exp Med,* 161**,** 20.

Rous, P. 1910. A transmissible avian neoplasm (sarcoma of the common fowl). *J. Exp. Med.,* 12**,** 10.

Rzymski, T. & Harris, A. L. 2007. The unfolded protein response and integrated stress response to anoxia. *Clin Cancer Res,* 13**,** 2537-40.

Sachlos, E., Risueño, R. M., Laronde, S., Shapovalova, Z., Lee, J. H., Russell, J., et al. 2012. Identification of drugs including a dopamine receptor antagonist that selectively target cancer stem cells. *Cell,* 149**,** 14.

Santos, S. A. & Paulo, A. 2013. Small molecule inhibitors of multidrug resistance gene (MDR1) expression: preclinical evaluation and mechanisms of action. *Curr Cancer Drug Targets,* 13**,** 15.

Schork, N. J. 2015. Personalized medicine: Time for one-person trials. *Nature,* 520**,** 3.

Scott, A. M., Wolchok, J. D. & Old, L. J. 2012. Antibody therapy of cancer. *Nat Rev Cancer,* 12**,** 278-87.

Seeman, P., Corbett, R. & Van Tol, H. H. M. 1997. Atypixal Neuroleptics Have Low Affinity for Dopamine D2 Receptor or Are selective for D4 Receptors *Neuropsychpoharmacology,* 16**,** 93-110.

Semenza, G. L. 2003. Targeting HIF-1 for cancer therapy. *Nat Rev Cancer,* 3**,** 721-32.

Semenza, G. L. 2010. Defining the role of hypoxia-inducible factor 1 in cancer biology and therapeutics. *Oncogene,* 29**,** 625-34.

Semenza, G. L. 2012. Hypoxia-inducible factors: mediators of cancer progression and targets for cancer therapy. *Trends Pharmacol Sci.,* 33**,** 207–214.

Semenza, G. L. 2014. Oxygen sensing, hypoxia-inducible factors, and disease pathophysiology. *Annu Rev Pathol,* 9**,** 47-71.

Shayman, J. A. & Abe, A. 2013. Drug induced phospholipidosis: an acquired lysosomal storage disorder. *Biochim Biophys Acta,* 1831**,** 602-11.

Shin, D. H., Li, S. H., Chun, Y. S., Huang, L. E., Kim, M. S. & Park, J. W. 2008. CITED2 mediates the paradoxical responses of HIF-1alpha to proteasome inhibition. *Oncogene,* 27**,** 1939-44.

Silver, P. J. & Stull, J. T. 1983. Effects of the calmodulin antagonist, fluphenazine, on phosphorylation of myosin and phosphorylase in intact smooth muscle. *Mol Pharmacol,* 23**,** 6.

Smith, B. & Bhowmick, N. 2016. Role of EMT in Metastasis and Therapy Resistance. *Journal of Clinical Medicine,* 5**,** 17.

Smith, E. L. & Schuchman, E. H. 2008. The unexpected role of acid sphingomyelinase in cell death and the pathophysiology of common diseases. *FASEB J,* 22**,** 3419-31.

Sowter, H. M., Ratcliffe, P. J., Watson, P., Greenberg, A. H. & Harris, A. L. 2001. HIF-1-dependent Regulation of Hypoxic Induction of the Cell Death Factors BNIP3 and NIX in Human Tumors. *Cancer Res,* 61**,** 6.

Subramanian, A., Tamayo, P., Mootha, V. K., Mukherjee, S., Ebert, B. L., Gillette, M. A., et al. 2005. Gene set enrichment analysis: a knowledge-based approach for interpreting genome-wide expression profiles. *Proc Natl Acad Sci U S A,* 102**,** 15545-50.

Sudhakar, A. 2009. History of Cancer, Ancient and Modern Treatment Methods. *J Cancer Sci Ther,* 1**,** 1-4.

Sui, X., Chen, R., Wang, Z., Huang, Z., Kong, N., Zhang, M., et al. 2013. Autophagy and chemotherapy resistance: a promising therapeutic target for cancer treatment. *Cell Death and Disease,* 4**,** e838.

Sullivan, R., Pare, G. C., Frederiksen, L. J., Semenza, G. L. & Graham, C. H. 2008. Hypoxia-induced resistance to anticancer drugs is associated with decreased senescence and requires hypoxia-inducible factor-1 activity. *Mol Cancer Ther,* 7**,** 1961-73.

Sun, Y. 2016. Tumor microenvironment and cancer therapy resistance. *Cancer Lett,* 380**,** 205-15.

Swami, M. 2010. Proteomics: A discovery strategy for novel cancer biomarkers. *Nature Reviews Cancer,* 10**,** 597-597.

Swinney, D. C. & Anthony, J. 2011. How were new medicines discovered? *Nat Rev Drug Discov,* 10**,** 507-19.

Talevi, A. 2015. Multi-target pharmacology: possibilities and limitations of the "skeleton key approach" from a medicinal chemist perspective. *Front Pharmacol,* 6**,** 205.

Tan, C., De Noronha, R. G., Roecker, A. J., Pyrzynska, B., Khwaja, F., Zhang, Z., et al. 2005. Identification of a novel small-molecule inhibitor of the hypoxia-inducible factor 1 pathway. *Cancer Res,* 65**,** 8.

Taniguchi, M., Ogiso, H., Takeuchi, T., Kitatani, K., Umehara, H. & Okazaki, T. 2015. Lysosomal ceramide generated by acid sphingomyelinase triggers cytosolic cathepsin B-mediated degradation of X-linked inhibitor of apoptosis protein in natural killer/T lymphoma cell apoptosis. *Cell Death and Disease,* 6**,** e1717.

Teppo, S., Sundquist, E., Vered, M., Holappa, H., Parkkisenniemi, J., Rinaldi, T., et al. 2013. The hypoxic tumor microenvironment regulates invasion of aggressive oral carcinoma cells. *Experimental Cell Research,* 319**,** 376-389.

The-International-Human-Genome-Mapping-Consortium 2001. A physical map of the human genome. *Nature,* 409**,** 8.

Thoma, C. R., Zimmermann, M., Agarkova, I., Kelm, J. M. & Krek, W. 2014. 3D cell culture systems modeling tumor growth determinants in cancer target discovery. *Adv Drug Deliv Rev,* 69-70**,** 29-41.

Thomas, D. W., Burns, J., Audette, J., Carroll, A., Dow-Hygelund, C. & Hay, M. 2016. *Clinical Development Success Rates 2006-2015* [Online]. Available: https://www.bio.org/sites/default/files/Clinical%20Development%20Success%20Rates%2

02006-2015%20-%20BIO,%20Biomedtracker,%20Amplion%202016.pdf [Accessed 28.August 2017].
Tidow, H. & Nissen, P. 2013. Structural diversity of calmodulin binding to its target sites. *FEBS Journal,* 280**,** 15.
Townsend, D. M. & Tew, K. D. 2003. The role of glutathione-S-transferase in anti-cancer drug resistance. *Oncogene,* 22**,** 7369-75.
Treindl, F., Ruprecht, B., Beiter, Y., Schultz, S., Döttinger, A., Staebler, A., et al. 2016. A bead-based western for high-throughput cellular signal transduction analyses. *Nature Communications,* 7**,** 12852.
Trendowski, M. 2015. Using cytochalasins to improve current chemotherapeutic approaches. *Anticancer Agents Med Chem,* 15**,** 9.
Tsai, Y.-P. & Wu, K.-J. 2014. Epigenetic regulation of hypoxia-responsive gene expression: Focusing on chromatin and DNA modifications. *International Journal of Cancer,* 134**,** 249-256.
Ulanovskaya, O. A., Cui, J., Kron, S. J. & Kozmin, S. A. 2011. A pairwise chemical genetic screen identifies new inhibitors of glucose transport. *Chem Biol,* 18**,** 222-30.
Upreti, M., Jamshidi-Parsian, A., Koonce, N. A., Webber, J. S., Sharma, S. K., Asea, A. a. A., et al. 2011. Tumor-Endothelial Cell Three-dimensional Spheroids: New Aspects to Enhance Radiation and Drug Therapeutics. *Translational Oncology,* 4**,** 365-IN3.
Van 'T Veer, L. J., Dai, H., Van De Vijver, M. J., He, Y. D., Hart, A. a. M. & Mao, M. 2001. Gene expression profiling predicts clinical outcome of breast cancer. *Nature,* 415**,** 7.
Vandonselaar, M., Hickie, R. A., Quail, J. W. & Delbaere, L. T. 1994. Trifluoperazine-induced conformational change in Ca(2+)-calmodulin. *Nat Struct Biol,* 1**,** 7.
Vaupel, P. & Mayer, A. 2007. Hypoxia in cancer: significance and impact on clinical outcome. *Cancer Metastasis Rev,* 26**,** 225-39.
Vaupel, P., Thews, O. & Hoeckel, M. 2011. Treatment resistance of solid tumors: role of hypoxia and anemia. *Med Oncol,* 18**,** 59.
Virchow, R. L. K. 1863. *Cellular pathology as based upon physiological and pathological histology.,* Philadelphia, J.B. Lippincott.
Volmer, R. & Ron, D. 2015. Lipid-dependent regulation of the unfolded protein response. *Curr Opin Cell Biol,* 33**,** 67-73.
Von Hansemann, D. 1890. Ueber asymmetrische Zelltheilung in epithel Krebsen und deren biologische Bedeutung. *Virchow's Arch. Path. Anat.,* 119.
Wagner, E. F. & Nebreda, Á. R. 2009. Signal integration by JNK and p38 MAPK pathways in cancer development. *Nature Reviews Cancer,* 9**,** 537-549.
Walko, C. M. & Lindley, C. 2005. Capecitabine: a review. *Clin Ther,* 27**,** 22.
Wan, J. C., Massie, C., Garcia-Corbacho, J., Mouliere, F., Brenton, J. D., Caldas, C., et al. 2017. Liquid biopsies come of age: towards implementation of circulating tumour DNA. *Nat Rev Cancer,* 17**,** 223-238.
Wang, M. & Kaufman, R. J. 2014. The impact of the endoplasmic reticulum protein-folding environment on cancer development. *Nat Rev Cancer,* 14**,** 581-97.
Wang, W., Li, Q., Yamada, T., Matsumoto, K., Matsumoto, I., Oda, M., et al. 2009. Crosstalk to stromal fibroblasts induces resistance of lung cancer to epidermal growth factor receptor tyrosine kinase inhibitors. *Clin Cancer Res,* 15**,** 6630-8.
Ward, M. C., Ciezki, J. P. & Stephans, K. L. 2015. Brachytherapy. 79-96.
Watson, J. D. & Crick, F. H. C. 1953. Molecular Structure of Nucleic Acids: A Structure for Deoxyribose Nucleic Acid. *Nature,* 171**,** 2.
Weiss, B., Prozialeck, W., Cimino, M., Barnette, M. S. & Wallace, T. L. 1980. Pharmacological regulation of calmodulin. *Ann N Y Acad Sci,* 356**,** 27.
Wenzel, C., Otto, S., Prechtl, S., Parczyk, K. & Steigemann, P. 2015. A novel 3D high-content assay identifies compounds that prevent fibroblast invasion into tissue surrogates. *Exp Cell Res,* 339**,** 35-43.

Wenzel, C., Riefke, B., Grundemann, S., Krebs, A., Christian, S., Prinz, F., et al. 2014. 3D high-content screening for the identification of compounds that target cells in dormant tumor spheroid regions. *Exp Cell Res,* 323**,** 131-43.

White, E. 2012. Deconvoluting the context-dependent role for autophagy in cancer. *Nature Reviews Cancer,* 12**,** 401-410.

Who.Int. 2017. *Cancer* [Online]. Available: http://www.who.int/mediacentre/factsheets/fs297/en/ [Accessed 24. July 2017].

Wilson, W. R. & Hay, M. P. 2011. Targeting hypoxia in cancer therapy. *Nat Rev Cancer,* 11**,** 393-410.

Wouters, B. G. & Koritzinsky, M. 2008. Hypoxia signalling through mTOR and the unfolded protein response in cancer. *Nat Rev Cancer,* 8**,** 851-64.

Wu, C.-H., Bai, L.-Y., Tsai, M.-H., Chu, P.-C., Chiu, C.-F., Chen, M. Y., et al. 2016. Pharmacological exploitation of the phenothiazine antipsychotics to develop novel antitumor agents–A drug repurposing strategy. *Scientific Reports,* 6**,** 27540.

Wu, S. Y., Lopez-Berestein, G., Calin, G. A. & Sood, A. K. 2014. RNAi therapies: drugging the undruggable. *Sci Transl Med,* 6**,** 240ps7.

Wynder, E. L. & Graham, E. A. 1950. Tobacco smoking as a possible etiologic factor in bronchiogenic carcinoma. *JAMA,* 143**,** 7.

Xu, J. P. 2016. *Cancer Inhibitors from Chinese Natural Medicines*, CRC Press – Taylor & Francis Group.

Yang, C., He, L., He, P., Liu, Y., Wang, W., He, Y., et al. 2015. Increased drug resistance in breast cancer by tumor-associated macrophages through IL-10/STAT3/bcl-2 signaling pathway. *Med Oncol,* 32**,** 352.

Yang, Y., Zhang, J., Liu, H., Wang, J., Xin, J. & Deng, M. 2013. Changes in levels of hypoxia-induced mediators in rat hippocampus during chronic cerebral hypoperfusion. *Neurochem Res,* 38**,** 2433-9.

Yates, L. R. & Campbell, P. J. 2012. Evolution of the cancer genome. *Nat Rev Genet,* 13**,** 795-806.

Yeh, C. T., Wu, A. T., Chang, P. M., Chen, K. Y., Yang, C. N., Yang, S. C., et al. 2012. Trifluoperazine, an antipsychotic agent, inhibits cancer stem cell growth and overcomes drug resistance of lung cancer. *Am J Respir Crit Care Med,* 186**,** 1180-8.

Yip, K. W. & Reed, J. C. 2008. Bcl-2 family proteins and cancer. *Oncogene,* 27**,** 6398-406.

Yoon, H., Lim, J. H., Cho, C. H., Huang, L. E. & Park, J. W. 2011. CITED2 controls the hypoxic signaling by snatching p300 from the two distinct activation domains of HIF-1alpha. *Biochim Biophys Acta,* 1813**,** 2008-16.

Yuan, G., Nanduri, J., Bhasker, C. R., Semenza, G. L. & Prabhakar, N. R. 2005. Ca2+/calmodulin kinase-dependent activation of hypoxia inducible factor 1 transcriptional activity in cells subjected to intermittent hypoxia. *J Biol Chem,* 280**,** 4321-8.

Zaytseva, Y. Y., Valentino, J. D., Gulhati, P. & Evers, B. M. 2012. mTOR inhibitors in cancer therapy. *Cancer Lett,* 319**,** 1-7.

Zeng, L., Xiao, Q., Chen, M., Margariti, A., Martin, D., Ivetic, A., et al. 2013. Vascular endothelial cell growth-activated XBP1 splicing in endothelial cells is crucial for angiogenesis. *Circulation,* 127**,** 1712-22.

Zhang, W. & Liu, H. T. 2002. MAPK signal pathways in the regulation of cell proliferation in mammalian cells. *Cell Res,* 12**,** 10.

Zhou, J., Schmid, T., Schnitzer, S. & Brune, B. 2006. Tumor hypoxia and cancer progression. *Cancer Lett,* 237**,** 10-21.

List of abbreviations

Abbreviation	Full name
(D)PBS	(Dulbecco's) Phosphate-Buffered Saline
2D	Two-dimensional
3D	Three-dimensional
ASMase	Acid sphingomyelinase
ATF4	Activating transcription factor 6
ATF6	Activating transcription factor 4
ATP	Adenosine triphosphate
BNIP3	BCL2/adenovirus E1B 19 kDa protein-interacting protein 3
BSA	Bovine serum albumin
Ca^{2+}-CaM	Calcium-Calmodulin
CAD	Cationic amphiphilic drug
CAFs	Cancer associated fibroblasts
cDNA	complementary DNA
cfDNA	Cell-free DNA
CHOP	C/EBP homologous protein
CITED2	Cbp/p300-interacting transactivator 2
cpd	Compound
c_T	Threshold cycle
ctDNA	Circulating tumor DNA
DDIT4	DNA-damage-inducible transcript 4 protein
DFO	Deferoxamine
DMEM	Dulbecco's Modified Eagle Medium
DMSO	Dimethyl sulfoxide
DNA	Deoxyribonucleic acid
EC50	half maximal effective concentration
ECM	Extracellular matrix
EGFR	Epidermal growth factor receptor
EMT	Epithelial-mesenchymal transition
ER	Endoplasmic reticulum
FCS	Fetal calf serum
FDA	Food and Drug Administration
FP	Fluphenazine
GLUT	Glucose transporter
GST	Glutathione S-transferase
HCA	High-Content analysis
HIF	Hypoxia-inducible transcription factor
HRE	Hypoxia response element
HTS	High-throughput screening
IF	Immunofluorescence
IRE1	Inositol-requiring protein 1
Lamp2	Lysosome-associated membrane protein 2
LMP	Lysosome membrane permeabilization
Luc	Luciferase

lysoPC	Lysophosphatidylcholine
MAPK	Mitogen-activated protein kinase
MOA	Mode of action
mRNA	Messenger RNA
mTOR	Mechanistic target of rapamycin
NER	Nucleotide excision repair
ON	overnight
P/S	Penicillin/Streptomycin
PC	Phosphocholine
PCR	Polymerase chain reaction
PERK	Protein kinase R-like ER kinase
PFA	Paraformaldehyde
PHD	Prolyl hydroxylase domain-containing protein
PI3K	Phosphoinositide 3-kinase
Rb	Retinoblastoma-protein
RFU	Relative fluorescence units
RLU	Relative luminescence units
RNA	Ribonucleic acid
RNAi	RNA interference
RT	Room temperature
RT-qPCR	Real-time Quantitative PCR
S1P	Sphingosine-1-phosphate
SD	Standard deviation
SDS-PAGE	Sodium dodecyl sulfate polyacrylamide gel electrophoresis
shRNA	Short hairpin RNA
siRNA	Small interfering ribonucleic acid
siRNA	Small interfering RNA
SLC2A3	Solute carrier family 2 member 3
SM	Sphingomyelin
SMPD1	Sphingomyelin phosphodiesterase 1
SphK	Sphingosine kinase
TBST	Tris(hydroxymethyl)aminomethane (Tris)
TME	Tumor microenvironment
TP	Thymidine phosphorylase
UPR	Unfolded protein response
VEGFA	Vascular endothelial growth factor A
VHL	Von Hippel-Lindau tumor suppressor protein
XBP1	X-box-binding protein 1

List of figures

List of tables

Acknowledgement

At this point I would like to take the opportunity to express my gratitude to everyone who supported me throughout the course of this dissertation.

I would like to thank Carsten Wenzel, Luise Schulze, Nina Zablowsky, Sebastian Köpp, Sebastian Räse, Dennis Zilling, Nicole Kahmann, Larissa Hildebrandt, Birgitt Wykhoff, Jennifer Bell, Maria Buhl and Elisabeth Krahl for their excellent experimental support.

I also want to thank Matthias Keck and Björn Riefke for their support in the lipidomics experiments and analyses. Furthermore, I would like to give my thanks to Ralf Lesche and Andreas Schlicker for their help and advice analyzing the deep sequencing data. I also thank Stefan Kaulfuss for providing me with HCT116 tumor xenografts and Sven Christian for his support with the ASMase and SphK assay.

A special thanks goes to my supervisor Dr. Patrick Steigemann for his useful comments, advice and engagement during the course of this work.

Furthermore, I would like to thank Dr. Karsten Parczyk who gave me the opportunity to carry out my work with all the required facilities in the Screening Cell Biology department at Bayer AG.

I would also like to thank Professor Dr. Juri Rappsilber and Professor Dr. Roland Lauster for their support and evaluation of this work.

Last but not least, a great thank you goes to my family for supporting me throughout the course of this work. I would like to thank in particular my husband for his continues motivation and help.

Curriculum vitae

Saskia Klutzny (born Otto)

Professional experiences

10/2014 -10/2017	PhD student, Bayer AG – Screening Cell Biology - High Content Analysis, Berlin
01/2014 -08/2014	Internship (Master Thesis), Bayer Pharma AG – Screening Cell Biology - High Content Analysis, Berlin
07/2013 -12/2013	Internship, German Rheumatism Research Center (DRFZ) – Cell Biology, Berlin
03/2012 -08/2012	Student Research Assistant, Fraunhofer Institute for Biomedical Engineering - Cellular Biotechnology - Miniaturized Cell Assays, Potsdam
03/2011 -02/2012	Student Research Assistant, Fraunhofer Institute for Biomedical Engineering – Nanobiotechnology - Biomolecular Nanostructures, Potsdam

Education

10/2014 - present	Doctoral candidate - Biotechnology, Technical University of Berlin, Berlin
04/2013 -09/2014	MSc Biotechnology, Technical University of Berlin, Berlin (final grade: very good, 1.0)
09/2012 -05/2013	Postgraduate Diploma Biotechnology, University of the West of Scotland, Hamilton, UK (final grade: A with distinction)
10/2009 -08/2012	BSc Biotechnology, Technical University of Berlin, Berlin (final grade: very good, 1.3)
09/2001 -06/2008	Abitur, Von Saldern-Gymnasium, Brandenburg an der Havel (final grade: 1.4)

Awards and scholarships

11/2015	VDI - Verein Deutscher Ingenieure, Recognition for the excellent degree in Biotechnology at the Technical University of Berlin 2015
2013	University of the West of Scotland, Dr William JC Watt Medal for “Most Distinguished Student in the School of Science 2012-2013”
2012-2013	DAAD - German Academic Exchange Service, International Scholarship for the academic year 2012/2013

Scientific contributions

Publications

S. Klutzny, et al. (2018) “PDE5 inhibition eliminates cancer stem cells via induction of PKA signaling” submitted for publication. Cell Death Dis. 9(2):192. doi: 10.1038/s41419-017-0202-5.

S. Klutzny, et al. (2017) „Functional inhibition of acid sphingomyelinase by Fluphenazine triggers hypoxia-specific tumor cell death.” Cell Death and Disease. 8(3): e2709. doi: 10.1038/cddis.2017.130.
(Most parts of this article have been included into the dissertation)

H. Hernando, K. A. Gelato, R. Lesche, G. Beckmann, S. Koehr, S. Otto[1] et al. (2016) “EZH2 Inhibition Blocks Multiple Myeloma Cell Growth through Upregulation of Epithelial Tumor Suppressor Genes.” Mol Cancer Ther. 15(2):287-98.

C. Wenzel, S. Otto[1] et al. (2015) „A novel 3D high-content assay identifies compounds that prevent fibroblast invasion into tissue surrogates.” Exp Cell Res. 339(1):35-43.

S. Otto[1], U. Kaletta, F.F. Bier, C. Wenger, R. Hölzel (2014) “Dielectrophoretic immobilisation of antibodies on microelectrode arrays” Lab Chip. 14(5):998-1004

Conference talks

SLAS - VIII Spanish Drug Discovery Network Meeting 2016

SLAS - Cutting-Edge Technologies for Drug Target Validation Conference 2015

[1] Maiden name Saskia Otto

Appendix

A1 Materials

1. Chemicals and Solutions		
Material	**Manufacturer**	**Order number**
1,2-Dioleoyl-sn-glycero-3-phosphocholine (18:1 (Δ9-Cis) PC)	Sigma Aldrich (St. Louis, MO, USA)	P6354
10x Bolt™ Sample Reducing Agent (DTT)	Life Technologies by Thermo Fisher (Waltham, MA, USA)	B0004
1-stearoyl-2-arachidonoyl-sn-glycero-3-phosphocolin (18:0-20:4 PC)	Avanti lipids (Alabaster, AL, USA)	850469
1-stearoyl-2-docosahexaenoyl-sn-glycerol-3-phosphocolin (18:0-22:6 PC)	Avanti lipids (Alabaster, AL, USA)	850472
20x Bolt™ MES SDS Running Buffer	Life Technologies by Thermo Fisher (Waltham, MA, USA)	B0002
2-Deoxy-D-glucose (2-DG)	Sigma Aldrich (St. Louis, MO, USA)	D8375
2-Methylbutane	Sigma Aldrich (St. Louis, MO, USA)	M32631
32 % Paraformaldehyde (formaldehyde) aqueous solution	Electron Microscopy Sciences (Hatfield, PA, USA)	15714-S
4X Bolt™ LDS Sample Buffer	Life Technologies by Thermo Fisher (Waltham, MA, USA)	B0007
Acid Sphingomyelinase Assay Kit	Echelon Biosciences Inc. (Salt Lake City, UT, USA)	K-3200
Agarose NA	GE Healthcare (Little Chalfont, UK)	17-0554-01
Agilent DNA 1000 Chip Kit	Agilent Technologies (Santa Clara, CA, USA)	5067-1504
Antimycin A	Sigma Aldrich (St. Louis, MO, USA)	A8674
AZD8055	Selleckchem (Munich, Germany)	S1555
Bafilomycin A	Sigma Aldrich (St. Louis, MO, USA)	B1793
BAPTA-AM	Sigma Aldrich (St. Louis, MO, USA)	A1076
Bepridil	Sigma Aldrich (St. Louis, MO, USA)	B5016
Blocking Reagent	Sigma Aldrich (St. Louis, MO, USA)	11096176001 Roche
Calmidazolium	Sigma Aldrich (St. Louis, MO, USA)	C3930
Ceramide (from bovine spinal cord)	Sigma Aldrich (St. Louis, MO, USA)	22244
Chlorpromazine	Sigma Aldrich (St. Louis, MO, USA)	C8138
Clozapine	Sigma Aldrich (St. Louis, MO, USA)	C6305
Cytochalasin B	Sigma Aldrich (St. Louis, MO, USA)	C6762
Dantrolene	Sigma Aldrich (St. Louis, MO, USA)	D9175
Deferoxamine mesylate (DFO)	Sigma Aldrich (St. Louis, MO, USA)	D9533
Dimethyl sulfoxide (DMSO)	Sigma Aldrich (St. Louis, MO, USA)	D2650
DMEM / Ham's F12	Gibco by Thermo Fisher (Waltham, MA, USA)	31331-028
DMEM medium	Gibco by Thermo Fisher (Waltham, MA, USA)	32430-027
DPBS, no calcium, no magnesium	Life Technologies by Thermo Fisher (Waltham, MA, USA)	14190-094
E6 berbamine	Santa Cruz Biotechnology (Dallas, TX, USA)	73885-53-7

EGTA	Sigma Aldrich (St. Louis, MO, USA)	E3889
Ethanol	Sigma Aldrich (St. Louis, MO, USA)	270741
Fetal Bovine Serum (FBS)	PAA Laboratories by GE Healthcare (Little Chalfont, UK)	A15-151
Fluphenazine	Sigma Aldrich (St. Louis, MO, USA)	F4765
Fluspirilene	Sigma Aldrich (St. Louis, MO, USA)	F100
GeneAmp® RNA PCR Kit	Life Technologies by Thermo Fisher (Waltham, MA, USA)	N8080143
GF 109203X	Sigma Aldrich (St. Louis, MO, USA)	G2911
Glucose	Sigma Aldrich (St. Louis, MO, USA)	G0350500
Haloperidol	Sigma Aldrich (St. Louis, MO, USA)	H1512
Halt Protease and Phosphatase Inhibitor Cocktail	Thermo Fisher (Waltham, MA, USA)	78440
Halt™ Protease and Phosphatase Inhibitor Cocktail (100x)	Thermo Fisher (Waltham, MA, USA)	78440
Hygromycin B	Invitrogen by Thermo Fisher (Carlsbad, Ca, USA)	10687010
Insulin	Gibco by Thermo Fisher (Waltham, MA, USA)	12585014
Ionomycin	Sigma Aldrich (St. Louis, MO, USA)	I3909
KAPA Library Quantification Kit	Kapa Biosystems (Wilmington, MA, USA)	KK4824
Latrunculin B	Sigma Aldrich (St. Louis, MO, USA)	L5288
LC-MS based AbsoluteIDQ p180 Kit	Biocrates Life Sciences AG (Innsbruck, Austria)	-
Lipofectamine® RNAiMAX Transfection Reagent	Life Technologies by Thermo Fisher (Waltham, MA, USA)	13778150
MagicMark™ XP Western Protein Standard	Life Technologies by Thermo Fisher (Waltham, MA, USA)	LC5602
Methanol	Sigma Aldrich (St. Louis, MO, USA)	322415
ML7	Sigma Aldrich (St. Louis, MO, USA)	I2764
ML9	Sigma Aldrich (St. Louis, MO, USA)	C1172
N-N-Dimethylsphingosine	Sigma Aldrich (St. Louis, MO, USA)	SML0311
N-Palmitoyl-D-sphingomyelin	Sigma Aldrich (St. Louis, MO, USA)	91553
Ophiobolin A	Sigma Aldrich (St. Louis, MO, USA)	SML1478
Opti-MEM™ medium	Gibco by Thermo Fisher (Waltham, MA, USA)	11058021
Penicillin-Streptomycin	Sigma Aldrich (St. Louis, MO, USA)	P0781
PF-543	Sigma Aldrich (St. Louis, MO, USA)	PZ0234
Pierce™BCA protein assay kit	Thermo Fisher (Waltham, MA, USA)	23225
Pimonidazole	Hypoxyprobe (Burlington, MA, USA)	HP6-100Kit
Pimozide	Sigma Aldrich (St. Louis, MO, USA)	P1793
Protein block	Dako by Agilent Technologies (Santa Clara, CA, USA)	X090930-2
Puromycin	Sigma Aldrich (St. Louis, MO, USA)	P9620
Rapamycin	Sigma Aldrich (St. Louis, MO, USA)	R0395
RevertAid H Minus First Strand cDNA Synthesis Kit	Thermo Fisher (Waltham, MA, USA)	K1632
RIPA-Lysis Buffer	Merck Millipore (Billerica, MA, USA)	20-188
RNeasy Plus Mini Kit	Quiagen (Venlo, Netherlands)	74134
Roti-Stock 10x TBST	Carl Roth (Karlsruhe, Germany)	1061.1

RPMI 1640 medium	Gibco by Thermo Fisher (Waltham, MA, USA)	21875-034
Ryanodine	Sigma Aldrich (St. Louis, MO, USA)	SML1106
S1P	Sigma Aldrich (St. Louis, MO, USA)	S9666
Screen-Well® ICCB Known Bioactives library	Enzo Life Sciences (Farmingdale, NY, USA)	BML-2840-0100
Siramesine	Sigma Aldrich (St. Louis, MO, USA)	SML0976
SKI-II	Sigma Aldrich (St. Louis, MO, USA)	S5696
SlowFade® Gold Antifade Reagent	Life Technologies by Thermo Fisher (Waltham, MA, USA)	S36936
Sodium chloride solution	Sigma Aldrich (St. Louis, MO, USA)	S8776
Sphingomyelin (from bovine brain)	Sigma Aldrich (St. Louis, MO, USA)	S7004
Sphingosine kinase 1, active	Echelon Biosciences Inc. (Salt Lake City, UT, USA)	E-K068
Sphingosine Kinase Activity Assay	Echelon Biosciences Inc. (Salt Lake City, UT, USA)	K-3500
Staurosporine	Sigma Aldrich (St. Louis, MO, USA)	S4400
Steady-Glo® Luciferase Assay System	Promega (Fitchburg, WI, USA)	E2510
Sucrose	Sigma Aldrich (St. Louis, MO, USA)	84097
SYTOX® Orange Nucleic Acid Stain	Life Technologies by Thermo Fisher (Waltham, MA, USA)	S-11368
Tamoxifen	Sigma Aldrich (St. Louis, MO, USA)	T5648
TaqMan® Fast Advanced Master Mix	Thermo Fisher (Waltham, MA, USA)	4444557
Temsirolimus	Sigma Aldrich (St. Louis, MO, USA)	PZ0020
Thioridazine	Sigma Aldrich (St. Louis, MO, USA)	T9025
Tissue-Tek® O.C.T.™	Sakura Inc. (Staufen, Germany)	4583
Trifluoperazine	Sigma Aldrich (St. Louis, MO, USA)	T8516
Triton™ X-100	Sigma Aldrich (St. Louis, MO, USA)	T8787
TruSeq RNA Sample Preparation Kit v2	Illumina (San Diego, CA, USA)	RS-122-2001
TrypLE™ Express	Life Technologies by Thermo Fisher (Waltham, MA, USA)	12604-013
W13	Tocris (Bristol, UK)	0361
W7	Tocris (Bristol, UK)	0369
Wiskostatin	Sigma Aldrich (St. Louis, MO, USA)	W2270

2. Antibodies and Dyes		
Material	**Manufacturer**	**Order number**
Alexa Fluor® 488 anti-mouse	Jackson Immuno Research (West Grove, PA, USA)	715-545-150
Alexa Fluor® 488 anti-rabbit	Jackson Immuno Research (West Grove, PA, USA)	711-545-152
Alexa Fluor® 594 anti-rabbit	Jackson Immuno Research (West Grove, PA, USA)	111-585-144
anti- Galectin 1	Abcam (Cambridge, UK)	ab25138
anti-ASM	Cell Signaling Technology (Cambridge, UK)	#3687
anti-beta-actin	Sigma Aldrich (St. Louis, MO, USA)	A5316
anti-CD31	Abcam (Cambridge, UK)	ab28364
anti-HIF1-α	Abcam (Cambridge, UK)	ab51608
anti-Lamp2	Santa Cruz Biotechnology (Dallas, TX, USA)	sc-18822
anti-pimonidazole–FITC	Hypoxyprobe Inc. (Burlington, MA, USA)	HP6-100Kit
BODIPY® FL C12-Sphingomyelin	Invitrogen by Thermo Fisher (Carlsbad, Ca, USA)	D7711
Hoechst 33342	Life Technologies by Thermo Fisher (Waltham, MA, USA)	H1399
IRDye® 680RD-anti-mouse IgG	Licor (Lincoln, NE, USA)	926-68070
IRDye® 800CW-anti-rabbit IgG	Licor (Lincoln, NE, USA)	926-32211
LipidTOX™ Red Phospholipidosis Detection Reagent	Invitrogen by Thermo Fisher (Carlsbad, Ca, USA)	H34351
LysoTracker® Red DND-99	Invitrogen by Thermo Fisher (Carlsbad, Ca, USA)	L7528
SYTOX® Green nucleic acid stain	Life Technologies by Thermo Fisher (Waltham, MA, USA)	S7020

3. Other Consumables		
Material	**Manufacturer**	**Order number**
12 well TPP® tissue culture plates	Sigma Aldrich (St. Louis, MO, USA)	Z707775
6 well TPP® tissue culture plates	Sigma Aldrich (St. Louis, MO, USA)	Z707759
Blot Transfer Stacks, nitrocellulose	Life Technologies by Thermo Fisher (Waltham, MA, USA)	IB23001
Cell scraper	Sigma Aldrich (St. Louis, MO, USA)	SIAL0010
CellCarrier-384 Black, Optically Clear Bottom, Tissue CultureTreated	Perkin Elmer (Waltham, MA, USA)	6007550
Corning® cell culture flasks 75cm²	Sigma Aldrich (St. Louis, MO, USA)	CLS3276
Corning® Costar® cell culture flasks 162cm²	Sigma Aldrich (St. Louis, MO, USA)	CLS3151
MicroAmp® optical 384-well reaction plate	Applied Biosystems by Thermo Fisher (Waltham, MA, USA)	4309849
MicroAmp® Optical 96-Well Reaction Plate	Applied Biosystems by Thermo Fisher (Waltham, MA, USA)	N8010560
MicroAmp® Optical Adhesive Film	Applied Biosystems by Thermo Fisher (Waltham, MA, USA)	4360954
NHS-PEG12-Biotin	Thermo Fisher (Waltham, MA, USA)	21312
NuPAGE™ 4-12 % Bis-Tris protein gels	Invitrogen by Thermo Fisher (Carlsbad, Ca, USA)	NP0335BOX
PVDF membranes	Merck Millipore (Billerica, MA, USA)	IPVH00010
SuperFrost Plus slides	Menzel-Glaser	J1800AMNZ

4. Equipment and Software	
Equipment/Software	**Manufacturer**
AB7900 qPCR machine	Applied Biosystems by Thermo Fisher (Waltham, MA, USA)
Autotechnicon (Leica ASP 200S)	Leica Biosystems (Wetzlar, Germany)
CASY Model TT cell counter	Roche Applied Science (Penzberg, Germany)
Centrifuge Biofuge 4K	Heraeus (Hanau, Germany)
Centrifuge Biofuge Fresco	Heraeus (Hanau, Germany)
CO_2-Inkubator BBD6220	Heraeus (Hanau, Germany)
Cryo-Star HM 560 Cryostat	MICROM International (Walldorf, Germany)
CyBi-Well 384-well pipetting system	Analytik Jena AG (Jena, Germany)
Genedata Screener® for high-content screening and Genedata Condoseo modules	Genedata AG (Basel, Switzerland)
Hummingbird plate replicator	Digilab Inc. (Marlborough, MA, USA)
iBlot Gel Transfer Device	Life Technologies by Thermo Fisher (Waltham, MA, USA)
Illumina HiSeq® 2500	Illumina (San Diego, CA, USA)
Image Studio Lite Version 4	Licor (Lincoln, NE, USA)
ImageXpress Micro widefield imaging system	Molecular Devices (Sunnyvale, CA, USA)
Incubator chamber C16 for hypoxia	Labotect (Rosdorf, Germany)
Infinite M1000 microplate reader	Tecan Trading AG (Männedorf, Switzerland)
In-house HCA Data Management software	in-house
MetaXpress High Content Image Acquisition & Analysis Software	Molecular Devices (Sunnyvale, CA, USA)
Microm EC350-1	Thermo Fisher (Waltham, MA, USA)
Microsoft Office Professional Plus 2010	Microsoft (Redmond, WA, USA)
Multidrop Combi	Thermo Fisher (Waltham, MA, USA)
NanoDrop 1000	Thermo Fisher (Waltham, MA, USA)
Odyssey® CLx Imaging System	Licor (Lincoln, NE, USA)
Opera confocal imaging system	Perkin Elmer (Waltham, MA, USA)
PHERAstar plate reader	BMG Labtech (Ortenberg, Germany)
Prism Scientific Presentation Software	GraphPad Software (La Jolla, CA, USA)
Sciex 5500 mass spectrometer	Sciex (Framingham, MA, USA)
UHPLC	Shimadzu (Kyoto, Japan)
Electronic cutting tool	Silhouette SD
FLEXMAP 3D®	Luminex (Austin, TX, USA)
Umetrics SIMCA-P software	MKS Data Analytics Solutions (Malmö, Sweden)

A2 Supplementary data

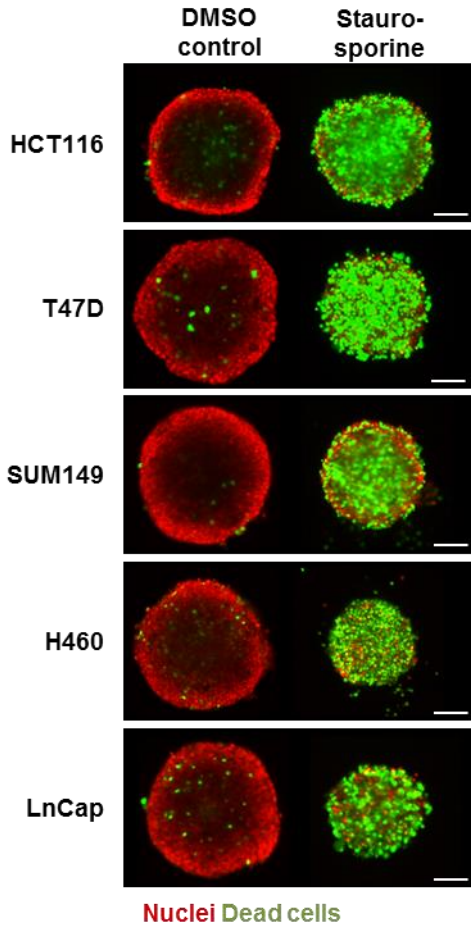

Supplementary Figure 1: 3D spheroid generation from single cell suspension of different tumor cells lines in agarose-covered 384-well plates. Single cell suspension of either HCT116 (colon cancer), T47D (breast cancer), SUM149 (breast cancer), H460 (lung cancer) or LnCap (prostate cancer) cells was seeded in agarose-covered 384-well plates. Cells were incubated for 4 days to form spheroids, followed by 3 days incubation with either DMSO control (solvent control) or 10 µM staurosporine (cell death control). After 7 days spheroids were stained with Hoechst (red) and dead cells were stained with SytoxGreen (green). Exemplary images of multiple experiments shown (n ≥ 2). Scale bar 100 µm.

Supplementary Table 1: DigiWest analysis of tumor spheroids. Protein or protein modifications that were significantly up-regulated (≥ 2x) in hypoxic HCT116 spheroids compared to normoxic spheroids. HCT116 Spheroids were incubated for 24 h in normoxia or hypoxia. Spheroids were collected and protein extracts were analyzed for expression of over 600 proteins or protein modifications by quantitative Western blot (DigiWest).

Protein / Protein Modification	Signal Intensity [arbitrary unit]			Reported Pathway / Function
	Hypoxia	Normoxia	Ratio Hypoxia/ Normoxia	
Fibronectin	2030.0	490.0	**4.1**	Adhesion
ZO-1	601.0	175.0	**3.4**	Adhesion
Akt	1464.0	705.0	**2.1**	Akt signaling / Metabolism
PEA-15 (PED)	906.0	369.0	**2.5**	Apoptosis / Autophagy
APG7L	1677.0	672.0	**2.5**	Autophagy
PKC substrates - phospho Ser	1042.0	273.0	**3.8**	Ca / cAMP / Lipid Signaling
CDK3	1587.0	484.0	**3.3**	Cell Cycle / Checkpoint
MCM2	10938.0	3416.0	**3.2**	Cell Cycle / Checkpoint
TOPK (PBK ,Lymphokine-activated killer T-cell-originated protein kinase)	3004.0	142.0	**21.2**	Cell Cycle / Checkpoint
Pbx1 (PRL)	15155.0	6996.0	**2.2**	Cell growth / Differentiation
ILK1 - phospho Ser246	124379.0	9915.0	**12.5**	Cell-cell adhesion
ILK1 - phospho Thr173	42852.0	4528.0	**9.5**	Cell-cell adhesion
Bmi1	3148.0	1566.0	**2.0**	Chromatin regulation / Epigenetics
Histone deacetylase 6 (HDAC6)	3760.0	1797.0	**2.1**	Chromatin regulation / Epigenetics
Histone H3 - acetyl Lys14	1026.0	326.0	**3.1**	Chromatin regulation / Epigenetics
Histone H3 - acetyl Lys18	35915.0	14073.0	**2.6**	Chromatin regulation / Epigenetics
Histone H3 - acetyl Lys23	11205.0	4212.0	**2.7**	Chromatin regulation / Epigenetics
Histone H3 - acetyl Lys9	38687.0	19100.0	**2.0**	Chromatin regulation / Epigenetics
Histone H3 - acetyl Lys9/Lys14	64238.0	19121.0	**3.4**	Chromatin regulation / Epigenetics
Histone H3 - monomethyl Lys4	3148.0	1016.0	**3.1**	Chromatin regulation / Epigenetics
Histone H3 - trimethyl Lys27	25485.0	5747.0	**4.4**	Chromatin regulation / Epigenetics
Histone H3 - trimethyl Lys9	153634.0	63313.0	**2.4**	Chromatin regulation / Epigenetics
RING1A	333.0	129.0	**2.6**	Chromatin regulation / Epigenetics
SUZ12	540.0	199.0	**2.7**	Chromatin regulation / Epigenetics
alpha 1-Actin	118180.0	56390.0	**2.1**	Cytoskeletal regulation / Adhesion
Rac1/cdc42	6985.0	2877.0	**2.4**	Cytoskeletal Signaling
53BP1	615.0	195.0	**3.2**	DNA Damage
SPRY3 (Spry-3, Sprouty 3)	1927.0	854.0	**2.3**	EGFR signaling

Src family - phospho Tyr416	671.0	259.0	**2.6**	Hippo signaling
SOCS-3	1363.0	279.0	**4.9**	Immunology / Inflammation
IGFBP-2	913.0	383.0	**2.4**	Insulin signaling
DUSP16 (MKP-7)	13838.0	866.0	**16.0**	MAPK signaling
JNK/SAPK	397.0	153.0	**2.6**	MAPK signaling
p38 MAPK	275.0	95.0	**2.9**	MAPK signaling
p38 MAPK - phospho Thr180/Tyr182	236.0	91.0	**2.6**	MAPK signaling
RKIP (PBP, PEBP, PEBP1)	8250.0	2645.0	**3.1**	MAPK signaling
RSK 1 (p90RSK) - phospho Thr573	514.0	245.0	**2.1**	MAPK Signaling
SPRY4 (Spry-4, Sprouty 4)	9964.0	2231.0	**4.5**	MAPK Signaling
FABP4	15405.0	2774.0	**5.6**	Metabolism
Glucose 6 phosphatase alpha	1207.0	345.0	**3.5**	Metabolism
HSP 70	468.0	137.0	**3.4**	Protein Folding
eEF2	12183.0	5819.0	**2.1**	Protein Translation
C/EBP beta	553.0	218.0	**2.5**	Transcription factor
HNF-4 alpha (HNF-4A) - phospho Ser304	2926.0	551.0	**5.3**	Transcription factor
HNF-4 alpha (HNF-4A) - phospho Ser313	5441.0	2467.0	**2.2**	Transcription factor
RNA Polymerase II - phospho Ser5	1963.0	877.0	**2.2**	Transcription/ RNA synthesis
PPAR gamma	32792.0	15768.0	**2.1**	Transcriptional Activator
PPAR gamma - phospho Ser112	5788.0	2761.0	**2.1**	Transcriptional Activator
eEF-2K	549.0	218.0	**2.5**	Translational control
eIF4E	12370.0	2234.0	**5.5**	Translational control
eIF4E - phospho Ser209	1316.0	543.0	**2.4**	Translational control
PKR - phospho Thr446	1734.0	362.0	**4.8**	Translational control
Bip	510.0	216.0	**2.4**	Translational control / RNA regulation
NDRG1 - phospho Thr346	1291.0	261.0	**4.9**	Tumor suppressor
Axl	215.0	99.0	**2.2**	Tyrosine Kinase / Adaptors
FAK	875.0	124.0	**7.1**	Tyrosine Kinase / Adaptors
EphA2 - phospho Ser897	635.0	216.0	**2.9**	tyrosine kinase receptor-mediated cell signaling
SHP-2	653.0	267.0	**2.4**	Tyrosine phosphatase
Caseinkinase 1 epsilon	323.0	122.0	**2.6**	Wnt / Hedgehog signaling
MMP13	34261.0	11902.0	**2.9**	
PHD2	1485.0	734.0	**2.0**	

Supplementary Table 2: EC50 generation of hypoxia specific hits in T47D spheroids under hypoxic conditions. T47D spheroids were treated for 72 h in normoxic or hypoxic conditions. Dead cells were stained with SytoxGreen and fluorescent intensities in spheroids were measured. Values were normalized with solvent (DMSO) control (0 %) and staurosporine (10 µM) as positive control (100 %) for cell death. (adapted from Klutzny et al. (2017))

Compound	EC50 (cell death) in T47D tumor spheroids [M]
Trifluoperazine	8.18E-06
E6 berbamine	4.12E-06
Wiskostatin	NA
Latrunculin B	inactive
ML9	3.86E-06
GF-109203X	9.62E-06
Tamoxifen	inactive
ML7	9.29E-06
Cytochalasin B	3.30E-06

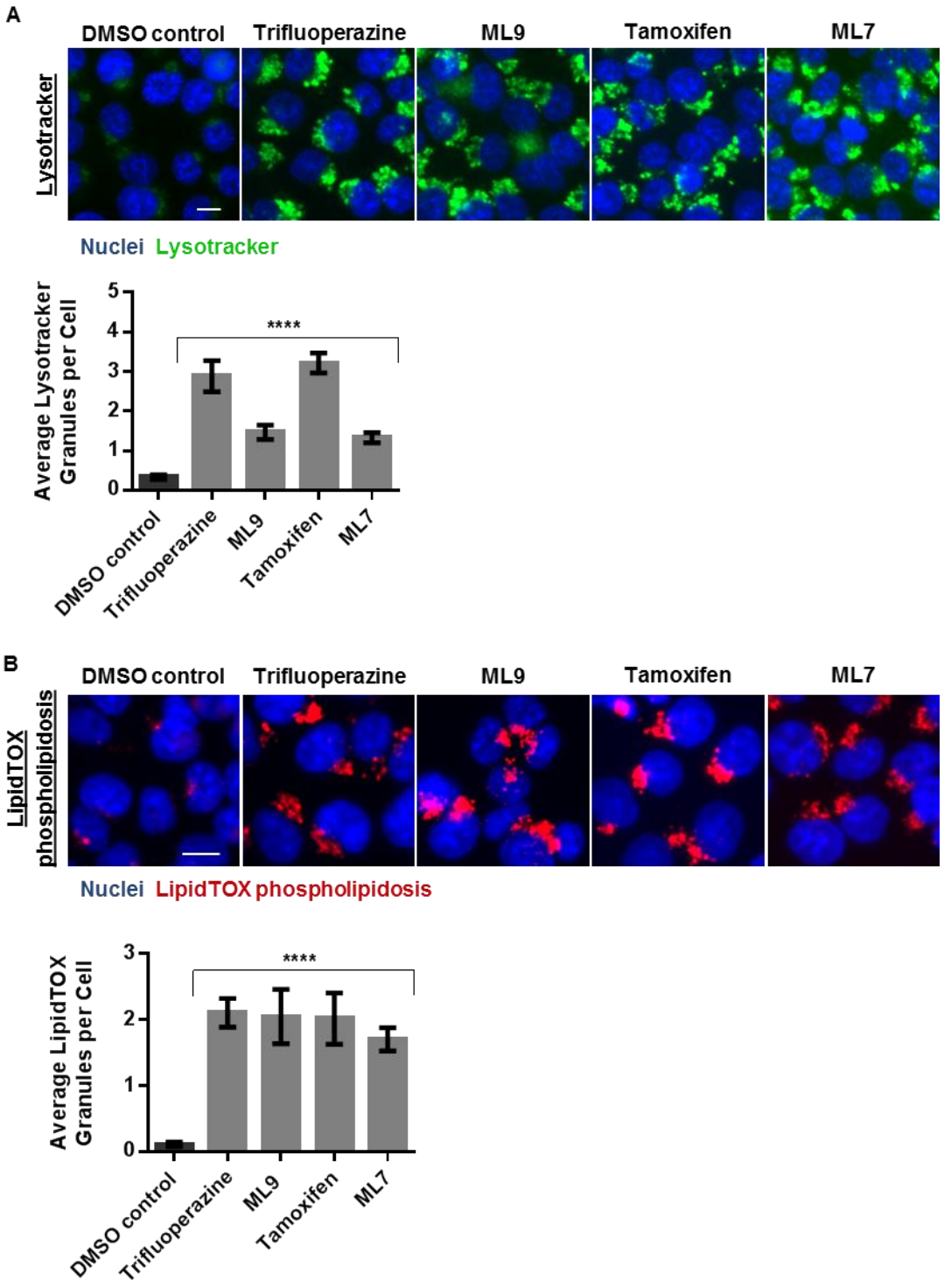

Supplementary Figure 2: Hypoxia-selective and 3D specific hits impair lysosomal function. HCT116 cells were treated for 24 h with either DMSO control or 5 µM compound. Cells were either stained A) for acidic vesicles using Lysotracker or B) for the accumulation of undigested phospholipids using the LipidTOX phospholipidosis staining. Nuclei were stained with Hoechst. Exemplary images of multiple experiments shown (n = 3). Scale bar 10 µm. Quantification of stainings shown below images. Bars show mean with SD (n = 3). **** p-value < 0.0001.

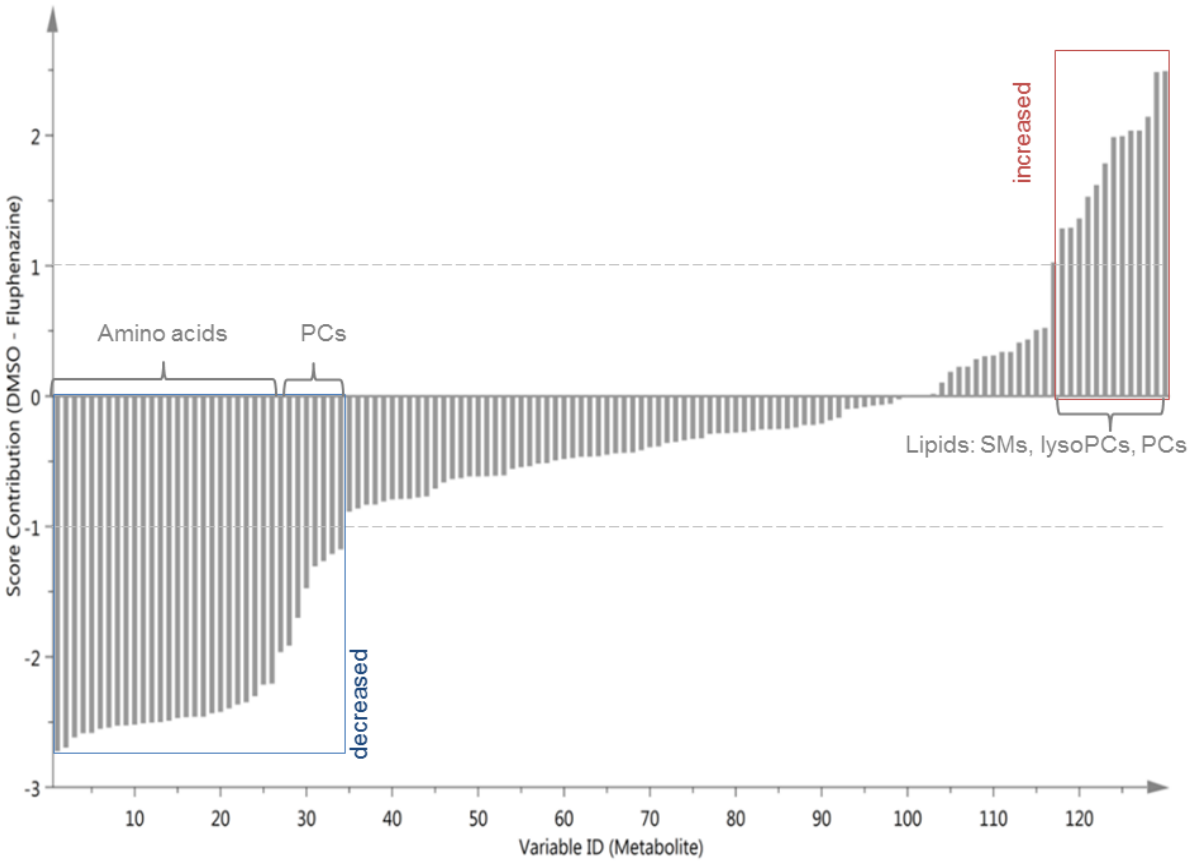

Supplementary Figure 3: Fluphenazine alters cellular lipid composition of HCT116 cells. Global analysis of 188 metabolites in HCT116 cells treated for 24 h with either DMSO control or 5 µM fluphenazine (median of 4 replicates). PC: phosphatidylcholine, lysoPC: lysophosphatidylcholine, SM: sphingomyelin. (adapted from Klutzny et al. (2017))

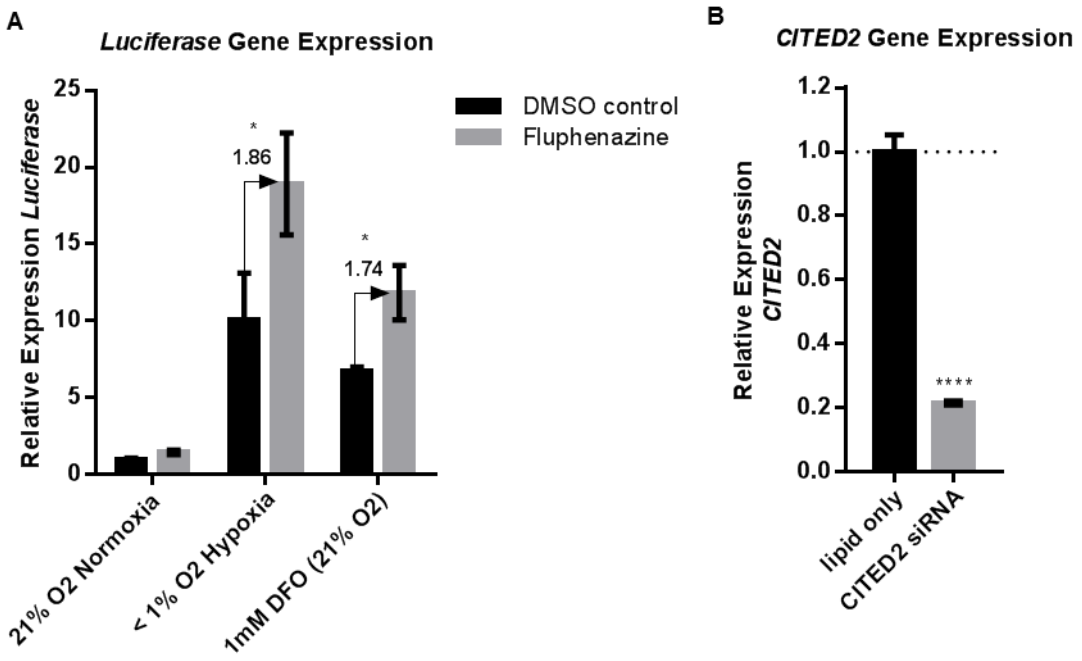

Supplementary Figure 4: *Luciferase* and *CITED2* mRNA expression level in HCT116-HRE-Luc cells.
A) HCT116-HRE-Luc cells were treated for 24 h with DMSO control or 5 µM fluphenazine control and incubated either in normoxia, hypoxia or in combination with DFO. Gene expression analysis was performed for *luciferase* by RT-qPCR. Ct values of each sample were normalized with the internal control *RPL32* and normalized to the normoxia DMSO control sample. Bars show mean with SD (n = 3). * p-value < 0.05. B) HCT116-HRE-Luc cells were incubated for 72 h with lipid only control or CITED2 siRNA. Gene expression analysis was performed for *CITED2* by RT-qPCR. Ct values of each sample were normalized with the internal control *RPL32* and normalized to lipid only control. Bars show mean with SD (n = 3). **** p-value < 0.0001. (adapted from Klutzny et al. (2017))

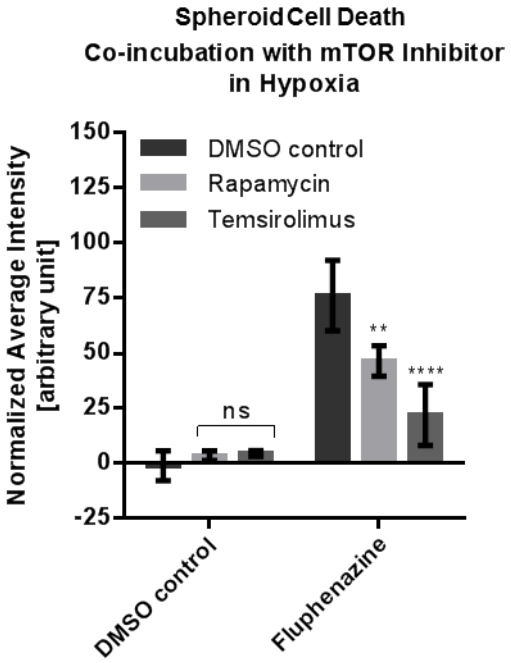

Supplementary Figure 5: Effect of mTOR inhibition on spheroid cell death. HCT116 spheroids were treated for 3 days with DMSO control, 5 µM fluphenazine or 10 µM staurosporine and co-treated with either DMSO control or 7 µM mTOR inhibitor (rapamycin or temsirolimus) under hypoxic conditions. Dead cells were stained with SytoxGreen and fluorescent intensities in spheroids were measured. Values were normalized with DMSO/DMSO control (0) and staurosporine/DMSO cell death control (100). Bars show mean with SD (n ≥ 3). **** p-value < 0.0001, ** p-value < 0.01, ns – not significant.

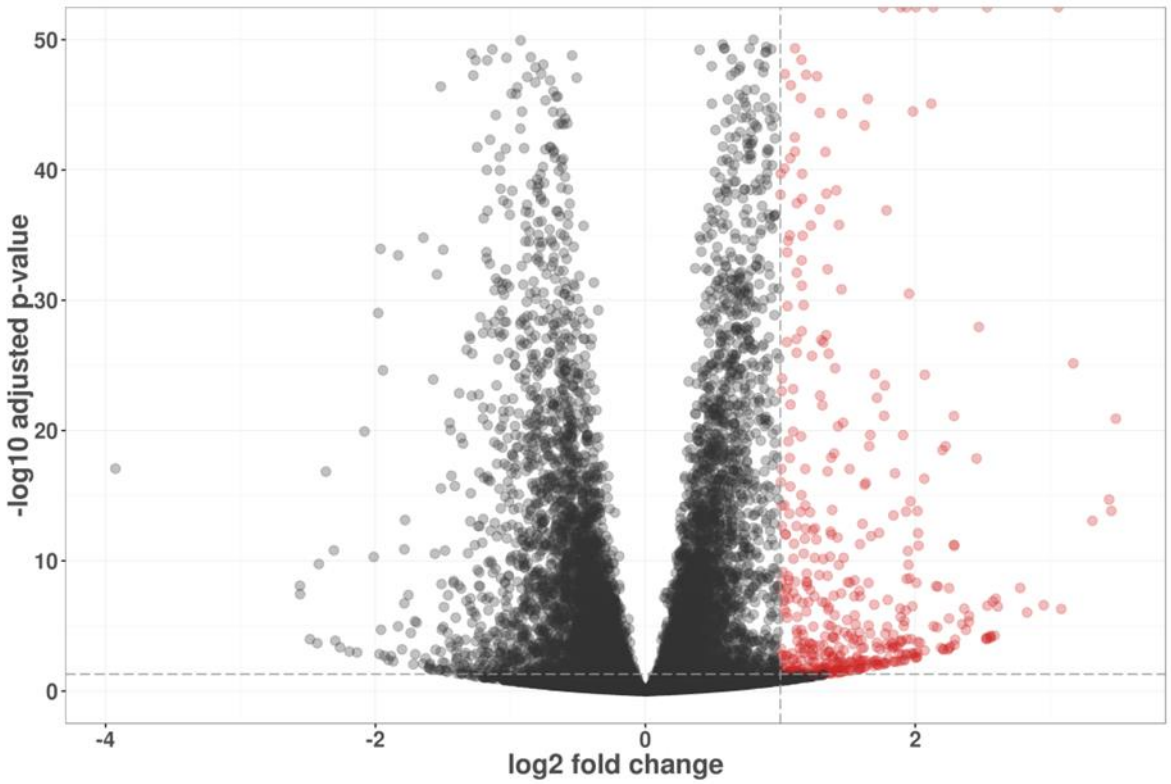

Supplementary Figure 6: Analysis of all protein-encoding genes (~ 20.000 genes) by deep sequencing of fluphenazine treated HCT116 cells. Volcano plot showing gene expression changes of cells treated with 1 mM DFO + 5 µM fluphenazine vs 1 mM DFO alone. In red: genes upregulated at least 2-fold in co-treated cells compared to DFO alone treated cells (adjusted p-value < 0.05). Mean of 4 replicates. (adapted from Klutzny et al. (2017))

Supplementary Table 3: Deep sequencing analysis of HCT116 cells treated for 24 h with either 1 mM DFO or 1mM DFO + 5 µM fluphenazine identifies several HIF-1 target genes to be upregulated (≥ 1,3 fold increased expression and adjusted p-value < 0.05) upon co-treatment. (adapted from Klutzny et al. (2017))

Gene	Fold Change
ADM	**1.62**
ANGPT2	**3.75**
BNIP3	**1.34**
CTGF	**2.34**
DDIT4 (REDD1)	**2.09**
EGLN3	**1.66**
MCL1	**1.42**
NDRG1	**1.32**
NR4A1	**1.47**
PFKFB3	**1.57**
PLAUR (uPAR)	**1.47**
SERPINE1	**1.74**
SLC2A3	**1.76**
SNAI1	**1.70**
SNAI2	**2.65**
STC2	**2.22**
VEGF	**2.14**
ZEB1	**2.01**

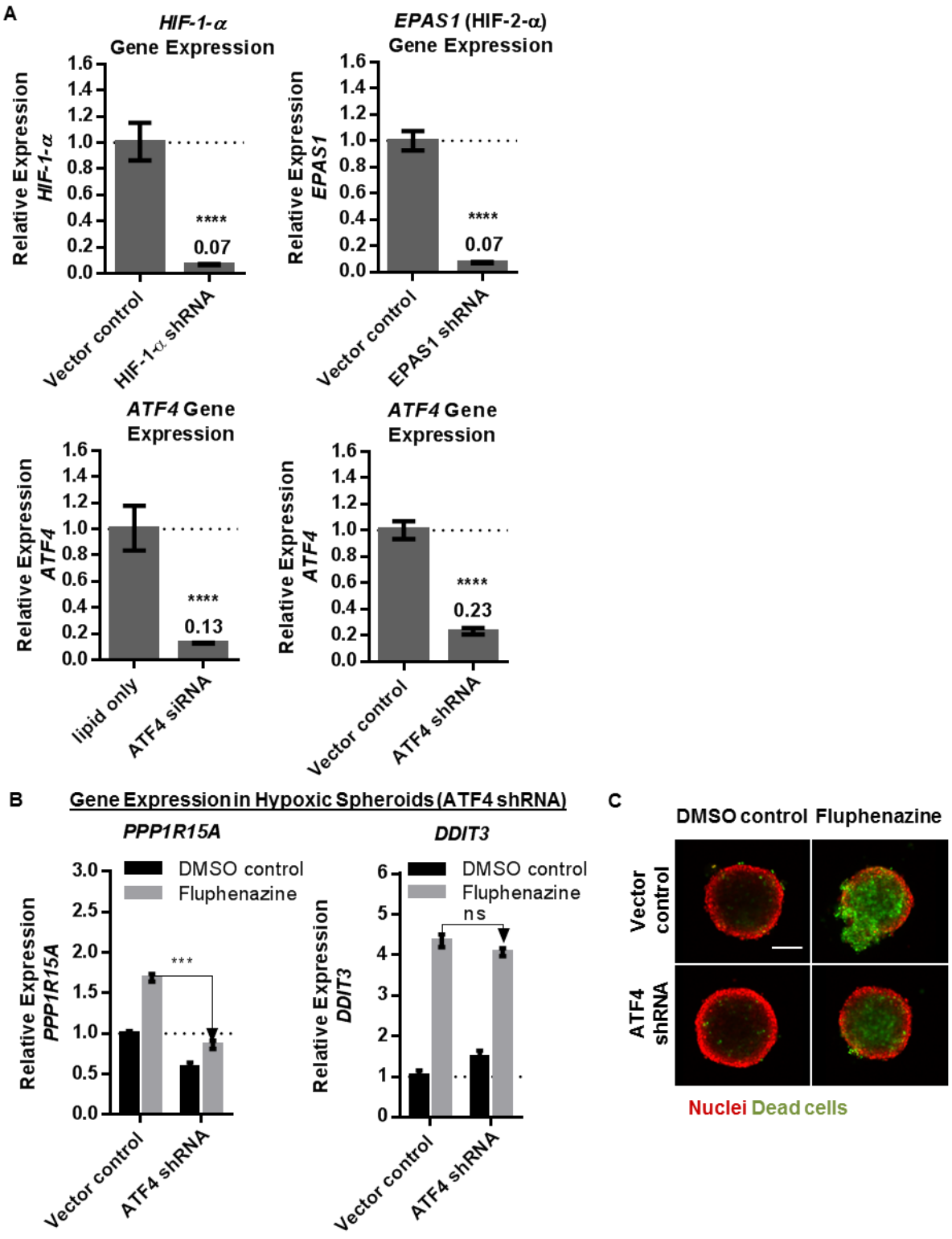

Supplementary Figure 7: Gene knockdown in HCT116 spheroids with HIF-1-α shRNA, EPAS1 (HIF-2-α), ATF4 shRNA and ATF4 siRNA. A) Knockdown efficacies: siRNA treated cells grown as spheroids (for *ATF4*) or spheroids from HCT116 cells stably transfected with HIF shRNA (see material and methods) were harvested and mRNA extracted. Ct values of each sample were normalized with the internal control *RPL32* and normalized to the lipid only or vector control sample. Bars show mean with SD (n = 3). **** p-value < 0.0001. B) Spheroids generated from HCT116 cells stably transfected with ATF4 shRNA were incubated for 24 h under hypoxia with DMSO control or 5 µM fluphenazine. Gene expression level for ATF4 target genes

PPP1R15A and *DDIT3* were determined using RT-qPCR. Ct values of each sample were normalized with the internal control *RPL32* and the hypoxia vector control sample. Bars show mean with SD (n = 3). *** p-value < 0.001, ns – not significant. C) Spheroids generated from HCT116 cells stably transfected with ATF4 shRNA were treated with either DMSO control or 5 µM fluphenazine for 3 days under hypoxia. Spheroid nuclei were stained with Hoechst (red) and dead cells were stained with SytoxGreen (green). Representative images of multiple experiments shown (n = 3). Scale bar 100 µm. (adapted from Klutzny et al. (2017))

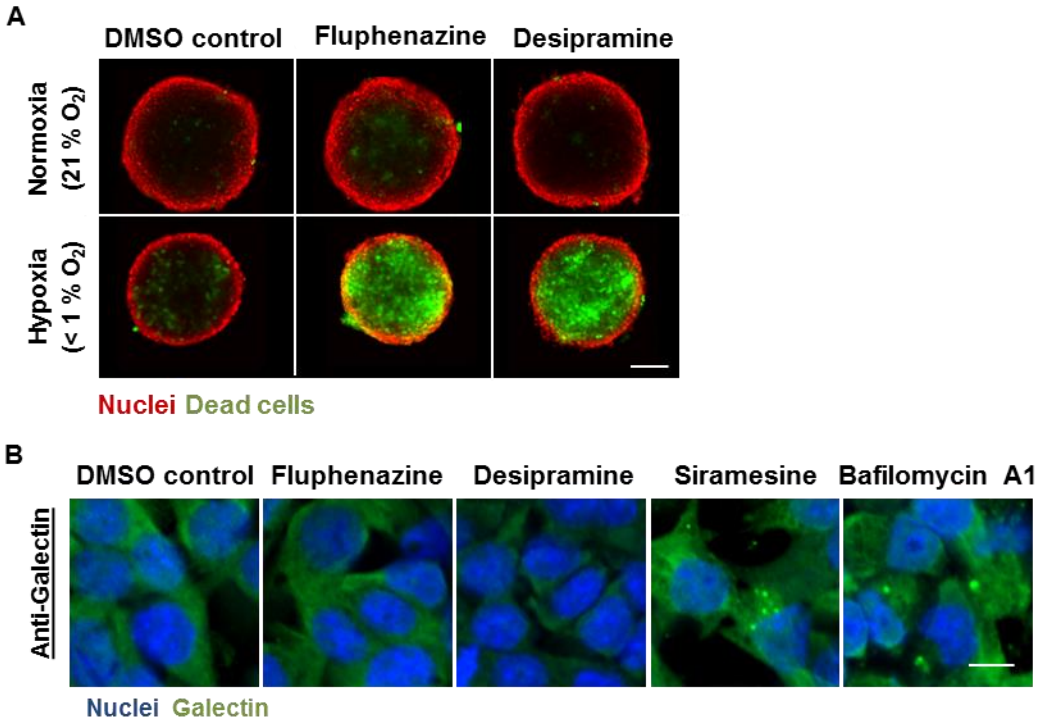

Supplementary Figure 8: Desipramine shows similar phenotype as fluphenazine. A) HCT116 Spheroids were treated for 3 days with either DMSO control, 5 µM fluphenazine or 5 µM desipramine under normoxic or hypoxic conditions. Spheroid nuclei were stained with Hoechst (red) and dead cells were stained with SytoxGreen (green). Representative images of multiple experiments shown (n ≥ 2). Scale bar 100 µm. B) HCT116 cells were treated for 24 h with either DMSO control, 5 µM fluphenazine, 5 µM desipramine, 5 µM siramesine or 200 nM bafilomycin A1. Cells were stained for Galectin. Representative images of multiple experiments shown (n ≥ 2). Scale bar 10 µM.